UNIVERSITÉ DE LILLE – UNIVERSITÄT MÜNSTER

Ecole Doctorale Biologie Santé de Lille (n°446)

DOCTORAT

Aspects Moléculaires et Cellulaires de la Biologie

Targeting the calcium-activated potassium channel $K_{Ca}3.1$ in pancreatic ductal adenocarcinoma

Benjamin Soret

16th of December 2024

Jury composition:

Prof. Natalia Prevarskaya – University of Lille – Jury President

Prof. Rosa Angela Cardone – University of Bari – Reviewer

Prof. Bruno Constantin – University of Poitiers – Reviewer

Prof. Alessandra Fiorio Pla – University of Turin – Examiner

Dr. Zoltán Pethö – University of Münster – Examiner

Prof. Albrecht Schwab – University of Münster – Thesis co-director

Dr. V'yacheslav Lehen'kyi – University of Lille – Thesis co-director

UNIVERSITÉ DE LILLE – UNIVERSITÄT MÜNSTER

Ecole Doctorale Biologie Santé de Lille (n°446)

DOCTORAT

Aspects Moléculaires et Cellulaires de la Biologie

Inhibition du canal potassique activé par le calcium $K_{Ca}3.1$ dans l'adénocarcinome canalaire pancréatique

Benjamin Soret

16 décembre 2024

Composition du jury :

Pr. Natalia Prevarskaya – Université de Lille – Présidente du jury

Pr. Rosa Angela Cardone – Université de Bari – Rapportrice

Pr. Bruno Constantin – Université de Poitiers – Rapporteur

Pr. Alessandra Fiorio Pla – Université de Turin – Examinatrice

Dr. Zoltán Pethö – Université de Münster – Examinateur

Pr. Albrecht Schwab – Université de Münster – Co-directeur de thèse

Dr. V'yacheslav Lehen'kyi – Université de Lille – Co-directeur de thèse

Co-tutelle carried out under the supervision of:

Prof. Dr. med. Albrecht Schwab – Institut für Physiologie II, Robert-Koch-Str. 27b, D-48149, Westfälische Wilhelms-Universität Münster, Germany

Dr. V'yacheslav Lehen'kyi – Laboratory of Cell Physiology, PHYCELL - INSERM U1003, University of Lille, Bâtiment SN3, 59655, Villeneuve d'Ascq, France

À **mes parents**, pour leur amour inconditionnel et leur soutien indéfectible,

À **mon frère**, dont la résilience et l'esprit combatif m'inspirent chaque jour,

À **Füsun**, pour son amour et son soutien sans faille, sans lesquels je ne serais pas arrivé jusqu'ici,

Et à **Winnie**, mon fidèle compagnon, qui ne m'a jamais quitté pendant mes longues nuits d'écriture.

ACKNOWLEDGEMENTS

I would like to express my heartfelt gratitude to all those who have supported me throughout the journey of completing this thesis.

First and foremost, I would like to thank Prof. Dr. Albrecht Schwab for allowing me to pursue my PhD in his lab. Your invaluable guidance, encouragement, and expertise have greatly enriched my work. Your exemplary qualities as a mentor, embodying professionalism, integrity, and a passion for research, have set a standard that I aspire to in my own career. I am truly grateful for the trust you placed in me and for the opportunity to learn under your mentorship. You will always represent the ideal of what a dedicated scientist and leader should be.

I would also like to extend my deepest thanks to Dr. V'yacheslav Lehen'kyi, who took a chance on me while I was still a bachelor student and mentored me in my early scientific life. I truly would not be here without your support and encouragement. You are the reason my scientific career took this turn, and for this, I will be forever grateful. I am thankful for your belief in my potential and for the opportunity to pursue my PhD through this cotutelle program. Your guidance has been instrumental in shaping my academic journey, and I appreciate everything you have done for me.

I am sincerely grateful to my colleague and friend, Dr. Zoltán Pethö, whose unwavering support was invaluable throughout my thesis journey. Your insights and encouragement gave me the confidence to overcome obstacles, and I genuinely appreciate the camaraderie we developed along the way. Thank you for being both a mentor and a friend.

In addition, I wish to thank those who provided experimental assistance throughout this project. A special thank you to Ilka Neumann, Weronika Wilczak, Sarah Sargin, Sandra Schimmelpfennig, Elke Nass, Dr. Andrea Oeckinghaus, and Dr. Serena Pillozzi. Your assistance was essential to the progress and success of my research.

I would like to extend my sincere thanks to Christina Kick and Prof. Dr. Bernhard Wünsch for their generous gift of the mitochondrially targeted-senicapoc compounds: WMS – 98 02, WMS – 98 03, and WMS – 98 04. I truly appreciate the trust and resources you invested in this project.

I would also like to express my gratitude to all the members of the Institut für Physiologie II and of The Laboratory of Cell Physiology. Your collaborative spirit, support, and encouragement have made this journey enjoyable and fulfilling. I would like to extend my sincere gratitude to Prof. Natalia Prevarskaya for inviting me to be a part of her lab.

Throughout these three years, I have had the privilege of meeting many remarkable individuals whom I am now happy to call friends. Each of you has made a meaningful impact on my journey. I would like to specifically acknowledge: Dr. Micol Rugi, Dr. Gonçalo Mesquita, Dr. Luca Matteo Todesca, Rieke Schleinhege, Dr. Jakub Mitrega, Dr. Aurélien Haustrate, Dr. Thorsten Loeck, Dominika Ciechanska, Dr. Karolina Najder and Dr. Héctor Noguera Hurtado. Thank you all for your friendship, support during this journey, and for the countless memories we've created together.

Thank you all for being part of this journey.

FUNDINGS

I am particularly grateful to those who made this research possible. This work was conducted as part of a co-tutelle doctorate program between the University of Lille and the University of Münster within the framework of the Internationally Associated Laboratory CaPANCInv.

I would like to extend my sincere gratitude for the financial support provided by the University of Lille and the Deutsche Forschungsgemeinschaft (SCHW 407/25-1). Additionally, I acknowledge the generous funding from the Deutsche Forschungsgemeinschaft (SCHW 407/22-1; GRK 2515/1, ChemBion), as well as the European Union through the Marie Skłodowska-Curie Actions Innovative Training Network (Grant 813834—pHioniC—H2020-MSCA-ITN-2018), awarded to AS.

PUBLICATIONS

Soret, B., Hense, J., Lüdtke, S., Thale, I., Schwab, A., & Düfer, M. (2022). Pancreatic $K_{Ca}3.1$ channels in health and disease. Biological chemistry, 404(4), 339–353. https://doi.org/10.1515/hsz-2022-0232

Loeck, T., Rugi, M., Todesca, L. M., Kalinowska, P., **Soret, B.**, Neumann, I., Schimmelpfennig, S., Najder, K., Pethő, Z., Farfariello, V., Prevarskaya, N., & Schwab, A. (2023). The context-dependent role of the Na^+/Ca^{2+}-exchanger (NCX) in pancreatic stellate cell migration. *Pflugers Archiv : European journal of physiology*, *475*(10), 1225–1240. https://doi.org/10.1007/s00424-023-02847-3

Mesquita, G., Haustrate, A., Mihalache, A., **Soret, B.**, Cordier, C., Desruelles, E., Duval, E., Pethö, Z., Prevarskaya, N., Schwab, A., & Lehen'kyi, V. (2023). TRPV6 Channel Is Involved in Pancreatic Ductal Adenocarcinoma Aggressiveness and Resistance to Chemotherapeutics. Cancers, 15(24), 5769. https://doi.org/10.3390/cancers15245769

Haustrate, A., Cordier, C., Shapovalov, G., Mihalache, A., Desruelles, E., **Soret, B.**, Essonghé, N. C., Spriet, C., Yassine, M., Barras, A., Marines, J., Alcaraz, L. B., Szunerits, S., Robin, G., Gosset, P., Prevarskaya, N., & Lehen'kyi, V. (2024). Trpv6 channel targeting using monoclonal antibody induces prostate cancer cell apoptosis and tumor regression. *Cell death & disease*, *15*(6), 419. https://doi.org/10.1038/s41419-024-06809-0

Rugi, M., Hofschröer, V., Pethő, Z., **Soret, B.**, Loeck, T., & Schwab, A. (2024). $K_{2P}2.1$ channels modulate the pH- and mechanosensitivity of pancreatic stellate cells. *Pflugers Archiv : European journal of physiology*, 10.1007/s00424-024-03021-z. Advance online publication. https://doi.org/10.1007/s00424-024-03021-z

Pending publication:

Soret, B., Pethő, Z., Neumann, I., Wilczak, W., Rugi, M., Sargin, S., Schimmelpfennig, S., Nass, E., Mesquita, G., Ciechanska, D., Oeckinghaus, A., Pillozzi, S., Prevarskaya, N., Lehen'kyi, V., & Schwab, A. Targeting plasma membrane $K_{Ca}3.1$ channels in pancreatic ductal adenocarcinoma impairs cancer progression.

SUMMARY

Pancreatic ductal adenocarcinoma (PDAC) is the most common and aggressive form of pancreatic cancer, accounting for over 90% of cases, with a poor 5-year relative survival rate of only 10% to 12%. Due to its asymptomatic early progression and the lack of effective diagnostic tools, PDAC is often diagnosed at advanced stages when metastasis has already occurred. Additionally, its high resistance to conventional therapies complicates treatment, highlighting the urgent need for novel strategies.

The development of PDAC is intricately linked to the unique physiology and microenvironment of the exocrine pancreas. The activation of pancreatic stellate cells (PSCs) creates a dense fibrotic stroma that contributes to cancer progression. This desmoplastic stroma interacts with tumor, immune, and endothelial cells, resulting in a hypoxic and poorly vascularized environment that hinders treatment delivery.

Research in oncology increasingly focuses on the role of ion channels in tumor development. Traditionally studied in excitable tissues, ion channels are now recognized as critical regulators in various cancers. Modulating these channels has shown potential for anticancer effects. Among these, potassium channels have garnered attention for their roles in the tumor microenvironment and their potential as therapeutic targets.

Among these, the calcium-activated potassium channel $K_{Ca}3.1$ has emerged as an important regulator of cancer signaling pathways and as a prognostic biomarker in PDAC, influencing processes such as migration, invasion, and apoptosis resistance. Additionally, $K_{Ca}3.1$ is expressed in PSCs making it particularly relevant in the tumor microenvironment of PDAC. Despite its therapeutic potential, the data regarding $K_{Ca}3.1$ targeting in PDAC are limited. Given its expression in both cancer cells and tumor microenvironment—including in immune and endothelial cells—predicting the effects of targeting $K_{Ca}3.1$ in PDAC is complex. Moreover, the differential expression of $K_{Ca}3.1$ in the plasma membrane and in the mitochondrial inner membrane of PDAC cells suggests that targeting these channels in specific cellular compartments may present distinct effects.

While *in vitro* studies provided valuable insights into the biological functions of $K_{Ca}3.1$, *in vivo* data were still lacking. It was the aim of my thesis to contribute to closing this gap. We conducted qPCR analysis of patient samples which showed that elevated $K_{Ca}3.1$ expression was associated with poorer survival outcomes. This led to an investigation of $K_{Ca}3.1$ inhibition using TRAM-34 and maurotoxin, both as monotherapies and in combination with gemcitabine. The KPfC (*Kras*$^{wt/LSL-G12D}$ *Tp53*$^{fl/+}$ *Pdx1-Cre*) mouse model was used, alongside a 3D spheroid co-culture that incorporates pancreatic cancer cells and PSCs.

Maurotoxin exhibited superior efficacy compared to TRAM-34 in both models. *In vivo*, plasma membrane-specific $K_{Ca}3.1$ inhibition led to a decrease in tumor node size without inducing excessive fibrosis. RNA sequencing of $K_{Ca}3.1$ CRISPR knockout spheroids revealed alterations in pathways related to IFN-α/γ, epithelial-mesenchymal transition (EMT), and G2-M checkpoint regulation. Subsequent analysis of the KPfC tissue indicated that $K_{Ca}3.1$ inhibition was associated with increased cell death and reduced EMT. *In vitro*, the inhibition of the plasma membrane $K_{Ca}3.1$ channel by maurotoxin resulted in decreased invasiveness and enhanced cell death in the 3D spheroid model. These results highlight the differential effects of $K_{Ca}3.1$ based on its subcellular

localization; plasma membrane-specific inhibition reduced tumor invasiveness, while TRAM-34 that blocks both plasma membrane and mitochondrial channels yielded less pronounced effects.

This research explores the intricate dynamics of $K_{Ca}3.1$ inhibition in PDAC and validates its potential as a promising therapeutic target for impairing cancer progression.

Keywords: Pancreatic cancer; $K_{Ca}3.1$; Tumor microenvironment; Spheroids; 3D Migration; Fibrosis.

Statement of significance: This study follows up on the correlation between elevated $K_{Ca}3.1$ channel expression and poor patient overall survival. Combining an immunocompetent murine PDAC model, 3D spheroid models and RNAseq analysis, we show that inhibiting $K_{Ca}3.1$ leads to decreased invasive potential and tumor growth as well as increased cell death. We propose $K_{Ca}3.1$ inhibition as an alternative strategy for pancreatic cancer treatment.

RÉSUMÉ

L'adénocarcinome canalaire pancréatique (PDAC) est la forme de cancer du pancréas la plus courante et la plus agressive, représentant plus de 90 % des cas, avec un taux de survie à 5 ans de seulement 10 % à 12 %. En raison de sa progression précoce asymptomatique et de l'absence d'outils diagnostiques efficaces, le PDAC est souvent diagnostiqué à un stade avancé, où le cancer a déjà métastasé. Sa forte résistance aux thérapies conventionnelles complique également le traitement, soulignant le besoin urgent de stratégies novatrices.

Le développement du PDAC est lié à la physiologie et au microenvironnement du pancréas exocrine. L'activation des cellules stellaires pancréatiques (PSCs) engendre un stroma fibreux dense qui contribue à la progression du cancer. Ce stroma desmoplastique interagit avec les cellules tumorales, immunitaires et endothéliales, créant un environnement hypoxique et peu vascularisé qui entrave l'efficacité des traitements.

La recherche en oncologie se concentre de plus en plus sur le rôle des canaux ioniques dans le développement tumoral, les ayant identifiés comme des régulateurs essentiels dans divers cancers. En particulier, le canal potassique activé par le calcium $K_{Ca}3.1$ a suscité un intérêt accru en raison de son rôle dans le microenvironnement tumoral et son potentiel en tant que cible thérapeutique.

$K_{Ca}3.1$ est impliqué dans des processus tels que la migration, l'invasion et la résistance à l'apoptose. De plus, son expression dans les PSCs le rend particulièrement pertinent dans le microenvironnement tumoral. Toutefois, les données concernant l'inhibition de $K_{Ca}3.1$ dans le PDAC restent limitées. Au vu de son expression à la fois dans les cellules cancéreuses et dans le microenvironnement tumoral, y compris dans les cellules immunitaires et endothéliales, il est complexe de prédire les effets de l'inhibition de $K_{Ca}3.1$ dans le PDAC. En outre, l'expression différentielle de $K_{Ca}3.1$ dans la membrane plasmique et dans la membrane interne mitochondriale des cellules suggère que cibler ces canaux dans des compartiments cellulaires spécifiques pourrait avoir des effets distincts.

Bien que les études *in vitro* aient fourni des informations précieuses sur $K_{Ca}3.1$, les données *in vivo* sont insuffisantes. L'objectif de cette thèse est de contribuer à combler cette lacune. Nous avons réalisé une analyse qPCR d'échantillons de patients, révélant qu'une expression élevée de $K_{Ca}3.1$ était associée à un pronostic défavorable. Cela a conduit à l'exploration de l'efficacité thérapeutique de l'inhibition de $K_{Ca}3.1$ en utilisant TRAM-34 et la maurotoxine, en monothérapies et en combinaison avec la gemcitabine dans le modèle murin KPfC (*Kras*$^{wt/LSL-G12D}$ *Tp53*$^{fl/+}$ *Pdx1-Cre*) ainsi que dans une co-culture de sphéroïdes 3D incorporant des cellules cancéreuses pancréatiques et des PSCs.

La maurotoxine a montré une efficacité supérieure à celle de TRAM-34 dans les deux modèles. *In vivo*, l'inhibition spécifique de $K_{Ca}3.1$ dans la membrane plasmique a entraîné une diminution de la taille des tumeurs sans induire de fibrose excessive. Le séquençage RNA des sphéroïdes $K_{Ca}3.1^{-/-}$ a révélé des altérations dans les voies liées à l'IFN-α/γ, à la transition épithélio-mésenchymateuse (EMT) et à la régulation du point de contrôle G2-M. L'analyse des tissus KPfC a montré que l'inhibition de $K_{Ca}3.1$ était associée à une augmentation de la mort cellulaire et à une réduction de la EMT. *In vitro*, l'inhibition de $K_{Ca}3.1$ par la maurotoxine a entraîné une diminution de la capacité d'invasion et une augmentation de la mort cellulaire dans les

sphéroïdes. Ces résultats soulignent le potentiel thérapeutique de $K_{Ca}3.1$ dans le traitement du PDAC ainsi que ses effets différentiels selon sa localisation subcellulaire : l'inhibition spécifique de la membrane plasmique a entravé la progression tumorale, tandis que l'inhibition par TRAM-34, affectant à la fois les canaux de la membrane plasmique et les canaux mitochondriaux, a produit des effets moins prononcés.

Mots-clés : Cancer du pancréas ; $K_{Ca}3.1$; Microenvironnement tumoral ; Sphéroïdes ; Migration 3D ; Fibrose.

Importance de l'étude : Cette étude approfondit la corrélation entre l'expression élevée du canal $K_{Ca}3.1$ et la survie globale réduite des patients atteints de cancer du pancréas. En combinant un modèle murin immunocompétent du PDAC, des modèles 3D de sphéroïdes et une analyse RNAseq, nous démontrons que l'inhibition de $K_{Ca}3.1$ conduit à une réduction du potentiel invasif et de la croissance tumorale, tout en favorisant la mort cellulaire. Ainsi, nous proposons que l'inhibition de $K_{Ca}3.1$ représente une option thérapeutique alternative pour le traitement du cancer du pancréas.

RÉSUMÉ SUBSTANTIEL

L'adénocarcinome canalaire pancréatique (PDAC) est la forme la plus fréquente et la plus agressive du cancer du pancréas, représentant plus de 90 % des cas diagnostiqués. Son pronostic est particulièrement préoccupant, avec un taux de survie à 5 ans ne dépassant pas 10 à 12 % (Park et al., 2021). Actuellement, le PDAC est la quatrième cause de décès par cancer dans les pays occidentaux et pourrait devenir la deuxième cause de mortalité par cancer aux États-Unis dans les années à venir (Park et al., 2021; Tirpe et al., 2024). Ce pronostic alarmant est principalement attribuable au fait que les stades précoces du PDAC sont souvent asymptomatiques, ainsi qu'à l'absence d'outils et de traitements efficaces pour un diagnostic précoce. Cette situation conduit à des diagnostics tardifs (Park et al., 2021), souvent à un stade où le cancer a déjà métastasé. De plus, le PDAC se caractérise par une forte résistance aux thérapies conventionnelles telles que la gemcitabine (Koltai et al., 2022). Ces défis mettent en lumière l'urgence de développer de nouvelles stratégies thérapeutiques.

Le développement du PDAC est étroitement lié à la physiologie et au microenvironnement spécifiques du pancréas exocrine. L'acidification intermittente du stroma pancréatique sain favorise la survie de cellules résistantes à de faibles niveaux de pH, ce qui contribue à la sélection de cellules agressives et stimule la croissance et l'invasion tumorales (Blaszczak & Swietach, 2021; S. F. Pedersen et al., 2017). Parallèlement, l'activation des cellules stellaires pancréatiques résidentes (PSC) entraîne la formation d'un stroma fibreux dense (desmoplasie). Ce stroma desmoplastique interagit avec les cellules tumorales, immunitaires et endothéliales, créant un microenvironnement complexe, hypoxique et peu vascularisé qui joue un rôle crucial dans la progression du cancer. Ce stroma peut agir comme une barrière, entravant l'administration efficace de traitements aux cellules cancéreuses (Provenzano et al., 2012; Sperb et al., 2020; Tao et al., 2021).

La recherche en oncologie met de plus en plus en lumière le rôle des canaux ioniques dans la progression tumorale. Bien que traditionnellement associés aux tissus excitables, tels que les systèmes nerveux et cardiovasculaire, les canaux ioniques ont récemment été identifiés comme des régulateurs critiques dans plusieurs cancers (incluant le PDAC). La modulation de ces canaux s'est révélée prometteuse pour induire des effets anticancéreux, soit en inhibant directement la croissance tumorale, soit en renforçant l'efficacité d'autres traitements antitumoraux existants (Kischel et al., 2019; M. Li et al., 2023) Leur implication dans des processus clés tels que la prolifération, la migration, l'invasion et la mort cellulaire suggère qu'ils pourraient ouvrir de nouvelles perspectives pour le traitement du cancer. Parmi ces canaux, les canaux potassiques ont suscité un intérêt particulier en raison de leur influence sur le microenvironnement tumoral et de leur potentiel en tant que cibles thérapeutiques.

Le canal potassique activé par le calcium $K_{Ca}3.1$ est apparu comme une cible thérapeutique potentielle en oncologie. Dans le PDAC, $K_{Ca}3.1$ est surexprimé (Kovalenko et al., 2016; Storck et al., 2017) et a été identifié comme un marqueur pronostique (S. Jiang et al., 2017). Il joue un rôle crucial dans des processus tels que la migration, l'invasion (Bonito et al., 2016), la prolifération (Jäger et al., 2004) cellulaire et la résistance à l'apoptose (Mo et al., 2022), influençant ainsi directement le comportement tumoral. Il influence la motilité des cellules cancéreuses en régulant l'homéostasie du calcium et le volume cellulaire, deux éléments essentiels au potentiel métastatique. Une expression élevée de $K_{Ca}3.1$ est associée à un pronostic défavorable et à une diminution de la survie chez les patients atteints de PDAC. De plus, $K_{Ca}3.1$ est également

fonctionnellement exprimé dans les PSCs, où il est associé à leur migration, ce qui lui confère une importance particulière dans le microenvironnement tumoral du PDAC (Storck et al., 2017). Étant donné son rôle essentiel, $K_{Ca}3.1$ se présente comme une cible thérapeutique prometteuse dans le traitement du PDAC.

Malgré son potentiel, les études sur l'inhibition de $K_{Ca}3.1$ dans le PDAC restent limitées. Son expression dans les cellules cancéreuses et le microenvironnement tumoral (y compris au sein des cellules immunitaires (Ghanshani et al., 2000; Wulff et al., 2004) et endothéliales (Pinilla et al., 2021)), complique la prédiction des effets liés à son inhibition sur la progression du PDAC (Hofschröer et al., 2021). Cette complexité est particulièrement marquée dans le contexte des cellules immunitaires. Bien que des effets bénéfiques aient été observés à la suite de l'activation de $K_{Ca}3.1$ dans d'autres types de cancer (Chimote et al., 2018), l'impact de la modulation de $K_{Ca}3.1$ sur les cellules immunitaires dans le cadre du PDAC n'a pas encore été exploré. De plus, la présence de $K_{Ca}3.1$ à la fois dans la membrane plasmique et dans la membrane interne mitochondriale des cellules du PDAC ajoute une complexité supplémentaire à la prédiction de ses effets lorsque son activité est inhibée (Kovalenko et al., 2016).

Bien que des études *in vitro* aient déjà fourni des informations importantes sur les fonctions biologiques de $K_{Ca}3.1$, il reste encore un manque de données *in vivo* sur son rôle dans le contexte du PDAC (Bachmann et al., 2022). Les modèles actuels ne tiennent souvent pas compte du microenvironnement tumoral et des interactions entre les cellules stromales, immunitaires et endothéliales, toutes cruciales pour le comportement agressif du PDAC et sa résistance au traitement. La majorité des études réalisées antérieurement se sont concentrées sur des modèles de culture cellulaire bidimensionnels (2D) en étudiant uniquement les canaux $K_{Ca}3.1$ dans la membrane plasmique de cellules cancéreuses. Par conséquent, ces études négligent le microenvironnement tridimensionnel (3D) spécifique du PDAC et le rôle des cellules non cancéreuses dans la réponse des cellules tumorales aux traitements. Ainsi, il existe un besoin urgent de nouveaux modèles *in vitro* utilisant des systèmes de co-culture 3D.

Pour combler ces lacunes, cette étude s'est penchée sur le potentiel thérapeutique de l'inhibition du canal $K_{Ca}3.1$ dans le PDAC. Une analyse par qPCR d'échantillons de patients atteint de PDAC a révélé qu'une expression élevée de $K_{Ca}3.1$ était associée à diminution significative de la survie. Cette découverte a conduit à l'exploration de l'inhibition de $K_{Ca}3.1$ à l'aide de deux inhibiteurs du canal : TRAM-34 et la maurotoxine. TRAM-34 est un inhibiteur spécifique du canal $K_{Ca}3.1$ (Wulff et al., 2000), il bloque les canaux $K_{Ca}3.1$ présents à la fois dans la membrane plasmique et les dans les mitochondries. La maurotoxine, un peptide, a été utilisée pour inhiber spécifiquement les canaux $K_{Ca}3.1$ situés à la membrane plasmique des cellules (Castle et al., 2003). Ces inhibiteurs ont été utilisés seuls ou en combinaison avec la gemcitabine, une chimiothérapie de référence dans le traitement du PDAC (Koltai et al., 2022)

Nous avons utilisé le modèle murin KPfC (*Kras$^{wt/LSL–G12D}$ Tp53$^{fl/+}$ Pdx1-Cre*) (Hingorani et al., 2003; Olive et al., 2004) et un système de co-culture sphéroïde 3D, qui reproduit le microenvironnement tumoral du PDAC en intégrant à la fois des cellules cancéreuses pancréatiques et des PSCs.

In vivo, l'inhibition spécifique de $K_{Ca}3.1$ à la membrane plasmique a conduit à une réduction de la taille des tumeurs sans provoquer de production excessive de fibrose. Des analyses mécanistiques, basées sur le séquençage de l'ARN de sphéroïdes composé de cellules cancéreuse $K_{Ca}3.1^{-/-}$ (réalisé via CRISPR) et de PSCs, ont révélé des altérations dans les voies de signalisation associées à l'IFN-α/γ, à la transition épithéliale-mésenchymateuse (EMT) et au contrôle du cycle cellulaire au stade G2-M. Ces résultats ont été confirmés par une analyse

immunohistochimique des tissus provenant du modèle murin KPfC, qui a montré qu'à la suite de l'inhibition du canal $K_{Ca}3.1$, on observait une diminution des processus liés à la transition épithélio-mésenchymateuse, avec un retour vers un phénotype épithélial, une restauration des fonctions immunitaires, ainsi qu'une augmentation de la mort cellulaire dans les tissus des souris étudiées.

Parallèlement, *in vitro*, l'inhibition du canal $K_{Ca}3.1$ à la membrane plasmique par la maurotoxine a conduit à une réduction du potentiel invasif des cellules et à une augmentation de la mortalité cellulaire dans le modèle sphéroïde 3D.

La maurotoxine a montré une efficacité supérieure à celle de TRAM-34, tant *in vitro* qu'*in vivo*. En monothérapie ou en combinaison avec la gemcitabine, elle a permis de réduire efficacement la taille des tumeurs tout en favorisant la mort cellulaire. De plus, cette association a atténué la fibrose généralement induite par la gemcitabine. Ces résultats soulignent l'importance de la localisation subcellulaire de $K_{Ca}3.1$: l'inhibition de la membrane plasmique a réduit l'invasivité tumorale, tandis que l'inhibition plus large de TRAM-34 (agissant sur la membrane plasmique et les canaux mitochondriaux), a produit des effets moins prononcés.

Ce projet de recherche offre de nouvelles perspectives sur le rôle de $K_{Ca}3.1$ dans le PDAC. Les résultats soulignent le potentiel thérapeutique de l'inhibition de $K_{Ca}3.1$, surtout lorsqu'elle est combinée à des chimiothérapies déjà établies. Les divers effets observés en fonction de la localisation de $K_{Ca}3.1$ mettent en lumière la complexité de la physiopathologie du PDAC, suggérant que le canal pourrait représenter une cible thérapeutique prometteuse pour diminuer la croissance tumorale, favoriser l'apoptose et ralentir la progression métastatique.

Mots-clés : Cancer du pancréas ; $K_{Ca}3.1$; Microenvironnement tumoral ; Sphéroïdes ; Migration 3D ; Fibrose.

Importance de l'étude : Cette étude approfondit la corrélation entre l'expression élevée du canal $K_{Ca}3.1$ et la survie globale réduite des patients atteints de cancer du pancréas. En combinant un modèle murin immunocompétent du PDAC, des modèles 3D de sphéroïdes et une analyse RNAseq, nous démontrons que l'inhibition de $K_{Ca}3.1$ conduit à une réduction du potentiel invasif et de la croissance tumorale, tout en favorisant la mort cellulaire. Ainsi, nous proposons que l'inhibition de $K_{Ca}3.1$ représente une option thérapeutique alternative pour le traitement du cancer du pancréas.

TABLE OF CONTENT

LIST OF FIGURES

LIST OF TABLES

ABBREVIATIONS

2D: Two-dimensional

3D: Three-dimensional

a.u.: Arbitrary units

ADM: Acinar-to-Ductal Metaplasia

AP-1: Activator Protein-1

ATP: Adenosine triphosphate

B cells: B lymphocytes

BSA: Bovine serum albumin

BRCA1: Breast Cancer Type 1 Susceptibility Protein

BRCA2: Breast Cancer Type 2 Susceptibility Protein

bFGF: Basic fibroblast growth factor

Ca^{2+}: Calcium

$[Ca^{2+}]i$: intracellular Ca^{2+} concentration

$CaCl_2$: Calcium chloride

CaM: Calmodulin

CaMBD: Calmodulin-Binding Domain

CAF: Cancer-Associated Fibroblast

CASP8: Caspase-8

CaV: Voltage-gated calcium channel

CCL20: Chemokine (C-C motif) ligand 20

CD47: Cluster of Differentiation 47

CD69: Cluster of Differentiation 69

CDKN2A: Cyclin Dependent Kinase Inhibitor 2A

cDNA: Complementary DNA

Cl^-: Chloride

CPM: Counts per million

CXCL5: Chemokine (C-X-C motif) ligand 5

CXCL-1: C-X-C Motif Chemokine Ligand 1

CXCR2: C-X-C Chemokine Receptor 2

DAB: 3,3'-Diaminobenzidine

DDR: Discoidin Domain Receptors

dNTP: Deoxynucleotide triphosphate

dNTPs: Deoxynucleotide triphosphates

DNA: Deoxyribonucleic acid

E-cadherin: Epithelial cadherin

E. coli: Escherichia coli

ECM: Extracellular Matrix

EGA: European Genome-phenome Archive

EGFR: Epidermal growth factor receptor

EMT: Epithelial-to-Mesenchymal Transition

ERK: Extracellular signal-regulated kinase

FAK: Focal Adhesion Kinase

FCS: Fetal calf serum

FDR: False discovery rate

Fgsea: Fast Gene Set Enrichment Analysis

FOLFIRINOX: A chemotherapy regimen consisting of 5-fluorouracil, leucovorin, irinotecan, and oxaliplatin

GABRP: Gamma-aminobutyric acid receptor subunit pi

GAPDH: Glyceraldehyde-3-phosphate dehydrogenase

GEM: Gemcitabine

GEO: Gene Expression Omnibus

GSEA: Gene Set Enrichment Analysis

gRNA: Guide RNA

H&E: Hematoxylin and eosin

H_2O_2: Hydrogen peroxide

HCO_3^-: Bicarbonate

hENT1 - Human Equilibrative Nucleoside Transporter 1

HEPES: 4-(2-hydroxyethyl)-1-piperazineethanesulfonic acid

HISAT2: Hierarchical Indexing for Spliced Transcript Alignment

HRP: Horseradish peroxidase

iCAFs - Inflammatory Cancer-Associated Fibroblasts

IFI35: Interferon-induced 35 kDa protein

IFN-α: Interferon-alpha

IFN-γ: Interferon-gamma

IHC: Immunohistochemistry

IK: Potassium Intermediate/Small Conductance Calcium-Activated Channel, Subfamily N, Member 4

IL-4R: Interleukin 4 receptor

IL-6: Interleukin 6

IL-8: Interleukin 8

IP3: Inositol trisphosphate

IPMNs: Intraductal Papillary Mucinous Neoplasms

IPTG: Isopropyl-β-D-1-thiogalactopyranosid

IRF2: Interferon regulatory factor 2

IVCs: Individually ventilated cages

JNK: c-Jun N-terminal kinase

K^+: Potassium

K_{2P}: Two-Pore Domain Potassium Channels

K-BAPTA: Potassium salt of 1,2-bis(o-aminophenoxy)ethane-N,N,N',N'-tetraacetic acid

K_{Ca}: Calcium-Activated Potassium Channels

$K_{Ca}3.1$: Potassium Intermediate/Small Conductance Calcium-Activated Channel, Subfamily N, Member 4

KCl: Potassium chloride

K_{ir}: Inwardly Rectifying Potassium Channels

KPfC: *Kras*$^{wt/LSL-G12D}$ *Tp53*$^{fl/+}$ *Pdx1-Cre*$^{+}$

KRAS: Kirsten Rat Sarcoma Viral Oncogene Homolog

K_v: Voltage-Gated Potassium Channels

LANUV: Landesamt für Natur, Umwelt und Verbraucherschutz

LSL: Lox-STOP-Lox

MAPK: Mitogen-Activated Protein Kinase

Miglyol-812: Medium-chain triglyceride oil

MTX: Maurotoxin

Mg-ATP: Magnesium adenosine triphosphate

$MgCl_2$: Magnesium chloride

MDSCs: Myeloid-Derived Suppressor Cells

myCAFs - Myofibroblastic Cancer-Associated Fibroblasts

Na-BAPTA: Sodium salt of 1,2-bis(o-aminophenoxy)ethane-N,N,N',N'-tetraacetic acid

NaCl: Sodium chloride

N-cadherin: Neural cadherin

NaGTP: Sodium guanosine triphosphate

NaPi: Sodium phosphate

NDPK-B: Nucleoside Diphosphate Kinase-B

NF-κB: Nuclear factor kappa-light-chain-enhancer of activated B cells

NK cells: Natural killer cells

NSCLC: Non-small cell lung cancer

PALB2: Partner and Localizer of BRCA2

PanINs: Pancreatic Intraepithelial Neoplasias

PBS: Phosphate-buffered saline

PDAC: Pancreatic Ductal Adenocarcinoma

PFA: Paraformaldehyde

PI3K-AKT - Phosphoinositide 3-Kinase - AKT signaling pathway

PKA: Protein Kinase A

PKC: Protein Kinase C

PLC: Phospholipase C

PSCs: Pancreatic Stellate Cells

RNA: Ribonucleic acid

RNAseq: RNA sequencing

ROS: Reactive oxygen species

RRID: Research Resource Identifier

RRM1: Ribonucleotide Reductase M1 Subunit

RT-qPCR: Reverse transcription quantitative polymerase chain reaction

SBRT: Stereotactic Body Radiation Therapy

SEM: Standard error of the mean

SLC1A4: Solute Carrier Family 1 Member 4

SMAD4: Mothers Against Decapentaplegic Homolog 4

STAT3: Signal transducer and activator of transcription 3

T cells: T lymphocytes

TAMs: Tumor-associated macrophages

TCGA: The Cancer Genome Atlas

TGF-β: Transforming Growth Factor Beta

TGF-β1: Transforming Growth Factor Beta 1

TME: Tumor Microenvironment

TP53 - Tumor Protein p53

TRAFD1: TNF receptor-associated factor domain-containing protein 1

TRP: Transient Receptor Potential

TRPC3: Transient receptor potential cation channel, subfamily C, member 3

TUNEL: Terminal deoxynucleotidyl transferase dUTP nick end labeling

U.S.: United States

VEGF: Vascular endothelial growth factor

VitC: Vitamin C

WT: Wild-Type

INTRODUCTION

Pancreatic ductal adenocarcinoma

The pancreas is a soft, elongated organ, located in the upper abdomen, between the stomach and the spine. It consists of several important cell types: acinar cells responsible for producing digestive enzymes, ductal cells that release bicarbonate, endocrine cells within islets that secrete hormones, and relatively dormant stellate cells (Kleeff et al., 2016). Pancreatic cancer occurs when mutations in the DNA of pancreatic cells lead to uncontrolled cell growth, ultimately forming tumors (Hu et al., 2021).

Epidemiology of PDAC

Pancreatic ductal adenocarcinoma (PDAC) is the most common type of pancreatic cancer, accounting for more than 90% of cases (Park et al., 2021). While "pancreatic cancer" broadly refers to any malignant growth within the pancreas, PDAC specifically arises from the ductal cells that line the pancreatic ducts, where the production of digestive enzymes takes place (Kleeff et al., 2016). PDAC remains one of the deadliest and most aggressive forms of cancer with a five-year survival rate of 11% (Siegel et al., 2022). It ranks as the fourth leading cause of cancer-related death in Western countries and is anticipated to rise as the second most common cause of cancer-related mortality in the U.S. (Rahib et al., 2021). The incidence of PDAC is increasing (62,210 estimated new cases in the U.S. in 2022) (Siegel et al., 2022), at a time when many other cancers are in decline (Henley et al., 2020). This form of cancer is particularly deadly because, by the time it is detected, it has often progressed to an advanced stage and spread to other organs, limiting treatment options (Sarantis et al., 2020).

Risk factor for PDAC

Numerous risk factors, both modifiable and non-modifiable, are linked to the development of PDAC. Non-modifiable factors include elements such as age, gender, ethnicity, genetic background, ABO blood type, microbiota composition, and conditions like diabetes mellitus. In contrast, modifiable factors include lifestyle choices such as smoking, alcohol intake, an unhealthy diet, obesity, chronic pancreatitis, infections, and socioeconomic status (Hu et al., 2021).

Pathogenesis and tumor development

PDAC is largely characterized by the presence of malignant ductal cells that have undergone genetic and molecular alterations, leading to uncontrolled growth and metastatic potential. While these malignant cells are in the minority within the tumor mass, they drive the aggressiveness of the disease (Halbrook et al., 2023).

At least two pathways leading to PDAC have been recognized in the pancreas (Halbrook et al., 2023). In both, intraductal precursors evolve from low-grade to high-grade lesions, gradually accumulating cytological abnormalities and genetic mutations.

The first and most frequently observed precursor lesions are microscopic pancreatic intraepithelial neoplasias (PanINs). The pancreas is composed of various cell types, including acinar, ductal, and endocrine cells. Acinar cells are particularly known for their plasticity enabling them to respond to environmental stresses or injury by transforming into more ductal-like cells

through a process known as acinar-to-ductal metaplasia (ADM) (Orth et al., 2019). Under certain conditions, such as tissue damage or inflammation, these acinar cells can undergo ADM, acquiring characteristics similar to progenitor cells. This change, however, makes them more vulnerable to oncogenic mutations, leading to the development of PanINs (Kanda et al., 2012). PanINs are early non-invasive lesions found in the smaller pancreatic ducts and are categorized into low-grade (PanIN-1 and PanIN-2) and high-grade (PanIN-3) lesions. The stepwise progression of PanINs involves the accumulation of increasing cytological atypia and genetic mutations, gradually leading to invasive pancreatic cancer (Hu et al., 2021). Phylogenetic studies have confirmed this stepwise progression model and demonstrated that PanIN lesions are responsible for approximately 85%–90% of PDAC cases (Makohon-Moore et al., 2018).

The second pathway leading to invasive pancreatic cancer is associated with cystic precursors, such as intraductal papillary mucinous neoplasms (IPMNs). These larger macroscopic lesions develop within the main pancreatic duct or its branches. Although they contribute to only 10–15% of PDAC cases, IPMNs are significant in the disease's development (Halbrook et al., 2023).

Genomic alterations driving PDAC

PDAC is driven by a distinct set of genetic changes. The most common of these is a mutation in the *KRAS* gene (Mueller et al., 2018; Z. Zhang et al., 2023), which occurs in over 90% of PDAC cases. Mutations in the *KRAS* gene are commonly found in the majority of low-grade PanINs and IPMNs (Kanda et al., 2012). This mutation leads to the activation of the MAPK and PI3K-AKT signaling pathways, both of which are critical for initiating and sustaining abnormal cell growth. Besides *KRAS* alterations, other frequently affected genes in PDAC include *TP53* (70% of PDAC cases) (Maddalena et al., 2021), *SMAD4* (Bailey et al., 2016; Jones et al., 2008; Waddell et al., 2015), and *CDKN2A* (Klatte et al., 2023), all of which typically experience loss-of-function mutations. *TP53* mutations contribute to genomic instability, allowing tumor cells to bypass growth arrest and evade apoptosis. *CDKN2A* encodes p16, which is a key regulator of the G1/S checkpoint. The inactivation of *SMAD4*, a central player in the TGF-β signaling pathway, is also associated with a more aggressive phenotype and higher metastatic potential (Bailey et al., 2016; Jones et al., 2008; Klatte et al., 2023; Maddalena et al., 2021; Raphael et al., 2017). These changes interfere with critical cellular mechanisms, such as controlling the cell cycle and maintaining genomic stability. Furthermore, about 5–7% of PDAC patients carry inherited mutations in genes related to DNA repair such as *BRCA1*, *BRCA2*, and *PALB2* (Zhen et al., 2015).

These genetic alterations result in highly proliferative and invasive tumor cells, which can rapidly progress from pre-malignant lesions to fully invasive adenocarcinoma.

PDAC tumor microenvironment

A hallmark of PDAC is its unique and highly complex tumor microenvironment (TME) which plays a critical role in shaping the aggressive nature of the disease and its resistance to treatment. A defining feature of this microenvironment is the dense desmoplastic stroma which can constitute up to 90% of the tumor volume (Dougan, 2017). This stroma is primarily composed of cancer-associated fibroblasts (CAFs), extracellular matrix (ECM), and immune cells. This stroma not only provides structural support to the tumor but also facilitates its progression by creating a hypoxic and poorly vascularized environment that hinders the effectiveness of therapies and promotes immune evasion (Provenzano et al., 2012; Sperb et al., 2020; Tao et al., 2021) (Figure 1).

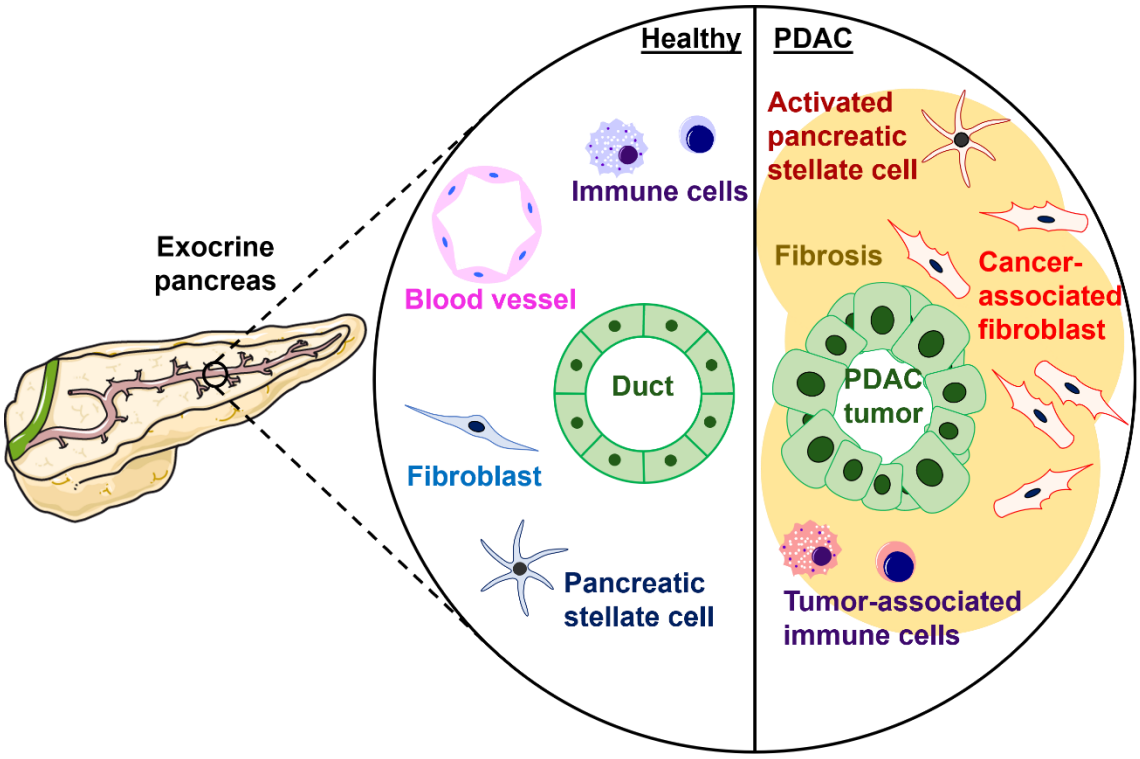

Figure 1. Schematic representation of the alteration in the microenvironment of the exocrine pancreas following PDAC development. *This figure illustrates the stark contrast between the healthy exocrine pancreas and the altered microenvironment observed in PDAC. In normal pancreatic ducts, the architecture is relatively simple, with a well-organized epithelial lining surrounded by minimal extracellular matrix components. However, in PDAC, this structure is disrupted, with a marked expansion of the desmoplastic stroma, an increase in CAFs, and dense ECM deposition following PSCs activation. These changes contribute to poor vascularization and hypoxia, creating a microenvironment that supports tumor growth and hinders effective therapeutic delivery. The immune cell population also shifts, which help the tumor evade immune detection and further promote its progression. Adapted from Soret et al., (2023).*

Cancer-associated fibroblasts and their role in PDAC

CAFs are the most abundant cells in the stroma and are primarily responsible for producing ECM components like collagen and hyaluronic acid (Provenzano et al., 2012). They originate from several sources, most notably pancreatic stellate cells (PSCs), which are typically quiescent but become activated in response to injury, inflammation, or hypoxia (Jacobetz et al., 2013; Melstrom et al., 2017). Upon activation, PSCs start producing large amounts of ECM components, including collagen, fibronectins, laminins, and hyaluronan, all of which contribute to the fibrotic, desmoplastic stroma (Jacobetz et al., 2013; Melstrom et al., 2017).

This ECM deposition drives the development of desmoplasia, a physical barrier that impedes the penetration of chemotherapeutic agents, reducing their efficacy (Jacobetz et al., 2013; Provenzano et al., 2012). Type I collagen is the most prevalent ECM protein in PDAC (Imamura et al., 1995). Beyond serving as a structural component, collagen also plays a role in signaling pathways that promote tumor cell migration, invasion, and immune suppression through interactions with receptors like discoidin domain receptors (DDRs) (Aguilera et al., 2014, 2017). Furthermore, CAFs play an active role in promoting tumor cell survival and proliferation by secreting growth factors, cytokines, and chemokines, creating a feedback loop that further

strengthens the stromal barrier and increases tumor aggression (Apte et al., 2012; G. Jin et al., 2020).

CAF populations within the stroma exhibit heterogeneity, with subtypes that have distinct functions. Myofibroblastic CAFs (myCAFs) are located close to the neoplastic cells and are involved in ECM production, while inflammatory CAFs (iCAFs) are found further away from the tumor and secrete pro-inflammatory cytokines such as IL-6 (Biffi et al., 2019; Öhlund et al., 2017). This functional heterogeneity is thought to contribute to the complexity of the PDAC microenvironment, as each CAF subtype interacts differently with tumor cells and other components of the TME (Biffi et al., 2019; Öhlund et al., 2017).

Hypoxia and its role in tumor progression

Hypoxia is a central feature of the PDAC microenvironment and is closely intertwined with desmoplasia. The dense ECM and poor vasculature within the stroma limit oxygen supply, leading to regions of hypoxia (Tao et al., 2021). Hypoxia, in turn, activates pancreatic stellate (PSCs) cells and contributes to the development of desmoplasia, creating a cycle that exacerbates tumor growth (Erkan et al., 2016; J. Li et al., 2018). Hypoxia also drives angiogenesis, but the new blood vessels formed are often dysfunctional, contributing to the persistence of the hypoxic environment. In addition to supporting tumor growth, hypoxia has been shown to play a role in immune evasion. Hypoxic conditions suppress the infiltration and activation of cytotoxic T cells within the TME, thus preventing effective anti-tumor immune responses (Daniel et al., 2019; Ene-Obong et al., 2013).

Immune evasion in PDAC

The immunosuppressive microenvironment in PDAC is another major challenge to effective treatment. This is intensified by the recruitment of immunosuppressive cells, such as myeloid-derived suppressor cells (MDSCs) and tumor-associated macrophages (TAMs), which are drawn into the tumor by chemokines such as TGF-β, IL-6, and CXCL-1 and adopt pro-tumorigenic, anti-inflammatory phenotypes (Clark et al., 2007; Mahajan et al., 2018). These immune cells contribute to the immunosuppressive environment, facilitating tumor growth and progression (Daniel et al., 2019; Ene-Obong et al., 2013) PDAC tumors are often referred to as "cold" tumors due to their low levels of immune cell infiltration, particularly of cytotoxic T cells (Hartupee et al., 2024). This lack of immune activation further reduces the effectiveness of immunotherapies. The presence of immunosuppressive cells and a dense ECM, combined with hypoxia, creates multiple layers of defense that the tumor utilizes to evade immune detection and resist treatment.

Understanding these interactions within the PDAC microenvironment, including the role of CAFs, collagen, and immune cells, is essential for developing new therapeutic strategies aimed at overcoming these barriers and improving treatment efficacy.

Metastatic Potential

PDAC tumor cells are highly invasive, with a propensity for early metastasis. Although the precise mechanisms behind metastasis in PDAC are still unclear, epithelial-to-mesenchymal transition (EMT) was identified as a key contributor (Rhim et al., 2012). The loss of adhesion molecules, such as E-cadherin, and the activation EMT pathways promote detachment from the primary tumor and migration through the ECM (Rhim et al., 2012). Tumor cells then invade the surrounding tissues, including the blood vessels and lymphatics, facilitating distant metastasis to organs like the liver and lungs. EMT is closely associated with resistance to therapy and poor prognosis, as

mesenchymal-like cells are often more resistant to apoptosis and capable of evading immune detection (Celià-Terrassa & Kang, 2024).

Challenges in treating PDAC

Treating PDAC remains highly challenging due to its aggressive nature, late-stage diagnosis, and resistance to conventional therapies. Chemotherapy and surgery are the main treatments, but only 15–20% of patients are eligible for surgery at diagnosis, as most present with advanced disease (Gillen et al., 2010; Kleeff et al., 2016; Werner et al., 2013). This often includes metastasis or involvement of critical blood vessels around the pancreas, making surgical removal ineffective or risky. Even when surgery is possible, it typically involves major operations, such as removing part of the pancreas and the duodenum, which can significantly affect digestion and metabolism. As a result, only patients in robust health can withstand and recover from the procedure (Gillen et al., 2010; Kleeff et al., 2016; Werner et al., 2013).

For the majority of patients who cannot undergo surgery, chemotherapy is the primary treatment. The combination regimens FOLFIRINOX (5-fluorouracil, leucovorin, irinotecan, and oxaliplatin) and gemcitabine with nab-paclitaxel have emerged as the first-line therapies (Conroy et al., 2011; Von Hoff et al., 2013). These treatments have shown survival benefits, but response rates are still modest. For patients whose disease progresses on first-line therapy, there are not universally accepted second-line treatments. Decisions are often based on the patient's health and the availability of clinical trials (Orth et al., 2019).

One of the biggest challenges in PDAC treatment is the high recurrence rate, even among patients who undergo surgery. Approximately 75% of patients experience disease recurrence within two years, indicating that micro-metastatic disease is often present even when the primary tumor appears localized (Groot et al., 2018). Studies suggest that tumor cells can enter the bloodstream before the primary tumor is detectable (Rhim et al., 2012), which complicates long-term disease control. To address this, adjuvant chemotherapy, typically using modified versions of FOLFIRINOX or gemcitabine-based regimens, is commonly administered after surgery to target any remaining cancer cells (Neoptolemos et al., 2017; Tempero et al., 2023).

There is also a growing use of neoadjuvant therapy, which involves administering chemotherapy or chemoradiation before surgery. This approach aims to shrink tumors, making them more manageable for surgical removal. Clinical trials have shown that patients who respond well to neoadjuvant therapy tend to have better survival outcomes. In one trial, patients who received neoadjuvant chemoradiation followed by surgery had a five-year survival rate of 20.5%, compared to 6.5% for those who underwent immediate surgery followed by adjuvant chemotherapy (Mavros et al., 2021; Versteijne et al., 2022).

Despite advancements in surgical techniques and chemotherapy regimens, PDAC remains a highly resistant cancer. Chemoresistance significantly limits the effectiveness of treatments like gemcitabine and FOLFIRINOX (Grasso et al., 2017; Manji et al., 2017). Overcoming these challenges will require a multifaceted approach that integrates earlier detection, personalized treatment plans, and novel therapies capable of addressing the resistance mechanisms of the tumor.

Overcoming Therapeutic Resistance

The resistance of PDAC cells to conventional therapies is a major obstacle. A critical focus in PDAC research is the identification of biomarkers that could predict chemoresistance. For instance, high expression levels of ribonucleotide reductase subunit M1 (RRM1) and human

equilibrative nucleoside transporter 1 (hENT1) have been associated with resistance to gemcitabine (Kurata et al., 2011; Nakahira et al., 2007; Nakano et al., 2007). However, their use in clinical practice remains limited due to inconsistent findings (Valsecchi et al., 2012).

Similarly, PDAC is highly resistant to radiotherapy, largely due to the dense and hypoxic tumor microenvironment, which reduces the effectiveness of radiation therapy (Mathews et al., 2011). To overcome this, researchers are exploring the combination of radiotherapy with radiosensitizing agents like gemcitabine or using stereotactic body radiation therapy (SBRT) to deliver higher doses of radiation to the tumor (Chang et al., 2009; Murphy et al., 2007). However, these strategies have yielded limited success, highlighting the need for new approaches to address the inherent resistance mechanisms of PDAC.

While these findings have yet to be fully integrated into clinical practice, they offer potential for tailoring based on the tumor molecular profile.

Innovative Therapeutic Approaches

Research is increasingly focused on targeting the genetic and molecular drivers of PDAC. Efforts to develop targeted therapies are increasingly focused on addressing the key genetic drivers of PDAC: *KRAS*, *CDKN2A*, *TP53*, and *SMAD4* (Raphael et al., 2017; Waddell et al., 2015). While these genes are typically viewed as "undruggable," there is ongoing research aimed at developing therapies that can target these mutations more effectively.

Targeting the TME has become a promising focus in the research for effective PDAC therapies. By disrupting the interaction between CAFs, ECM, and immune cells, the goal is to improve the delivery and efficacy of therapeutic agents. One such approach involves inhibiting focal adhesion kinase (FAK), a key regulator of CAF activation. Inhibiting FAK has shown potential in preclinical models, as it not only reduces desmoplasia but also enhances immune cell infiltration into the tumor, offering a promising target for improving immunotherapy outcomes (H. Jiang et al., 2016). Similarly, targeting cytokine and chemokine networks within the TME, particularly the CXCL-1/CXCR2, could significantly reduce the immunosuppressive environment, making immunotherapies more effective (J. Li et al., 2018).

Another innovative approach focuses on ion channels, which have gained recognition for their roles in cancer progression (Djamgoz et al., 2014; S. F. Pedersen & Stock, 2013). Ion channels regulate various cellular processes, including apoptosis and cell volume regulation, and are frequently upregulated or dysfunctional in PDAC. By modulating ion channel activity, therapeutic strategies may be able to interrupt signaling pathways crucial for tumor growth and survival (Hofschröer et al., 2021; Schnipper et al., 2020).

Ion channels in PDAC

Ion channels are membrane proteins responsible for the rapid transport of ions and fluids across cell membranes, playing a crucial role in maintaining the electrical and chemical balance within cells (Gouaux & MacKinnon, 2005; Niemeyer et al., 2001). When they open, they alter intracellular ion concentrations, setting off a variety of cellular processes, including gene expression, secretion of hormones, and intracellular signaling (Roux, 2017). Dysregulation of these processes can lead to various diseases, including cancer (Prevarskaya et al., 2018). In the context of PDAC, on channels are increasingly recognized as contributors to tumor progression, influencing the tumor microenvironment and promoting cellular invasion and metastasis (Hofschröer et al., 2021).

The exocrine pancreas relies heavily on ion channel-mediated bicarbonate secretion to regulate digestive processes (Ishiguro et al., 2012; Novak et al., 2013). In PDAC, ion channel function is disrupted, contributing to abnormal pancreatic fluid secretion and promoting tumor progression. This disruption also results in the loss of cellular polarity and adhesion, which facilitates metastasis (Coradini et al., 2011; S. F. Pedersen & Stock, 2013)

Many studies on the role of ion channels in cancer, including PDAC, highlight how targeting these channels could offer new therapeutic targets. For instance, aberrant ion channel expression has been associated with the hallmarks of cancer, such as increased proliferation, evasion of apoptosis, and enhanced metastatic potential (Djamgoz et al., 2014; Prevarskaya et al., 2018). This is particularly relevant in PDAC, where the matrix producing-PSCs have been shown to contribute to immune evasion and chemoresistance (Hessmann et al., 2020; Sperb et al., 2020; S. Wang et al., 2020). While the precise role of ion channels in the tumor microenvironment is still under investigation, there is a growing interest in exploring their potential as therapeutic targets.

Ion channels represent an attractive therapeutic target in PDAC because they are accessible on the cell surface and have been well-characterized in other diseases (Becker et al., 2014). Several ion channel-targeting drugs have already been developed for use in other conditions, such as sodium and potassium channel blockers for cardiovascular diseases (Pointer et al., 2017). These existing drugs could be repurposed for cancer therapy, reducing the time and cost associated with developing new treatments from scratch (Zheng et al., 2013). (Specifically, the $K_{Ca}3.1$ potassium channel has emerged as a potential target in PDAC, with drugs like senicapoc (a $K_{Ca}3.1$ inhibitor) showing promise in clinical trials for other diseases (Ataga et al., 2008).

In summary, ion channels are central to many cellular processes and may provide a new avenue for therapeutic intervention in PDAC. Targeting ion channels could address several aspects of PDAC pathology, including tumor cell proliferation, migration, and interactions within the tumor microenvironment. By repurposing existing drugs that modulate ion channel activity, there is potential to develop more effective treatments for PDAC, a cancer that has so far remained resistant to conventional therapies.

$K_{Ca}3.1$ channel

Potassium channels are transmembrane proteins that selectively mediate the flow of potassium ions across cell membranes according to their electrochemical gradient. Although traditionally associated with the regulation of cell excitability, many studies have highlighted their broader involvement in key cellular processes such as proliferation, migration, and angiogenesis. Importantly, their role in cancer has gained significant attention, positioning these channels as potential diagnostic markers and therapeutic targets in oncology (M. Li et al., 2023). Potassium channels are classified into four major categories based on their structure and functional mechanisms: voltage-gated potassium channels (K_v), inwardly rectifying potassium channels (K_{ir}), two-pore domain potassium channels (K_{2P}), and calcium-activated potassium channels (K_{Ca})(Vergara et al., 1998).

Among these K_{Ca}, the calcium-activated potassium channel $K_{Ca}3.1$ (SK4; IKCa; Potassium Intermediate/Small Conductance Calcium-Activated Channel, Subfamily N, Member 4) stands out due its intermediate conductance, sensitivity to intracellular Ca^{2+} levels and widespread expression across various tissues. It is one of the most extensively studied channels within this family.

The following sections will focus on the structure, regulation, and function of $K_{Ca}3.1$.

Structure

$K_{Ca}3.1$ is encoded by the *KCNN4* gene. It is a tetrameric transmembrane protein composed of four identical subunits. Each subunit consists of six transmembrane segments (S1-S6), with a pore-forming region located between the fifth (S5) and sixth (S6) transmembrane segments, which selectively allows the passage of potassium ions (K^+)(Sforna et al., 2018). The channel is regulated by its calmodulin-binding domain (CaMBD), located in the membrane-proximal C-terminal region. Upon an increase in intracellular Ca^{2+} concentration (100–350 nM), Ca^{2+}-bound calmodulin (CaM) binds to CaMBD, inducing the conformational changes required for channel activation and K^+ efflux (Fanger et al., 1999; Maylie et al., 2004; Sforna et al., 2018). Calmodulin is also crucial for the assembly and surface expression of $K_{Ca}3.1$ (Joiner et al., 2001).

Regulation

$K_{Ca}3.1$ is voltage-independent and primarily regulated by the intracellular Ca^{2+} concentration (Fanger et al., 1999). Its activity is highly sensitive to intracellular Ca^{2+}, typically within the range of 100-350 nM (Sforna et al., 2018). This allows the channel to respond quickly to changes in intracellular Ca^{2+} (Maylie et al., 2004). As K^+ exits the cell through the calmodulin-activated $K_{Ca}3.1$ channel, the membrane potential becomes hyperpolarized (Maylie et al., 2004). This hyperpolarization, in turn, enhances the electrochemical gradient for further Ca^{2+} influx, creating a feedback loop that promotes Ca^{2+} entry (Sforna et al., 2018). However, when co-expressed with voltage-gated calcium channels (Ca_V), the hyperpolarization caused by $K_{Ca}3.1$ can inhibit Ca_V-mediated Ca^{2+} entry, creating a negative feedback mechanism. $K_{Ca}3.1$ activity is also regulated by phosphorylation through various protein kinases: protein kinase A (PKA) phosphorylates the serine 334 site, decreasing channel activity by diminishing CaM binding (Gerlach et al., 2000; Wong & Schlichter, 2014). Protein kinase C has been shown to activate the channel (Wulf & Schwab, 2002), while nucleoside diphosphate kinase-B (NDPK-B) phosphorylates the histidine 358 (H358) residue, activating $K_{Ca}3.1$ by counteracting copper-mediated inhibition (Srivastava et al., 2016). Additionally, early studies suggested that $K_{Ca}3.1$ activity was decreasing in acidic environments (K. A. Pedersen et al., 2000; Strupp et al., 1993). However, recent research indicates

that while $K_{Ca}3.1$ has minimal pH sensitivity under normal conditions, intracellular acidity impairs its pharmacological (Cozzolino & Panyi, 2024).

Function

The $K_{Ca}3.1$ channel is widely expressed in various tissues, including secretory epithelial cells in the gastrointestinal tract and lungs (Todesca et al., 2021). Additionally, $K_{Ca}3.1$ is found in the immune system, in cells such as erythrocytes, lymphocytes, and macrophages, where it regulates processes such as migration, proliferation, and immune response by sustaining the necessary Ca^{2+} influx (Ghanshani et al., 2000; Schwab et al., 2012). $K_{Ca}3.1$ is also expressed in human enteric, sensory, and sympathetic neurons. In the central nervous system, the channel is expressed in the microglia where it plays a key neuroprotective role (Kshatri et al., 2018). More importantly for our study, $K_{Ca}3.1$ is also expressed in the healthy pancreas (Soret et al., 2023).

In addition to their well-established presence in the plasma membrane, there is growing evidence suggesting that $K_{Ca}3.1$ channels are also located in the inner membrane of mitochondria in certain cell types. These include cells from human colon carcinoma, cervix adenocarcinoma, non-small cell lung cancer (NSCLC) and PDAC (Kovalenko et al., 2016; Sassi et al., 2010; Todesca et al., 2024). The exact function of $K_{Ca}3.1$ in mitochondria remains a topic of ongoing research, but its localization in these organelles suggests a role in regulating mitochondrial ion homeostasis, influencing processes like cell metabolism and apoptosis, both of which are critical in cancer biology (Todesca et al., 2024).

Given its widespread expression and regulatory roles, dysregulation of $K_{Ca}3.1$ is linked to various pathological conditions. It has been implicated in neurological disorders, including ischemic stroke, Alzheimer's disease (Yi et al., 2016), and multiple sclerosis, as well as in vascular diseases like atherosclerosis and restenosis (Chou et al., 2008; Köhler et al., 2003; Sugunan et al., 2016). Additionally, $K_{Ca}3.1$ has garnered attention in cancer research, particularly PDAC, where its altered function promotes oncogenic processes such as cell migration and proliferation (Mohr et al., 2019; Soret et al., 2023).

The following sections will explore the function of the $K_{Ca}3.1$ channel in the exocrine pancreas, focusing on its physiological and pathological roles within the exocrine pancreatic tissue.

Role of the $K_{Ca}3.1$ channel in exocrine pancreatic function

The $K_{Ca}3.1$ channel was first cloned from human pancreatic tissue in 1997 by Ishii and colleagues, marking the discovery of its potential role in pancreatic physiology (Ishii et al., 1997) Since then, its expression and function in the pancreas have been investigated in numerous studies (Hayashi et al., 2012; Hayashi & Novak, 2013; Kovalenko et al., 2016; Mo et al., 2022; Nguyen & Moody, 1998; Thompson-Vest et al., 2006; J. Wang et al., 2013; Wulff & Castle, 2010). It was detected in several critical pancreatic cell types, including ductal epithelial cells, acinar cells, and pancreatic stellate cells (PSCs), all of which play vital roles in pancreatic secretion and homeostasis.

Expression and localization in the exocrine pancreas

$K_{Ca}3.1$ is expressed in both the basolateral and apical membranes of exocrine pancreas cells, particularly in acinar cells and pancreatic ductal epithelial cells (Hayashi et al., 2012). Early studies in cultured dog pancreatic ductal epithelial cells identified the presence of $K_{Ca}3.1$ in the basolateral membrane, where it was shown to participate in regulating membrane potential and ion transport (Nguyen & Moody, 1998). Subsequent research confirmed its expression in human

pancreatic tissues, with immunohistochemistry revealing its localization in intercalated and interlobular ducts as well as in acinar cells (Thompson-Vest et al., 2006). Studies in Capan-1 cells revealed that $K_{Ca}3.1$ channels are functional in both the luminal and basolateral membranes, providing the electrochemical driving force for anion (Cl^-) secretion (Hayashi et al., 2012). The inhibition of $K_{Ca}3.1$ in these cells resulted in membrane depolarization, highlighting the critical role of the channel in maintaining the membrane potential and supporting physiological pancreatic ductal secretion (Hayashi et al., 2012).

$K_{Ca}3.1$ role in Ca^{2+} signaling and ductal secretion

The exocrine pancreas secretes digestive enzymes and bicarbonate-rich fluids that are essential for digestion and neutralization of gastric acid (Sarles, 2010). Ca^{2+} signaling plays a crucial role in the regulation of the secretory activity of the pancreatic ductal epithelial cells (Jung et al., 2006). $K_{Ca}3.1$ channels are directly involved in this process: pancreatic ductal epithelial cells express $P2Y_2$ and $P2Y_{11}$ receptors, which are coupled to phospholipase C (PLC) signaling. Upon activation by extracellular ATP, these receptors stimulate the production of inositol trisphosphate (IP3), which triggers the release of Ca^{2+} from intracellular stores (Jung et al., 2006). The rise in intracellular Ca^{2+} subsequently activates $K_{Ca}3.1$. This membrane potential change enhances chloride-dependent bicarbonate (HCO_3^-) secretion. The Ca^{2+}-dependent activation of $K_{Ca}3.1$ channels also creates a feedback loop that promotes sustained Ca^{2+} entry through other Ca^{2+}-permeable channels, such as Orai and Transient Receptor Potential (TRP) channels. This sustained Ca^{2+} signaling is necessary for ongoing pancreatic secretion and the maintenance of proper ductal function (Sforna et al., 2018).

$K_{Ca}3.1$ role in the stromal cells of the pancreas

$K_{Ca}3.1$ is not only expressed in epithelial cells but also in the stromal cells of the pancreas, including pancreatic stellate cells (PSCs) (Storck et al., 2017). PSCs play a critical role in maintaining the structural integrity of the pancreas and are involved in processes such as matrix turnover, immune regulation, and exocrine secretion (Apte et al., 2012). Under physiological conditions, PSCs are quiescent; however, they become activated in response to pancreatic injury or inflammation, contributing to fibrosis and tumor progression in diseases such as pancreatic cancer (Apte et al., 2012). The role of $K_{Ca}3.1$ in healthy PSCs remains under investigation. However, in PDAC, its expression suggests it may influence the activation and function of these cells, particularly in the context of desmoplasia. Moreover, $K_{Ca}3.1$ channels are expressed in immune cells such as T- and B-lymphocytes, which are present in the pancreatic microenvironment (Ghanshani et al., 2000; Wulff et al., 2004). $K_{Ca}3.1$ in these immune cells could influence the inflammatory response and immune surveillance within the pancreas, potentially contributing to both normal pancreatic physiology and the pathogenesis of diseases such as pancreatitis and PDAC.

Limitations and Future Directions

Despite extensive research into the expression of $K_{Ca}3.1$ in various pancreatic cell types, many questions remain regarding its full physiological role in the exocrine pancreas. $K_{Ca}3.1$ plays a key role in pancreatic ductal fluid secretion by regulating the membrane potential and ion transport processes essential for bicarbonate secretion. However, a deeper understanding of how $K_{Ca}3.1$ integrates into the broader network of ion channels and signaling pathways within the pancreas is needed.

Moreover, further studies are required to clarify the precise roles of $K_{Ca}3.1$ in PSCs, particularly in the context of pancreatic diseases such as chronic pancreatitis and PDAC. PSCs are known to

contribute to the fibrotic stroma seen in PDAC, and given that $K_{Ca}3.1$ is expressed in these cells, understanding how the channel influences PSCs activation, migration, and secretion may open new therapeutic avenues for managing fibrosis and stroma-related drug resistance in pancreatic cancer (Apte et al., 2012; Mato et al., 2009; Phillips et al., 2010).

Finally, exploring the role of $K_{Ca}3.1$ in regulating Ca^{2+} homeostasis, secretory pathways, and immune interactions in the pancreas is critical for gaining insights into both normal pancreatic function and the pathophysiology of pancreatic diseases. More research is necessary to determine whether modulation of $K_{Ca}3.1$ can serve as a therapeutic strategy for enhancing pancreatic secretion in conditions like cystic fibrosis or targeting its role in fibrosis and tumor progression in diseases like PDAC.

The $K_{Ca}3.1$ channel is a crucial player in the exocrine pancreas, influencing key processes such as ion transport, secretion, and cell signaling. Its widespread expression in pancreatic ductal epithelial cells, acinar cells, and PSCs underscores its importance in maintaining pancreatic homeostasis. However, the full extent of its physiological functions, especially in the context of disease, remains to be fully explored.

Role of the $K_{Ca}3.1$ channel in PDAC

$K_{Ca}3.1$ expression in cancer

$K_{Ca}3.1$ channels are overexpressed in many types of cancers and have been implicated in several processes of the hallmarks of cancer such as tumor growth, cell migration, invasion, and metastasis (Todesca et al., 2021). Interestingly, $K_{Ca}3.1$ channels have been identified not only in the plasma membrane but also in the inner mitochondrial membrane. This mitochondrial localization suggests a role in regulating mitochondrial ion homeostasis and processes such as apoptosis and cellular metabolism (Szabo & Zoratti, 2014).

Although there is limited direct evidence of the role of $K_{Ca}3.1$ in PDAC, in lung cancer, glioblastoma, hepatocellular carcinoma, colorectal, prostate, breast, and endometrial cancers, overexpression of $K_{Ca}3.1$ correlates with poor prognosis and increased tumor aggressiveness (Mohr et al., 2019; Todesca et al., 2021). These findings offer a compelling rationale for investigating the role of $K_{Ca}3.1$ in PDAC where similar oncogenic mechanisms may be at play.

For instance, in breast cancer, high $K_{Ca}3.1$ expression in both the primary tumor and metastatic cells has been associated with increased tumor progression. In a study using transgenic breast cancer models (MMTV-PyMT$^{tg/+}$ and MMTV-cNeu$^{tg/+}$), crossing these mice with $K_{Ca}3.1$ knockout mice revealed that cancer progression was significantly slowed in the absence of the channel (Steudel et al., 2017). Furthermore, in the breast cancer mouse model MMTV-PyMT, $K_{Ca}3.1$ was shown to confer resistance to radiation therapy. Overexpression of the channel was associated with enhanced survival of breast cancer cells following radiation exposure.

Although not yet observed in PDAC, another resistance mechanism involving $K_{Ca}3.1$ has been reported in NSCLC. The inhibition of $K_{Ca}3.1$ was shown to partially overcome resistance to epidermal growth factor receptor (EGFR) tyrosine kinase inhibitors, such as erlotinib (Glaser et al., 2021; Todesca et al., 2024). Blocking $K_{Ca}3.1$ with the inhibitor senicapoc, was found to enhance cell adhesion via β1-integrin expression, impair cancer cell migration, and increase mitochondrial reactive oxygen species (ROS) production. This ultimately sensitized NSCLC cells to erlotinib, reducing cell motility and promoting apoptosis (Todesca et al., 2024). These findings

suggest that targeting $K_{Ca}3.1$ could be a viable strategy to overcome drug resistance in cancer treatments.

$K_{Ca}3.1$ expression in PDAC

The $K_{Ca}3.1$ channel is greatly overexpressed in primary pancreatic cancer samples (Jäger et al., 2004). Studies have shown that mRNA expression of $K_{Ca}3.1$ is up to 66-fold higher in PDAC tissue compared to normal pancreatic tissue (Jäger et al., 2004). This dramatic increase in expression has been confirmed through various methods, including data mining of microarrays from microdissected patient samples, which also revealed a marked overexpression of $K_{Ca}3.1$ in PDAC (Storck et al., 2017; Zaccagnino et al., 2016). The upregulation of $K_{Ca}3.1$ in PDAC is controlled by the AP-1 transcription factor and is associated with a poor prognosis (Mo et al., 2022). Patients with higher $K_{Ca}3.1$ expression have significantly poorer survival outcomes compared to those with lower expression levels (S. Jiang et al., 2017; Mo et al., 2022).

$K_{Ca}3.1$ expression is not uniform across all pancreatic cancer cell lines. Studies have found that MiaPaCa-2 and BxPC-3 cells express higher levels of $K_{Ca}3.1$ compared to PANC-1 (Jäger et al., 2004). Compared to human pancreatic ductal epithelial (HPDE) cells, MiaPaCa-2 and BxPC-3 cells display a 6- to 11-fold increase in $K_{Ca}3.1$ mRNA levels (Bonito et al., 2016). This elevated expression correlates with increased Ca^{2+}-activated K^+ currents. Consequently, in this study, the inhibition of $K_{Ca}3.1$ with blockers such as clotrimazole or TRAM-34 almost completely abolished the proliferation in BxPC-3 and MiaPaCa-2 cells, but had little to no effect on PANC-1 cells. This suggests that KCa3.1 is more functionally relevant in certain pancreatic cancer subtypes.

Recent research has shown that $K_{Ca}3.1$ is not only expressed in the plasma membrane but also in the inner mitochondrial membrane. In MiaPaCa-2 cells, mitochondrial $K_{Ca}3.1$ expression correlates with several metabolic processes, such as a reduction in oxygen consumption and ATP production upon $K_{Ca}3.1$ inhibition (Kovalenko et al., 2016). Furthermore, Todesca et al., (2024) highlighted the broader relevance of mitochondrial $K_{Ca}3.1$, showing that inhibition of this channel affects mitochondrial membrane potential, disrupts ATP production, and ultimately reduces cell viability. While this research has not yet been directly linked to PDAC, these findings highlight the importance of mitochondrial $K_{Ca}3.1$ in cancer.

Targeting $K_{Ca}3.1$ and its effect on PDAC progression

Further insights into the role of $K_{Ca}3.1$in PDAC progression come from studies using siRNA-mediated knockdown of $K_{Ca}3.1$. In MiaPaCa-2 cells, silencing $K_{Ca}3.1$ almost completely suppressed the channel activity, leading to a significant inhibition of cell proliferation and a reduction of cell migration and invasion (Bonito et al., 2016). These *in vitro* results laid the groundwork for understanding the contribution of the channel to tumor growth, migration, and invasion.

However, this study uncovered an unexpected finding: blocking $K_{Ca}3.1$ with TRAM-34 or clotrimazole increased cell migration in treated cells (Bonito et al., 2016). This paradoxical effect may be attributed to disruptions in Ca^{2+} homeostasis caused by these inhibitors, or possibly due to $K_{Ca}3.1$ expression in mitochondria. The inhibition of the mitochondrial $K_{Ca}3.1$ channel leads to a hyperpolarization of the mitochondrial membrane, which can alter mitochondrial function, including its role in Ca^{2+} storage. This may, in turn, affect the cytosolic Ca^{2+} concentration, further complicating the effects of $K_{Ca}3.1$ inhibition in cancer cells (Bonito et al., 2016).

The role of $K_{Ca}3.1$ in PDAC progression has also been investigated in *in vivo* models. Transplantation of sh$K_{Ca}3.1$ ASPC-1 cells into immunodeficient NCG mice resulted in reduced

tumor growth compared to controls. Similarly, treatment with the $K_{Ca}3.1$ inhibitor TRAM-34 also led to a reduction in tumor size in these mice (Mo et al., 2022). Additionally, $K_{Ca}3.1$ has been implicated in promoting epithelial-mesenchymal transition (EMT), with evidence suggesting that the channel influences this process via the MET/AKT signaling pathway (Mo et al., 2022). These findings further emphasize the role of $K_{Ca}3.1$ in driving the aggressive behavior of PDAC and underscore its potential as a promising therapeutic target for future treatment strategies.

$K_{Ca}3.1$ in the tumor microenvironment of PDAC

In PDAC, $K_{Ca}3.1$ channels are expressed not only in tumor cells but also in stromal cells, including PSCs, immune cells, and endothelial cells (Soret et al., 2023).

Role of $K_{Ca}3.1$ channels in pancreatic stellate cells

While the precise role of $K_{Ca}3.1$ channels in PDAC-associated fibrosis is still under investigation, emerging evidence suggested that these channels contribute to PSCs activation and migratory behavior (Storck et al., 2017).

$K_{Ca}3.1$ channels were shown to be functionally expressed in pancreatic stellate cells (PSCs) through Western blot, immunofluorescence staining, and patch clamp analyses (Storck et al., 2017). The activation of PSCs by pancreatic cancer cells was described in co-culture studies where supernatants from PDAC cell lines such as PANC-1 and Colo357 were applied to PSCs. These supernatants induced significant PSC migration, a process that was effectively reversed by targeting $K_{Ca}3.1$ channels with the selective inhibitor TRAM-34 (Storck et al., 2017). The study also suggests that $K_{Ca}3.1$ channels play an indirect role in regulating intracellular Ca^{2+} concentration ($[Ca^{2+}]_i$) in PSCs by maintaining a hyperpolarized membrane potential. This hyperpolarization provides the driving force for Ca^{2+} entry through the TRPC3 channel, which is crucial for PSC activation and function (Storck et al., 2017). By facilitating TRPC3-mediated Ca^{2+} entry, $K_{Ca}3.1$ channels contribute to the signaling pathways that support PSC activation.

Another critical role of PSCs in PDAC is their involvement in immune evasion. PSCs have been shown to reduce the infiltration of cytotoxic T cells into tumors, thereby contributing to an immunosuppressive microenvironment (Garg et al., 2018) Further investigation is required to determine whether $K_{Ca}3.1$ regulation in PSCs contributes to shaping the immune environment within PDAC tumors.

Involvement of $K_{Ca}3.1$ channels in immune regulation in PDAC

$K_{Ca}3.1$ channels are also found in various immune cells within the PDAC microenvironment, including macrophages (Xu et al., 2017), neutrophils (Henríquez et al., 2016), natural killer cells (Koshy et al., 2013) as well as in T-lymphocytes (Ghanshani et al., 2000), regulatory-T cells (Estes et al., 2008) and B-lymphocytes (Wulff et al., 2004). Moreover, $K_{Ca}3.1$ channels are implicated in immune evasion mechanisms: PDAC cells secrete immunomodulatory agents that contribute to an immunosuppressive microenvironment, promoting tumor progression and invasiveness (S. H. Jiang et al., 2019). For instance, $K_{Ca}3.1$ interacts with the gamma-aminobutyric acid receptor subunit pi (GABRP) to activate the Ca^{2+}/NF-κB/CXCL5-CCL20 axis, promoting macrophage infiltration, which is linked to poor prognosis in PDAC (S. H. Jiang et al., 2019). Moreover, blocking $K_{Ca}3.1$ with TRAM-34 in tumor-associated macrophages (TAMs) has been shown to attenuate their pro-tumorigenic activity by reducing the release of cytokines such as IL-6 and IL-8 (Xu et al., 2017).

Given that $K_{Ca}3.1$ is expressed in a wide range of immune cells, understanding the full impact of channel modulation is complex (Hofschröer et al., 2021). More research is required to elucidate how targeting $K_{Ca}3.1$ influences the immune landscape in PDAC.

Role of $K_{Ca}3.1$ channels in tumor angiogenesis

Although $K_{Ca}3.1$ has not yet been directly associated with tumor angiogenesis in PDAC, several studies hint at its role in vascular processes. $K_{Ca}3.1$ was found in the vasculature of clear cell renal cell carcinoma (Rabjerg et al., 2015) and shows increased expression in the endothelium of tumor-adjacent mesenteric arteries in colorectal tumors (Köhler et al., 2000). In human umbilical vein endothelial cells and human microvascular endothelial cells factors such as basic fibroblast growth factor (bFGF) and vascular endothelial growth factor (VEGF) have been shown to promote $K_{Ca}3.1$ expression, promoting angiogenesis (Grgic et al., 2005). However, it remains unclear whether the hypovascularity seen in the microenvironment of PDAC is related to $K_{Ca}3.1$. The potential benefits of targeting tumor vasculature still require further clinical validation (Hosein et al., 2020).

Role of $K_{Ca}3.1$ in cell death

$K_{Ca}3.1$ channels play a role in apoptosis in various cancer types particularly by regulating apoptotic volume decrease. For example, inhibiting $K_{Ca}3.1$ channels in glioma cells (D54-MG) was shown to impair staurosporine-induced apoptosis (McFerrin et al., 2012). $K_{Ca}3.1$ is expressed in the mitochondria of PDAC cell lines, such as MiaPaCa-2. This suggests that that it may contribute to mitochondrial-dependent apoptosis in PDAC, though this is yet to be fully explored (Kovalenko et al., 2016). Knockdown of $K_{Ca}3.1$ in PDAC cells like ASPC-1 and PANC-1 increased apoptosis and induced cell cycle arrest in the S phase (Mo et al., 2022). Additionally, Todesca et al., (2024) showed in NSCLC that mitochondrial $K_{Ca}3.1$ is crucial in maintaining mitochondrial function and cell survival, further suggesting its involvement in apoptosis resistance in PDAC. Interestingly, the role of $K_{Ca}3.1$ in apoptosis resistance is not limited to PDAC. In insulinoma, an endocrine pancreatic tumor, $K_{Ca}3.1$ inhibition increasded apoptosis by inactivating the JNK/ERK signaling pathway (Karatug Kacar, 2020). This reinforces the idea that $K_{Ca}3.1$ plays a broader role in modulating apoptosis resistance across various tumor types.

Targeting $K_{Ca}3.1$ channels in PDAC

$K_{Ca}3.1$ channel blockers

The $K_{Ca}3.1$ channel has emerged as a promising therapeutic target in various cancers, including PDAC. Several inhibitors of $K_{Ca}3.1$ have demonstrated potential in preclinical models, with the most prominent being clotrimazole, TRAM-34, and senicapoc (Brown et al., 2018).

Clotrimazole was initially developed as an antifungal agent and was later identified as a $K_{Ca}3.1$ inhibitor. However, its clinical application has been limited by considerable toxicity. In response to these concerns, TRAM-34, a derivative of clotrimazole, was engineered to reduce toxicity while providing selective inhibition of $K_{Ca}3.1$. This compound binds to the inner pore of the channel and has become an important tool for studying $K_{Ca}3.1$ functions in both physiological and pathological conditions (Wulff et al., 2000).

Senicapoc, another clotrimazole-based inhibitor, functions similarly to TRAM-34 by blocking $K_{Ca}3.1$ channels (Stocker et al., 2003). Initially developed for the treatment of sickle cell disease, senicapoc has demonstrated safety in human trials, including a phase III clinical trial (Ataga et al.,

2008). Given its favorable safety profile, repurposing senicapoc for other $K_{Ca}3.1$-related diseases, such as Alzheimer's disease and stroke, is currently being explored (L. W. Jin et al., 2019; Staal et al., 2017). Among these inhibitors, TRAM-34 and senicapoc have shown considerable promise in targeting $K_{Ca}3.1$ in cancer.

Maurotoxin is another inhibitor of $K_{Ca}3.1$, originally isolated from *Scorpio maurus palmatus* venom. Maurotoxin selectively targets plasma membrane-bound $K_{Ca}3.1$ channels, unlike TRAM-34 and senicapoc, which also affect mitochondrial channels (Todesca et al., 2024). This specificity offers a more controlled inhibition, but recent studies suggest limited clinical efficacy.

$K_{Ca}3.1$ as a therapeutic target in PDAC

The broad expression of $K_{Ca}3.1$ channels in PDAC, not only in cancer cells but also in the surrounding tumor microenvironment, complicates predictions about the overall therapeutic effect of $K_{Ca}3.1$ inhibition. $K_{Ca}3.1$ is expressed in various cell types, including pancreatic stellate cells (PSCs), immune cells, and vascular cells, each contributing to the progression of PDAC (Soret et al., 2023). Consequently, the effects of $K_{Ca}3.1$ inhibition on the complex interactions within the tumor microenvironment are not fully understood (Mo et al., 2022). While inhibiting $K_{Ca}3.1$ has been shown to reduce the aggressive behavior of PDAC cells and dampen PSCs activation, these benefits must be balanced against potential drawbacks. Targeting the channel could suppress immune responses which may have unintended consequences for tumor control.

$K_{Ca}3.1$ inhibitors have demonstrated positive effects in heterotopic xenograft models of PDAC using immunodeficient mice. However, the absence of functional T, B, and NK cells in these models complicates the assessment of how $K_{Ca}3.1$ inhibitors would affect immune surveillance and tumor-immune interactions in human patients (Mo et al., 2022). Given these uncertainties, further research is essential to fully understand the implications of $K_{Ca}3.1$ targeting in PDAC.

Additionally, the subcellular localization of $K_{Ca}3.1$ in both plasma membranes and mitochondria adds to the complexity of the targeting strategies. Recent studies emphasize that mitochondrial $K_{Ca}3.1$ plays a critical role in cancer cell survival by regulating mitochondrial metabolism and ATP production Todesca et al., (2024) highlighted that inhibiting mitochondrial $K_{Ca}3.1$ channels with senicapoc induced significant cancer cell death in NSCLC models, whereas plasma membrane-targeting agents like maurotoxin had minimal impact. These findings suggest that selectively targeting mitochondrial $K_{Ca}3.1$ could be a more effective approach for treating cancers such as PDAC, where both mitochondrial and plasma membrane $K_{Ca}3.1$ are expressed (Kovalenko et al., 2016).

Figure 2 illustrates the inhibitory mechanisms of maurotoxin and TRAM-34 on $K_{Ca}3.1$ channels.

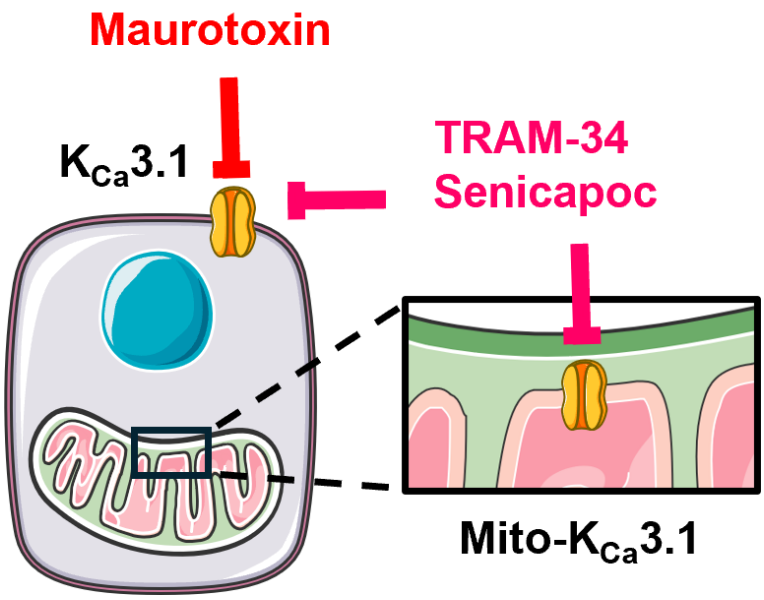

Figure 2. Schematic representation of the inhibitory mechanisms of maurotoxin, TRAM-34 and senicapoc. *Maurotoxin selectively inhibits $K_{Ca}3.1$ channels located in the plasma membrane, without impacting mitochondrial $K_{Ca}3.1$ (Mito-$K_{Ca}3.1$), whereas TRAM-34 and senicpoc effectively targets both plasma membrane and mitochondrial $K_{Ca}3.1$ channels. The figure includes elements created using Servier Medical Art, licensed under Creative Commons Attribution 3.0 unported.*

In summary, $K_{Ca}3.1$ channels have emerged as a promising therapeutic target in PDAC, offering potential for modulating cancer progression and the tumor microenvironment. However, the complexities of the role of $K_{Ca}3.1$ in PDAC, particularly its expression in various cell types and subcellular locations, underscore the need for further research.

PROJECT AIM

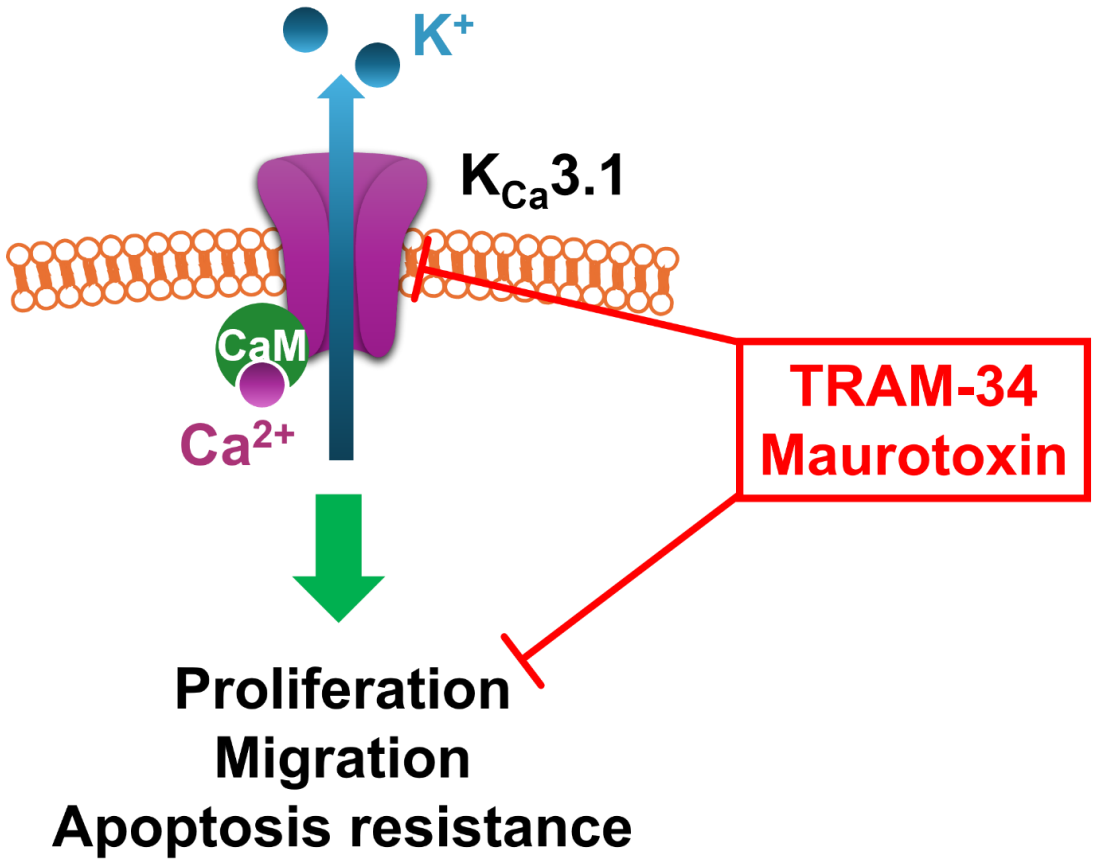

Figure 3. Targeting $K_{Ca}3.1$ in PDAC. *Schematic representation of the expected effects of $K_{Ca}3.1$ targeting in PDAC. $K_{Ca}3.1$ is associated with cell proliferation, migration, and apoptosis resistance. Thus, we asked whether $K_{Ca}3.1$ inhibition can impact these processes. The figure includes elements created using Servier Medical Art, licensed under Creative Commons Attribution 3.0 unported.*

PDAC is one of the deadliest forms of cancer, with poor survival rates, aggressive tumor biology, and resistance to conventional therapies. There is an urgent need to explore novel therapeutic strategies in PDAC progression. Emerging research indicates that ion channels, particularly potassium channels like $K_{Ca}3.1$, play a significant role in tumorigenesis by regulating key processes such as cell proliferation, migration, and survival. In PDAC, $K_{Ca}3.1$ is not only overexpressed in cancer cells but also in stromal components, including PSCs, immune cells, and endothelial cells, suggesting that this channel is intricately involved in the cancer progression of PDAC.

The primary aim of this project is to explore the therapeutic potential of targeting $K_{Ca}3.1$ in PDAC (Figure 3), with a specific focus on its role in cancer progression both within tumor cells and the surrounding stromal cells, particularly PSCs. This project evaluates the efficacy of selective $K_{Ca}3.1$ inhibitors, including TRAM-34 and maurotoxin, both as monotherapies and in combination with standard chemotherapy (e.g., gemcitabine) (Figure 4).

What distinguishes this project is its comprehensive approach to incorporating the tumor microenvironment. Unlike previous studies that relied primarily on 2D models, which fail to capture the complexity of PDAC, this project employs advanced *in vivo* and *in vitro* models. This study employs the KPfC (*Kras*$^{wt/LSL-G12D}$ *Tp53*$^{fl/+}$ *Pdx1-Cre*$^{+}$) mouse model of PDAC, which closely mirrors human PDAC. *In vitro*, this project employs advanced 3D spheroid co-culture systems that better replicate the PDAC tumor microenvironment by including both cancer cells and PSCs. This approach ensures that $K_{Ca}3.1$ is investigated within the broader context of the tumor microenvironment, capturing the intricate interactions between cancer and stromal cells.

The project examines how $K_{Ca}3.1$ inhibition impacts tumor growth, migration, invasion, and stromal remodeling. It places special emphasis on comparing the effects of maurotoxin, which specifically targets plasma membrane $K_{Ca}3.1$, with those of TRAM-34, which affects both plasma membrane and mitochondrial $K_{Ca}3.1$ channels. The research also evaluates the influence of $K_{Ca}3.1$ inhibition on immune cell infiltration and tumor-stromal interactions within these realistic models.

By taking the tumor microenvironment into account, this research aims to address critical gaps in understanding the role of $K_{Ca}3.1$ in PDAC, providing important insights into how the microenvironment influences the contribution of $K_{Ca}3.1$ to tumor progression and how its inhibition can disrupt these processes. Ultimately, this project aims to contribute to the development of more effective, targeted therapies for PDAC by leveraging ion channel modulation to inhibit tumor growth and improve patient outcomes.

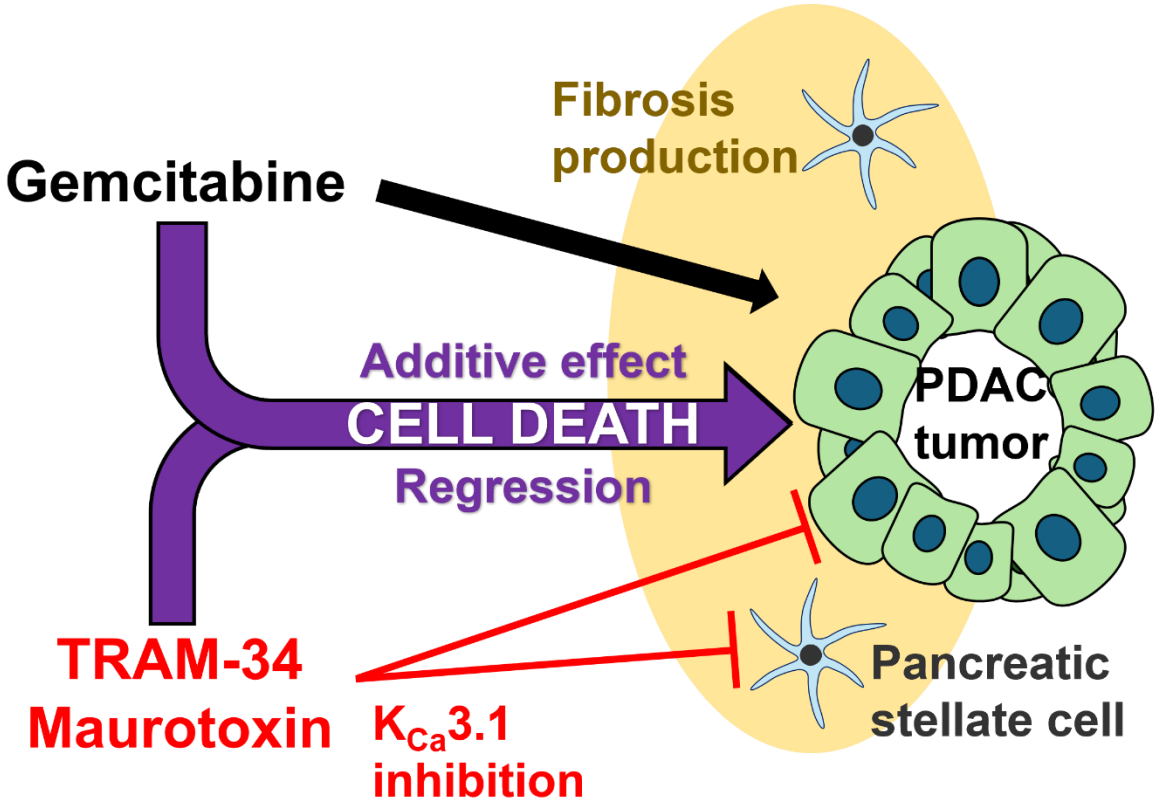

Figure 4. Combined targeting of PDAC. *Schematic representation of the expected effects of combining $K_{Ca}3.1$ inhibitors and gemcitabine in PDAC treatment. The figure includes elements created using Servier Medical Art, licensed under Creative Commons Attribution 3.0 unported.*

MATERIAL AND METHODS

Cell culture

Four cell lines were used in this study: the PDAC-derived PANC-1 (RRID: CVCL_0480; ATCC) and BxPC-3 (RRID: CVCL_0186; ATCC), the CRISPR/Cas9-mediated knockout PANC-1-$K_{Ca}3.1^{-/-}$ (PANC-1 *Kcnn4*$^{-/-}$), and the human pancreatic stellate cell line PS-1 (Froeling et al., 2009). Cells were cultured in DMEM/F12 medium (Sigma-Aldrich), supplemented with 10% fetal calf serum (FCS) superior and 1% penicillin/streptomycin. Cultures were incubated at 37°C in a humidified atmosphere containing 5% CO_2. The PANC-1-$K_{Ca}3.1^{-/-}$ cell line was generated by Cyagen Biosciences using the CRISPR/Cas9 gene-editing system, in which Cas9 and guide RNA (gRNA) vectors were co-electroporated into PANC-1 cells to achieve targeted knockout of the $K_{Ca}3.1$ gene.

Gene target	gRNA	Sequence	PAM Sequence
KCNN4	gRNA-B1	GGCGCGTGGCGCTGACCGGG	CGG
KCNN4	gRNA-B2	CAAGCGTGAGGCCGAGCAGC	AGG

Table 1. Guide RNA sequences targeting the Kcnn4 gene for CRISPR/Cas9

Individual clones were genotyped through PCR and DNA sequencing.

Type	Primer	Sequence
PCR primers	Forward	GTTCACTGTGTATCCTTAGCACATAG
	Reverse	GGCAACCAGGATCTAGTTCCAAT
Sequencing primers	Forward	AAGATGTCTTCCTCAAGTCC
	Reverse	GGTCAAAGTGTGAACTTTCT

Table 2. PCR and sequencing primers for genotyping of KCNN4

RNA isolation and cDNA synthesis

RNA was isolated from cultured cells using TRIzol (Life Technologies). Cells were grown in 100 mm culture dishes, lysed directly with 500 µL of TRIzol, and incubated at room temperature for 5 min. After adding 100 µL of chloroform, the samples were centrifuged at 12,000 x g at 4 °C for 15 min. The RNA-containing supernatant was mixed with 250 µL of isopropanol and centrifuged under the same conditions. The resulting pellet was washed with 70% ethanol, centrifuged again, and dissolved in RNase-free water. RNA concentrations were measured using a BioPhotometer (Eppendorf).

Complementary DNA (cDNA) was synthesized from 2 µg of RNA using SuperScript IV Reverse Transcriptase (ThermoFisher Scientific). To perform the reverse transcription, 2 µg of RNA were suspended in RNase-free water to a final volume of 13 µL, followed by the addition of 1 µL oligo(dT) primers (50 µM) and 1 µL dNTPs (10 mM). The mixture was then heated to 65 °C for 5 minutes to denature secondary structures, cooled on ice for 1 min, and left at room temperature for 5 min. The reverse transcription reaction was carried out by incubating the solution at 50 °C for 10 minutes, followed by heating to 80 °C for 10 min. The resulting cDNA was diluted with 75 µL of molecular-grade water and prepared for subsequent PCR experiments.

Quantitative real-time PCR

Data from RT-qPCR analyses were gathered from 34 PDAC patients (experiments was performed by Dr. Serena Pillozzi and her colleagues from the University of Florence), evenly split between males and females. These samples were obtained from individuals diagnosed with PDAC, without any intervention assigned within the scope of this study. The focus of the data was on $K_{Ca}3.1$ expression and its relationship with factors such as patient sex, cancer grade, tumor site, and overall survival.

RT-qPCR was carried out using Power Up SYBR Green master mix (Applied Biosystems) on a QuantStudio 3 Real-Time PCR System (Thermo Fisher Scientific). To perform the qPCR, 2 µL of each cDNA sample was combined with 10 µL of master mix, 1 µL of each forward and reverse primer (10 µM), and molecular biology-grade water to adjust the final volume to 20 µL. A negative control, consisting of water instead of cDNA, was included to ensure specificity. Specific primers for *KCNN4* (coding for $K_{Ca}3.1$ channels) and *GAPDH* were used (Table 3). The cycling conditions included an initial denaturation at 95 °C for 8 min, followed by 40 cycles of denaturation at 95 °C for 30 s, annealing at 57 °C for 30 s, and elongation at 72 °C for 30 s. Data analysis was performed using QuantStudio Design and Analysis Software (Thermo Fisher Scientific). Gene expression levels were quantified using the $2^{-\Delta Ct}$ method (Livak & Schmittgen, 2001), with *GAPDH* as the reference gene. All experiments were conducted in triplicate and repeated three times to ensure reliability and reproducibility. The primer sequences used are as follows:

Gene	Primer	Sequence
KCNN4	Forward	GGCCAAGCTTTACATGAACACGCA
	Reverse	AAAGGTGCCCAGTGGCATTAACAG
GAPDH	Forward	GAAGGTCGGTGTGAACGGA
	Reverse	GAAGATGGTGATGGGCTTCC

Table 3. Primer sequences for KCNN4 and GAPDH genes used in RT-qPCR

Animal experiments

The animal experiments conducted in this study were approved by the local authorities (Landesamt für Natur, Umwelt und Verbraucherschutz (LANUV); LANUV 81-02.04.2019.A281) and the Office of Animal Welfare of the University Clinic Münster. KPfC mice (genotype *Kras$^{wt/LSL-G12D}$ Tp53$^{fl/+}$ Pdx1-Cre^{+}*), a genetically engineered strain, were used in this study. These mice are characterized by a heterozygous loss of p53 and conditional expression of the K-Ras^{G12D} mutation from the endogenous locus in the pancreas (Hingorani et al., 2003; Olive et al., 2004). These mice were generated with a Lox-STOP-Lox (LSL) cassette, allowing for conditional expression of the K-Ras^{G12D} mutation specifically in the pancreas upon activation by Cre recombinase. Expression is driven by the Pdx1 promoter (Pdx1-Cre) which mediates recombination and excises the STOP cassette (Gannon et al., 2000).

Starting at week 20, mice were treated for 28 days with either TRAM-34 or maurotoxin, alone or in combination with gemcitabine. In the "TRAM-34" experiment, control mice received daily intraperitoneal (i.p.) injections of Miglyol-812 (caprylic/capric triglyceride, Spectrum Chemicals), while the "TRAM-34" and "TRAM-34+gemcitabine groups" were given daily i.p injections with 40mg/kg bodyweight TRAM-34 (kindly provided by Dr. H. Wulff from the University of California,

Davis) dissolved in Miglyol-812, with a total injection volume of 10ml/kg bodyweight. The dosage of TRAM-34 was derived from a previous study on a rat model of ischemia/reperfusion stroke (Chen et al., 2011). In the maurotoxin experiment, control mice received daily intraperitoneal injections of 0.9% saline, while the "maurotoxin" and "maurotoxin+gemcitabine" groups were administered maurotoxin (#STM-340, Alomone labs) at a dose of 0.139 mg/kg bodyweight, dissolved in saline, with an injection volume of 10 mL/kg. Since maurotoxin had not been previously tested in *in vivo* therapeutic studies, the dosage was adapted from a study involving margatoxin, a toxin with similar structure and function (Jang et al., 2011; Wu et al., 2020). Mice in the "gemcitabine", "TRAM-34+gemcitabine" and "maurotoxin+gemcitabine" treatment groups were administered four doses of 100 mg/kg bodyweight gemcitabine intraperitoneally (Ely Lilly) on days D_{19}, D_{22}, D_{25} and D_{28} (N=37 mice and N ≥ 3 for each group). The treatment schedule is shown in Figure 5. Equal numbers of male and female mice were distributed across the six experimental groups, although the total group sizes varied. Mice were housed in individually ventilated cages (IVCs) with access to nesting materials. Environmental conditions were kept stable, with the temperature set at 22 ± 2°C, humidity maintained at 55% ± 10%, and a 12 h light/dark cycle.

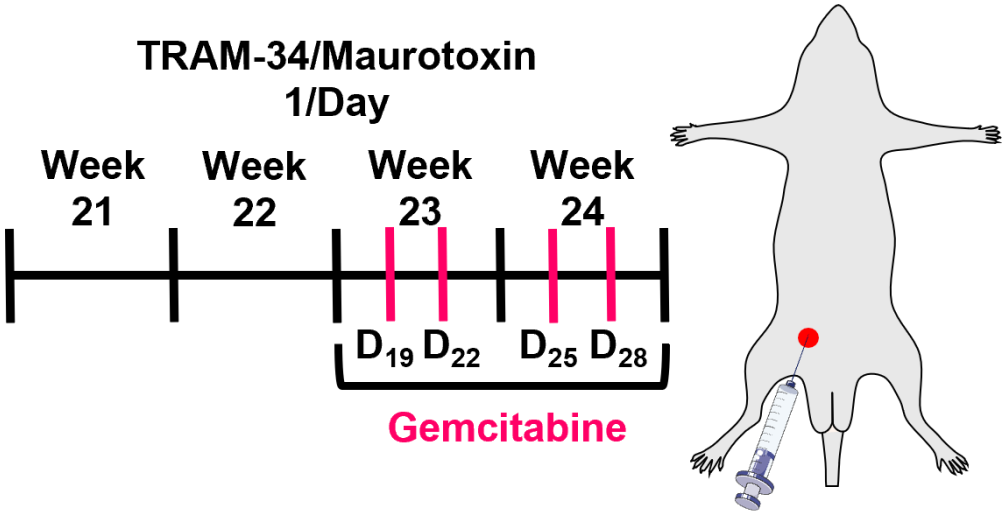

Figure 5. Schematic illustration of the 4-week treatment protocol in KPfC mice. *Twenty-week-old KPfC mice received daily intraperitoneal (i.p.) injections of either the $K_{Ca}3.1$ inhibitors TRAM-34 (40 mg/kg/day), maurotoxin (MTX) (0.139 mg/kg/day), or a vehicle control. Additionally, gemcitabine (GEM) was co-administered at a dose of 100 mg/kg via i.p. injection on days 19, 22, 25, and 28. N=38 mice; N ≥ 3 per treatment group.*

Histology and immunohistochemistry

Pancreata were initially fixed in a 4% paraformaldehyde solution and subsequently embedded in paraffin. Sections measuring 2 µm were sliced using an RM2125 microtome (Leica). The paraffin-embedded sections underwent deparaffinization with xylene, followed by a gradual rehydration process. Staining was performed with either hematoxylin/eosin or Sirius Red (Roche). Whole tissue slices were then digitally scanned using the Leica SCN400 scanner and its corresponding software (Leica). The analysis of the scanned tissue was conducted in a blinded manner using the the QuPath software (RRID: SCR_018257) (Bankhead et al., 2017). This approach ensured that the classification of the tissue slices into experimental groups occurred only after all samples had been evaluated. Hematoxylin/eosin-stained sections were carefully examined, allowing for the manual identification of each tumor node. Additionally, a pixel classifier was trained to

differentiate between fibrotic tissue positive for Sirius Red and non-fibrotic areas. This classifier was subsequently applied to all Sirius Red-stained sections, enabling the quantification of fibrosis levels within each tumor node (Figure 6). Data from the vehicle control groups in both the TRAM-34 and maurotoxin experiments were pooled, as no significant differences were found in the measured parameters, which included animal weight, tumor node number and size, as well as individual tumor node fibrosis. Similarly, data from the "gemcitabine" treatment groups were combined for analysis.

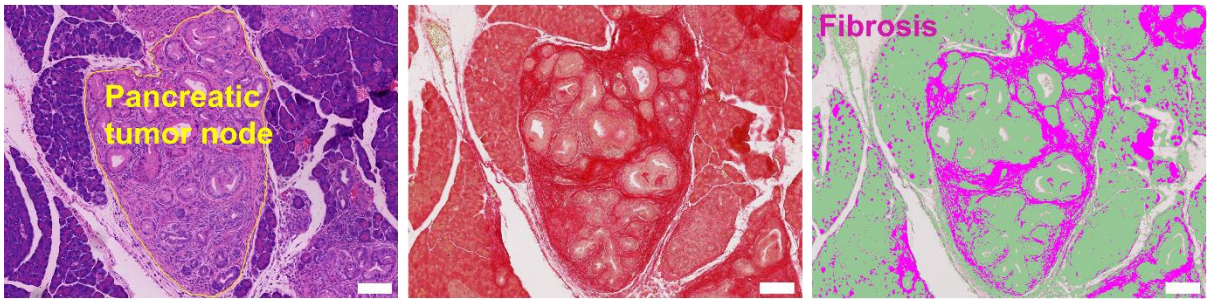

Figure 6. Analysis of immunohistochemical staining in KPfC mice. *To evaluate the tumor size, KPfC tissue section were H/E-stained and analyzed morphometrically with QuPath 0.3.1 (right panel). Fibrosis within the tissue was evaluated through Picrosirius red staining of KPfC sections (middle panel). An automated pixel classifier in QuPath 0.3.1 was employed to quantify the extent of fibrosis (left panel). Scale bar: 100 µm.*

For immunohistochemistry, following deparaffinization a 10 mM sodium citrate buffer (pH 6.0) was used for antigen retrieval. Tissue sections were heated in a steam cooker at 96°C for 30 min and then allowed to cool for 35-45 min. After cooling, the sections were washed twice with PBS. Permeabilization was achieved by treating the sections with PBS containing 1% bovine serum albumin (Sigma-Aldrich) and 0.5% Triton X-100 (Sigma-Aldrich) for 5 min, followed by two additional washes with PBS. To block endogenous peroxidase activity, the sections were incubated with 1.5% hydrogen peroxide (H_2O_2) in PBS for 15 min. The sections were then treated with Image-iT FX Signal Enhancer (Invitrogen) in a humidified chamber. Following this step, the sections were washed twice with PBS. Blocking was conducted using a solution containing 1% BSA and 0.1% Triton X-100 in PBS for 30 min, after which primary antibodies were incubated overnight in a humidified chamber at 4°C.

The primary antibody used were:

Antibody	Dilution	Supplier	Catalog number	RRID
Guinea pig anti-CK18	1:100	Progen	GP-CK18	AB_2909805
Rabbit anti-K_{Ca}3.1	1:200	Sigma-Aldrich	AV35098	AB_1852147
Rabbit anti-Ki67	1:250	Abcam	ab15580	AB_443209
Alexa Fluor 488-conjugated mouse anti-αSMA	1:600	Thermo Fisher Scientific	53-9760-82	AB_2574461
Goat anti-E-Cadherin	1:20	R&D Systems	AF748	AB_355568
Rabbit anti-N-cadherin	1:75	Proteintech	22018-1-AP	AB_2813891
Rabbit anti-CD3	1:25	Abcam	ab5690	AB_305055
Rat anti-CD8a	1:25	Thermo Fisher Scientific	14-0808-82	AB_2572861
Goat anti-PD1	1:20	R&D Systems	AF1021	AB_354541

Table 4. Primary antibodies used in immunohistochemical analysis.

Following three PBS washes, the following secondary antibodies were used:

Antibody	Dilution	Supplier	Catalog number	RRID
Cy3-conjugated donkey anti-guinea pig	1:1000	Jackson ImmunoResearch Labs	706-165-148	AB_2340460
Alexa Fluor 647-conjugated goat anti-rabbit	1:1000	Jackson ImmunoResearch Labs	111-606-047	AB_2338082
Cy3-conjugated goat anti-rabbit	1:1000	Jackson ImmunoResearch Labs	111-166-003	AB_2338007
Alexa Fluor 647-conjugated donkey anti-rat	1:1000	Abcam	ab150155	AB_2813835
Alexa Fluor 488-conjugated donkey anti-goat	1:1000	Jackson ImmunoResearch Labs	705-545-003	AB_2340428
Peroxidase-conjugated goat anti-rabbit	1:5000	Sigma-Aldrich	A0545	AB_257896

Table 5. Secondary antibodies used in immunohistochemical staining.

Ki-67-stained sections were counterstained with hematoxylin (1:200, Carl Roth) for 2 min. The slides were mounted by applying DAKO mounting medium (Agilent) with 0.001% DAPI (Sigma-Aldrich) and subsequently covered with coverslips. Within 24 hours, fluorescent images were obtained using the Nikon ECLIPSE Ti2 microscope, and the resulting images were processed using ImageJ (RRID: SCR_003070).

Protein extraction and Western blot

Total protein was extracted from cultured cells using RIPA Lysis and Extraction Buffer (Thermo Fisher Scientific), along with 1% Complete Mini Protease Inhibitor (Roche). Protein concentrations were measured with the Pierce BCA Protein Assay Kit (Thermo Fisher Scientific). The extracted proteins were mixed with a 5X SDS-PAGE Protein Loading Buffer and denatured by heating to 95 °C for 5 min. Each lane of a 10% polyacrylamide gel was loaded with 15 µg of the denatured protein, running at 80 mV. The proteins were then transferred to a PVDF membrane, which was kept at 4 °C overnight. To block nonspecific binding, the membrane was incubated for one hour in a solution of Tris-buffered saline containing 5% skim milk and 0.05% Tween. The membrane was then incubated overnight at 4 °C with the primary antibody, rabbit anti-$K_{Ca}3.1$ (1:500, Sigma-Aldrich Cat# AV35098, RRID: AB_1852147). After three washes with PBS, HRP-conjugated goat anti-rabbit (1:10,000, Sigma-Aldrich Cat# 12-348, RRID: AB_390191) was applied as the secondary antibody for one hour. The membrane underwent three additional washes before chemiluminescent detection using Clarity Max Western ECL Substrate (Bio-Rad) on the ChemiDoc Gel Imaging System (Bio-Rad). Band intensities were subsequently quantified using Image Lab software (Bio-Rad), with GAPDH (Mouse anti-GAPDH, 1:5000, Abcam Cat# ab125247, RRID: AB_11129118) used as the housekeeping control.

Immunocytochemistry

Cells were directly seeded onto glass-bottom dishes for immunocytochemistry. After washing with PBS, they were fixed with 4% paraformaldehyde (PFA) on ice for 30 minutes. The dishes were then rinsed twice with PBS, followed by permeabilization and blocking on ice for 30 min using 0.1% saponin PBS containing 10% FCS. The primary antibody against $K_{Ca}3.1$ (AV35098, 1:200, Sigma-Aldrich) was applied at 4°C for two hours. Afterwards, the cells were washed three times with PBS and incubated with Alexa 488-conjugated secondary anti-rabbit antibodies (1:500, Invitrogen) at 4°C for 30 min. Following three additional PBS washes, the cells were stained with 0.01% DAPI in 1 ml PBS. Images of the stained cells were captured within 24 h post-staining.

Spheroid formation and 3D emigration

PANC-1, BxPC-3, PANC-1-$K_{Ca}3.1^{-/-}$, PS-1, or a 50/50 mixture of cancer and PS-1 cells were suspended in a methylcellulose solution (Sigma-Aldrich) to create spheroids. Each spheroid was formed by mixing 10,000 cells with 0.31% methylcellulose in DMEM/F12 medium containing 10% FCS. The resulting cell/methylcellulose mixture was carefully placed as droplets on the inner side of a petri dish lid, which was inverted and incubated at 37°C in a humidified atmosphere with 5% CO_2 for 48 h. Spheroid formation was monitored under a microscope and confirmed by 3D visualization using the Cell3iMager Estier (SCREEN Holdings) (Figure 7).

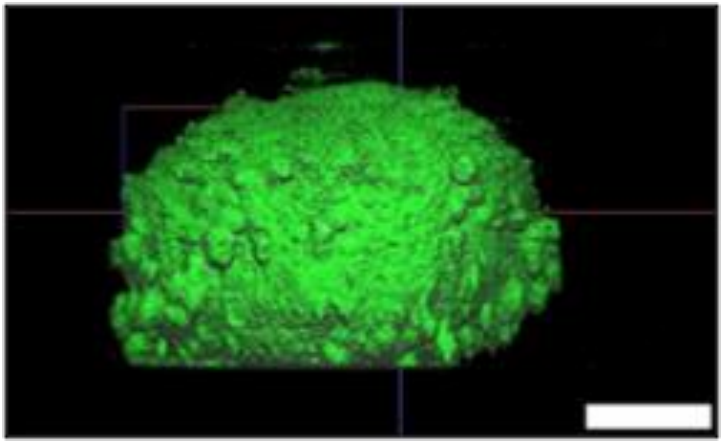

Figure 7. 3D architecture of a PANC-1/PS-1 spheroid. *Optical Coherence Tomography (OCT) image of a PANC-1/PS-1 spheroid, depicting its three-dimensional structure. Scale bar = 100 µm.*

Spheroids were embedded in a PDAC-like extracellular matrix composed of:

Matrix component	Concentration	Company
HEPES	14.9 mmol/L	-
RPMI	7.7 g/L	-
Rat tail collagen I	2,164 µg/mL	Corning
Laminin	74.4 µg/mL	Sigma-Aldrich
Fibronectin	74.4 µg/mL	Roche
Collagen III	26.8 µg/mL	BD
Collagen IV	12.1 µg/mL	Corning
pH	Adjusted to pH 7.4	-

Table 6. Composition of the PDAC-resembling extracellular matrix

The spheroid-matrix suspension was placed into 12.5 cm^2 tissue culture flasks. Spheroids were maintained in DMEM/F12 medium supplemented with 1% FCS. The experimental treatments administered to the spheroids were tailored according to the specific objectives of each experiment.

The treatment applied included: TRAM-34 (10µM), maurotoxin (20nM, Alomone Labs), gemcitabine (10µM, Ely Lilly) or their combinations. Additionally, several formulations of mitochondrial $K_{Ca}3.1$ specific inhibitors (synthesized by Christina Kick from Prof. Wünsch's working group, Department of Pharmaceutical and Medicinal Chemistry, University of Münster) were employed, including both a mitochondrially targeted-senicapoc (mito-senicapoc; WMS – 98 02) and its hydrosoluble variant (WMS – 98 03), along with a negative control (WM – 98 04) that comprised the identical mitochondrial transporter molecule (phosphonium moiety that causes the trapping of senicapoc in mitochondria) as mito-senicapoc but lacking the senicapoc component. For all three mito-senicapoc compounds, a concentration of 30 µM was utilized. Figure 8 illustrates the different mito-senicapoc compounds used in the experiments and Figure 9 shows the hydrolysis reaction of the hydrosoluble mito-senicapoc.

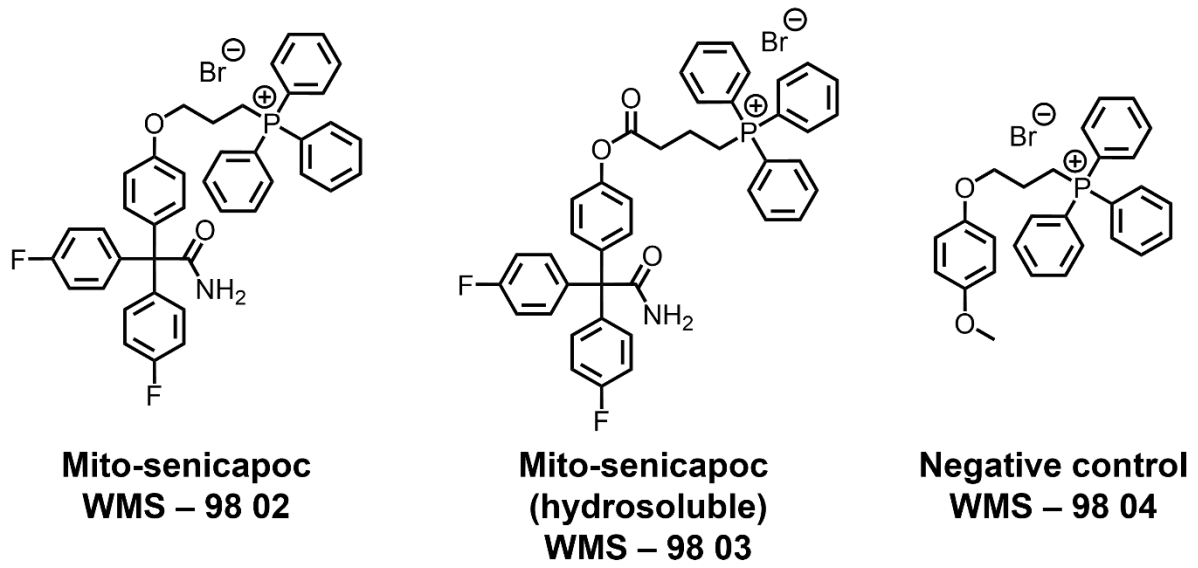

Figure 8. Chemical structures of the mitochondrial $K_{Ca}3.1$ inhibitors: mitochondrially targeted senicapoc (mito-senicapoc) and its derivatives.

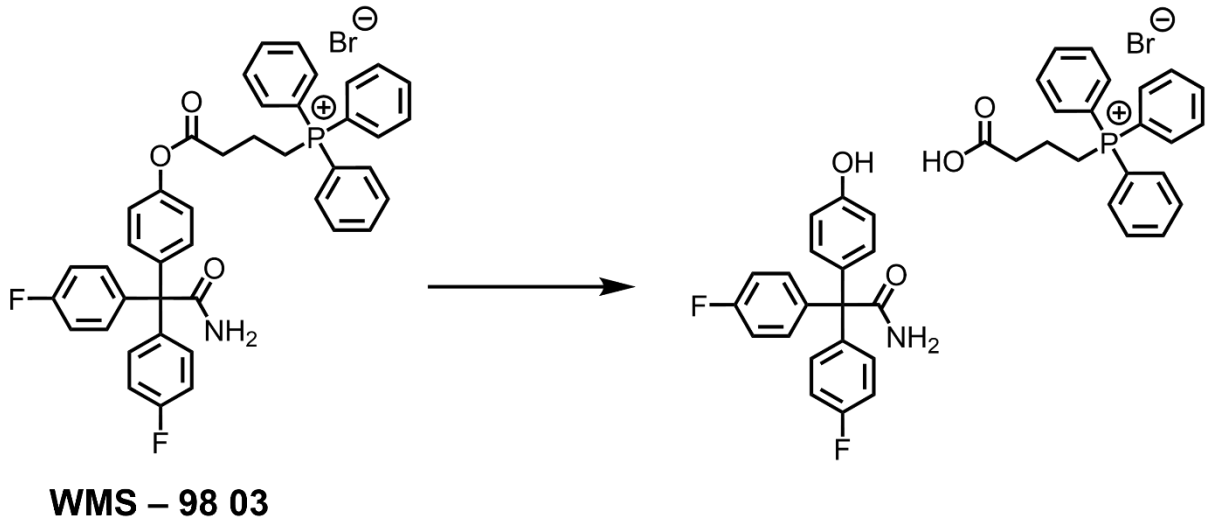

Figure 9. Hydrolysis mechanism of hydrosoluble mito-senicapoc (WMS – 98 03).

DMSO was used as the vehicle. Flasks were meticulously sealed to create an airtight environment and placed in chambers maintained at a controlled temperature of 37 °C. The emigration of cells out of the spheroids, both in the presence and absence of the inhibitors, was tracked through live-cell imaging conducted over a 48-h period using an inverted microscope (Zeiss Axiovert 40) and the MicroCamLab 3.1 software (Bresser). To assess the invasive potential of the spheroid cells, the projected area was measured over time using ImageJ software (v1.54k). The projected area of the invasive zone (in μm^2) was calculated by subtracting the initial core area of the spheroid (as described in Figure 10). The numerical values presented in the main text correspond to the size of the invasive area at t=48 h.

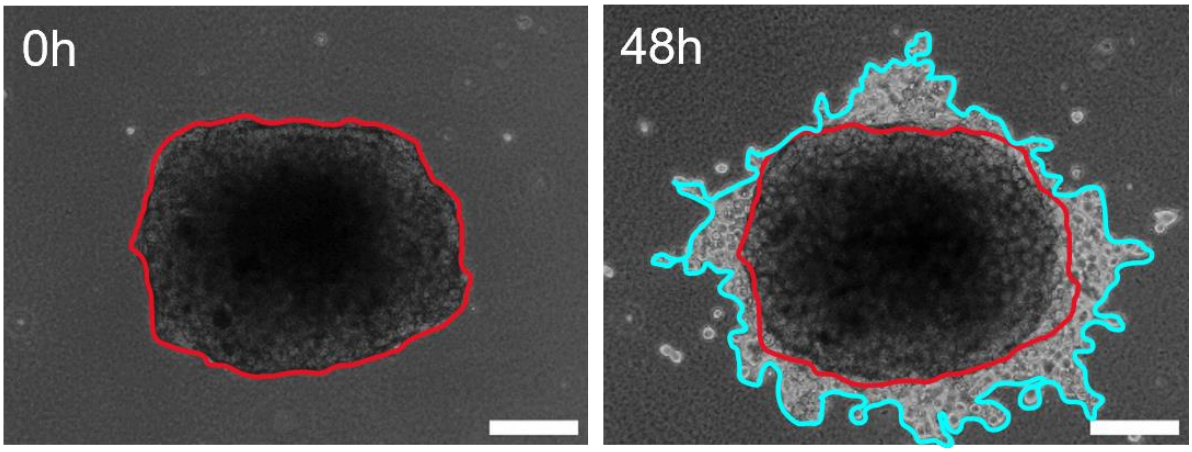

Figure 10. Quantification of the invasive potential of the spheroids. *The invasive capacity of the spheroids (here, PANC-1/PS-1) was assessed over time. The invasive zone of the spheroids was calculated by subtracting the initial area of the spheroid core (indicated in red). Scale bar=200 µm.*

mRNA-sequencing

At the end of a 3D emigration assay (as described above) (t=48 h), PANC-1/PS-1 and PANC-1-$K_{Ca}3.1^{-/-}$/PS-1 spheroids were harvested for RNA extraction. The RNA isolation process was conducted using the RNeasy Mini Kit (Qiagen), following the manufacturer's guidelines. RNA concentration and quality were measured using a NanoDrop 2000 spectrophotometer. Subsequently, RNA libraries were constructed and sequenced on Illumina Next-Seq 500 sequencing platform (High-Output Kit, 75 Cycles v2 Chemie) at the Genomics Core Facility (University Hospital Münster, Münster, Germany).

Bioinformatics analyses were performed on the the Galaxy platform (Afgan et al., 2018). Raw sequencing data in fastq format underwent alignment and mapping against the mm10 human reference genome, employing the HISAT2 algorithm v2.2.1 (RRID: SCR_015530) (D. Kim et al., 2015). Gene counts were obtained through featureCounts 2.0.1 (Liao et al., 2014), and differential gene expression analysis was done via limma 3.50.1 (Liu et al., 2015), filtering out genes with fewer than 0.5 counts per million (CPM) across at least two samples. Principal component analysis indicated consistency among biological replicates while highlighting differences among the treatments. Genes that exhibited a false discovery rate (FDR) p-value < 0.05 were considered significantly differentially expressed. These genes were subjected to further examination using gene set enrichment analysis (GSEA) with fgsea 1.8.0 (Korotkevich et al., 2021) and EGSEA 1.20.0 (Alhamdoosh et al., 2017). The RNA-Seq dataset has been made publicly accessible on the Gene Expression Omnibus under accession number GEO: GSE279207.

Matrix production assay

PS-1 or PANC-1 cells were seeded in a clear bottom black-walled 96-well plate (Thermo Fisher) at 80% confluence. The cells were maintained in DMEM/F12 medium (Sigma-Aldrich) supplemented with 0.5% FCS, vitamin C (284 µM, Sigma-Aldrich), and TGF-β1 (10 ng/mL, PeproTech) to stimulate matrix production. The cells were subsequently treated with TRAM-34 (10µM), maurotoxin (20nM),

gemcitabine (10μM) or their combinations. After 24 h, the cells were washed twice with PBS. Newly synthesized collagen I was labeled with CNA35-tdTomato (1:200, diluted in PBS) and kept at room temperature in the dark for 3 h. Fluorescence intensities were assessed using a fluorescence plate reader (Fluoroskan II), and representative images were captured using confocal microscopy (Nikon ECLIPSE Ti2 microscope). Fluorescence intensity values were blank corrected.

CNA-35-tdTomato production and purification

Competent *E. coli* BL21(DE3) bacteria (Novogen) were transformed with pET28a-tdTomato-CNA35 plasmid (Addgene plasmid #61606, RRID: Addgene_61606) following the method described by Aper et al., 2014. The bacteria were cultured in LB medium (BD Bioscience) with 10 μg/mL kanamycin until the optical density at 600 nm reached 0.6. Protein expression was then induced by adding 1 mM isopropyl-β-D-1-thiogalactopyranoside (IPTG, AppliChem PanReac) at 37°C for 20 h with continuous shaking (220 rpm). After centrifugation (4,000 g at 4°C for 20 minutes), the bacterial pellet was washed twice with 50 mM sodium phosphate (NaPi) and 300 mM sodium chloride (NaCl), pH 7.0 followed by further centrifugation (4,000 g at 4°C for 20 minutes). The pellet was then resuspended in a buffer containing lysozyme (10 mg/mL) and protease inhibitor cocktail III (Calbiochem) and incubated on ice for 30 min.

Triton X-100 (0.1%; Sigma Aldrich), DNase I (1 mg/mL; Invitrogen), RNase A (1 mg/mL; AppliChem PanReac) and 1 M $MgCl_2$ were added, followed by sonication on ice for three 60 s cycles. The cells were then lysed mechanically using a French press, and the lysate was cleared by centrifugation (12,500 g, 45 min, 4 °C).

The supernatant containing the protein was purified with nickel-nitrilotriacetic acid (Ni-NTA) agarose beads (Qiagen) according to the manufacturer's instructions. The bead-protein mixtures were incubated on ice for 60 min with continuous shaking to facilitate the binding of 6xHis-tagged CNA35-tdTomato protein to the beads. The resulting complexes were transferred into filter columns (Cytiva), washed thoroughly, and the bound proteins were then eluted with 250 mM imidazole. The eluate was concentrated using Amicon Ultra 0.5 ml 10k diafiltration filters followed by an additional washing step. The filters were inverted and centrifuged at 1,000 g for 2 min at 4°C to collect the concentrated CNA35-tdTomato protein. To ensure proper maturation of the fluorescent protein, the collected protein solution was incubated at 37°C overnight. The concentration of the purified CNA35-tdTomato (1.037 mg/mL) was measured using the BCA Protein Assay Kit (Pierce). The aliquoted protein solution was then stored at -70°C for later use.

Patch clamp recordings

Whole-cell patch-clamp technique was performed (by Mrs. Elke Nass from the University of Münster) on PANC-1 cells at room temperature, using borosilicate glass pipettes (GC150TF-10, Clark Electromedical Instruments, Pangbourne, UK) connected to an EPC-10 amplifier (HEKA Electronics, Lambrecht, Germany). Measurements were visualized and analyzed using Patch Master software (HEKA Electronics, Lambrecht, Germany). Patch-clamp recordings were performed to investigate the presence of voltage-dependent K^+ currents mediated by $K_V1.3$

channels. Cells were maintained at a holding potential of -90 mV for 2 seconds, followed by a stepwise depolarization for up to 2 seconds to +40 mV, and then returned to the holding potential. Following superfusion with maurotoxin (20 nM, Alomone Labs), the experimental protocol was repeated to assess the impact of the toxin on K^+ currents. The recording solutions were as follows: Extracellular solution (in mM): 150 NaCl, 5 KCl, 10 HEPES, 5,5 glucose, 1 $CaCl_2$ 1 $MgCl_2$; pH 7.35, osmolality 305 mOsm/kg. Intracellular solution (in mM): 10 NaCl, 10 KCl, 85 K-gluconate, 20 K_3-citrate, 10 HEPES, 3 K-BAPTA, 3 Mg-ATP, 0.5 Na-GTP, 15 phosphocreatine, 1 $MgCl_2$, 0.5 $CaCl_2$; pH 7.25, osmolality 295 mOsm/kg, respectively. Data were analyzed using Nest-o-Patch software.

Annexin-V staining

The PANC-1/PS-1 spheroids, embedded and treated as previously described, were stained with annexin-V to identify apoptotic cells after 24 h of treatment. The annexin-V staining was conducted using the Annexin V-FITC Apoptosis Detection Kit (Invitrogen), following the manufacturer's instructions. The stained spheroids were then imaged using a confocal Nikon ECLIPSE Ti2 fluorescence microscope with a 10x. A z-stack of the spheroids was acquired to encompass their entire volume. These z-stack images were subsequently merged into a single composite image using ImageJ software. To quantify the annexin V-positivity, a threshold was manually established in ImageJ based on a visual assessment of the images, allowing for the measurement of the area corresponding to green fluorescence intensity. Consistent threshold values were applied across all images to maintain uniformity in the quantification process. The percentage of annexin V-positive area was calculated by dividing the fluorescence area above the threshold by the total projected area of the spheroid.

Cell viability/cytotoxicity assay

PANC-1-PS-1 spheroids were seeded into a 96-well plate with clear bottom and black side walls (Falcon). After seeding, the treatments were applied as described in earlier sections. Cell viability and cytotoxicity were assessed using two distinct assays: the RealTime-Glo™ MT viability assay (Promega) and the CellTox™ Green cytotoxicity assay (Promega), following the manufacturer's instructions. Measurements were collected at four time points: immediately after treatment (t=0 h), and at t=24 h, t=48 h, and t=72 h.

Baseline values (in the absence of the vehicle) are referred to as "Medium," while the vehicle control (e.g., DMSO) is denoted as "Control." A background blank was also included for comparison. Detection was performed using a Promega GloMax® Discover microplate reader, enabling the multiplexing of real-time quantification of cell viability through luminescence and cell death via fluorescence. Data shown are blank adjusted. Numerical values given in the main text correspond to measurements performed at t=72h.

TUNEL assay

Following deparaffinization, the TUNEL assay was performed using the OneStep TUNEL Apoptosis Kit [Red, 555] (NBP3-12093, Novus Biologicals), in accordance with the manufacturer's protocol

for tissue section preparation. Slides were mounted using DAKO mounting medium (Agilent). Samples were imaged within 24 hours using a Nikon ECLIPSE Ti2 confocal microscope, with apoptotic cells being identified based on their characteristic perinuclear fluorescence. Image analysis was conducted using ImageJ software.

Statistical analysis

Biological replicates (N) represent the total number of mice used for *in vivo* experiments or the number of *in vitro* experiments repeated with cells from different passages. "n" indicates the number of individual data points for each experimental condition. The normality of data distribution was assessed using the D'Agostino-Pearson test. Normally distributed data are displayed as mean ± standard error of the mean (SEM), while non-normally distributed data are presented as median ± 95% confidence interval (CI). All experiments were conducted at least three times. Statistical analyses were performed with "n." For normally distributed data, 2-tailed unpaired Student's t-tests or one-way ANOVA test with Tukey's multiple comparison test was performed. In instances where data did not meet normal distribution, Mann-Whitney *U* test or nonparametric 1-way ANOVA-on-ranks (Kruskal-Wallis) statistical test with Dunn's multiple comparisons test was used. Multiple comparison tests over time were assessed using the repeated measure two-way ANOVA with Tukey's multiple comparison test. For statistical analysis and data presentation, GraphPad Prism 10 (RRID:SCR_002798) was employed. Statistical significance was established at a p-value < 0.05.

RESULTS

Elevated $K_{Ca}3.1$ expression is associated with poor survival in PDAC patients

This project aims to elucidate the molecular mechanisms by which $K_{Ca}3.1$ channels influence the progression of PDAC. The first step of our research project involved assessing the clinical relevance of $K_{Ca}3.1$. To achieve this objective, our research emphasized the acquisition and analysis of clinical data from PDAC patients. We analyzed qPCR data from PDAC patient samples to explore potential correlations between $K_{Ca}3.1$ expression and patient outcomes, particularly overall survival, along with key clinicopathological factors such as tumor grade, location, and patient sex.

To do this, we employed the Kaplan-Meier Plotter tool (Győrffy, 2024), a robust online resource for survival analysis in cancer research. This platform integrates clinical data from extensive RNA-seq datasets, allowing us to correlate how expression levels with overall survival. Drawing from data repositories such as GEO (Gene Expression Omnibus), EGA (European Genome-phenome Archive), and TCGA (The Cancer Genome Atlas). By comparing the gene expression levels of $K_{Ca}3.1$ specifically in PDAC patients, we accessed RNA-seq data from 177 individuals diagnosed with PDAC, categorized into two groups: 79 patients exhibiting high $K_{Ca}3.1$ expression and 98 with low expression. Kaplan-Meier survival analysis revealed that patients with higher $K_{Ca}3.1$ expression had significantly lower overall survival compared those with lower expression of the channels (Median survival: 15.7 months versus 23.4 months) (Figure 11).

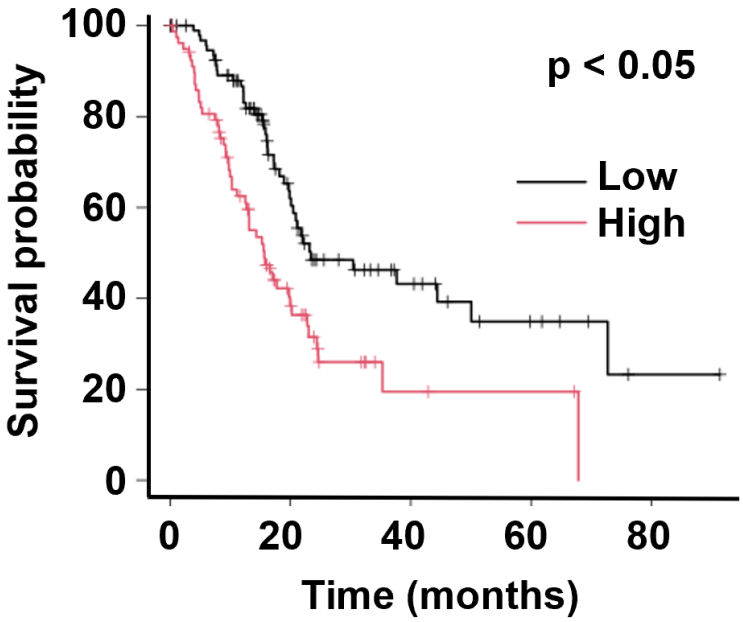

Figure 11. High $K_{Ca}3.1$ expression correlates with reduced survival in PDAC patients. *Kaplan-Meier survival analysis curve of PDAC patients according to their $K_{Ca}3.1$ expression levels.* The curve depicts the overall survival of 177 PDAC patients grouped by $K_{Ca}3.1$ expression levels, with high (N=79) and low (N=98) expression cohorts. *Data are derived from RNA-seq analyses using the Kaplan-Meier plotter tool and subsequently adapted for this study. p-value < 0.05.*

Given the compelling association between $K_{Ca}3.1$ expression and overall survival observed in the Kaplan-Meier analysis, we sought to further investigate this correlation using patient data from our collaboration partner. We analyzed RNA from PDAC samples through qPCR, focusing on $K_{Ca}3.1$ expression. 34 samples were examined and 31 showed varying degrees of $K_{Ca}3.1$ expression, emphasizing its clinical relevance in PDAC. Survival data (i.e., death status) was available for 27 of these 31 patients with measurable $K_{Ca}3.1$ expression. We used the median expression level (0.0585) as a threshold to dichotomize them into low and high $K_{Ca}3.1$ expression groups. Although the differences in survival rates between these two groups did not reach statistical significance (p=0.06), a notable trend emerged: 50% of high-expressing patients died after ~20 months compared to 50% of the low-expressing patients that survived up to ~32 months (Figure 12). While our findings were not statistically significant, this outcome could be attributed to the relatively small sample size in our study. However, the observed trends still provide valuable insights, aligning closely with the data from the Kaplan-Meier plotter database. This consistency reinforces the potential of $K_{Ca}3.1$ as a prognostic biomarker for poor survival in PDAC patients, highlighting the importance of further investigation into its role within this malignancy.

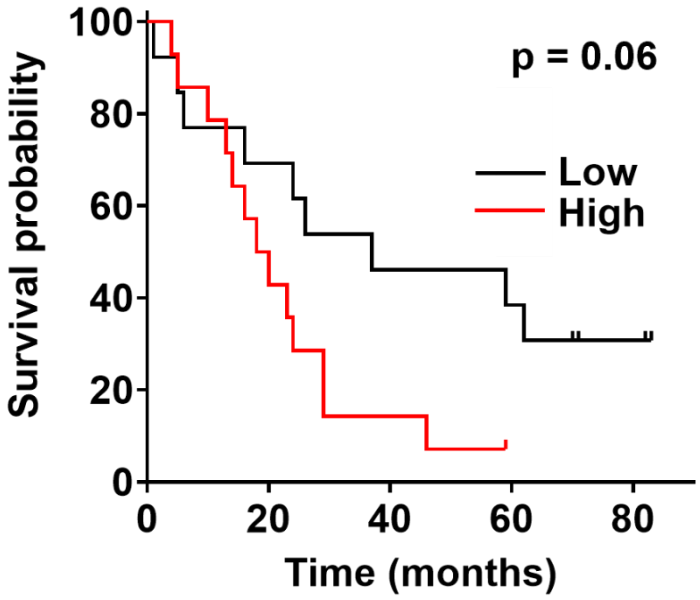

Figure 12. Survival analysis of PDAC patients dichotomized according to their $K_{Ca}3.1$ expression levels. *Kaplan-Meier curve showing the overall survival of our 27 PDAC patients. They were divided into high (n=14) and low (n=13) $K_{Ca}3.1$ expression groups based on the median expression level (0.0585). p=0.06; Statistical comparisons were performed using simple survival analysis (Kaplan-Meier).*

Continuing our investigation into key clinicopathological factors in our PDAC patient cohort, we observed no differences (p=0.45) in $K_{Ca}3.1$ expression based on gender (Female: 0.02, 95% CI, 0.01-0.18, N=16; Male: 0.05, 95% CI, 0.01-0.30, N=15) (Figure 13).

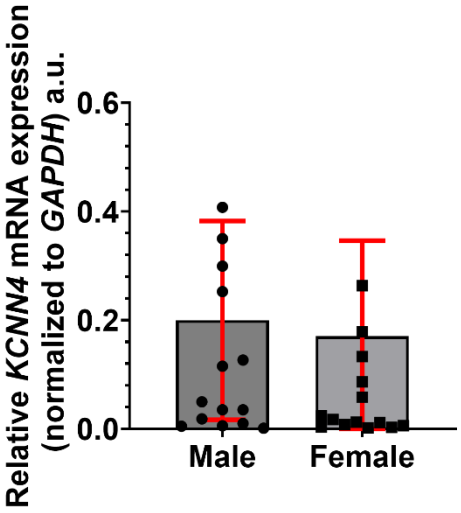

Figure 13. Comparison of $K_{Ca}3.1$ expression between male and female PDAC patients. *mRNA expression levels of KCNN4 were measured by qPCR using the $2^{-\Delta CT}$ method, with patients grouped by gender (Male: N=15; Female: N=16). GAPDH served as the housekeeping gene.*

Additionally, data on cancer grades were available for 27 patients, and while we did not find a statistically significant difference (p=0.15), there was a notable trend suggesting that patients with grade 2 PDAC exhibited higher $K_{Ca}3.1$ expression compared to those with grade 3 PDAC (Grade 2: 0.101, 95% CI, 0.006- 0.263, N=22; Grade 3: 0,017, 95% CI, 0,001- 0,300, N=7) (Figure 14).

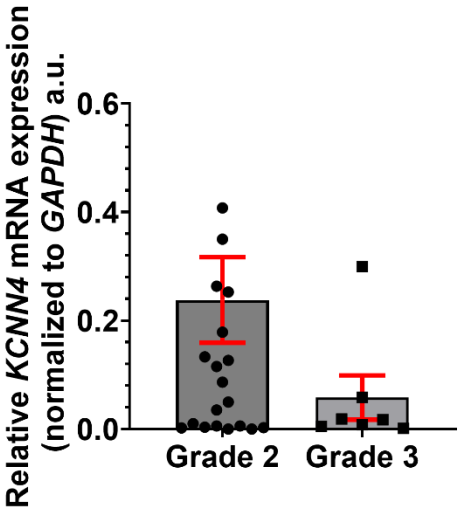

Figure 14. $K_{Ca}3.1$ Expression in grade 2 vs grade 3 PDAC patients. *mRNA expression levels of KCNN4 were assessed by qPCR using the $2^{-\Delta CT}$ method with GAPDH as the housekeeping gene. Patients were grouped by cancer grade (Grade 2: N=22; Grade 3: N=7).*

Data on tumor localization was available for 26 patients, categorizing the tumors into head, body, and tail regions of the pancreas. Notably, patients with tumors located in the tail of the pancreas showed higher $K_{Ca}3.1$ expression levels compared to those with tumors in the body (Body: 0. 010, 95% CI: 0.001-0.059, N=7; Tail: 0.263, 95% CI: 0.179-0.722, N=5) (Figure 15). This difference in expression could be linked to the fact that pancreatic tumors in the tail are often detected at more advanced stages, which may reflect a more aggressive tumor biology in this region (van Erning et al., 2018). Such a finding suggests that tumor location within the pancreas may influence the

behavior and progression of the disease, particularly in relation to $K_{Ca}3.1$ expression. However, it is important to note that our analysis did not show any differences in survival rates based on localization of the cancer within the pancreas (Figure 16).

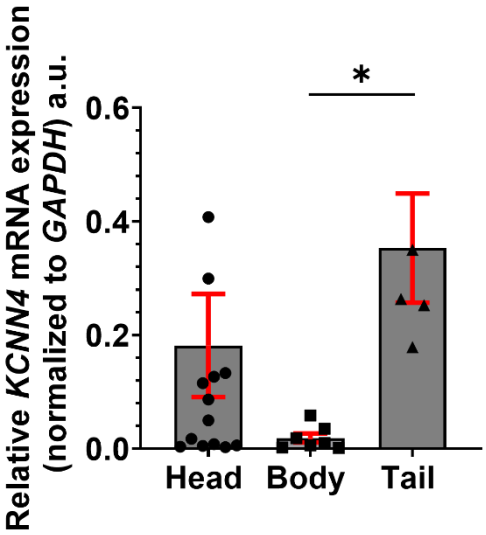

Figure 15: Patients with tumors in the tail of the pancreas show elevated $K_{Ca}3.1$ expression. *KCNN4 mRNA expression levels were analyzed using the $2^{-\Delta CT}$, with patients grouped by tumor location (Head: N=14; Body: N=7; Tail: N=5). GAPDH was used as the housekeeping gene. *p < 0.05. Statistical analysis was performed using the Kruskal-Wallis test followed by Dunn's post hoc test.*

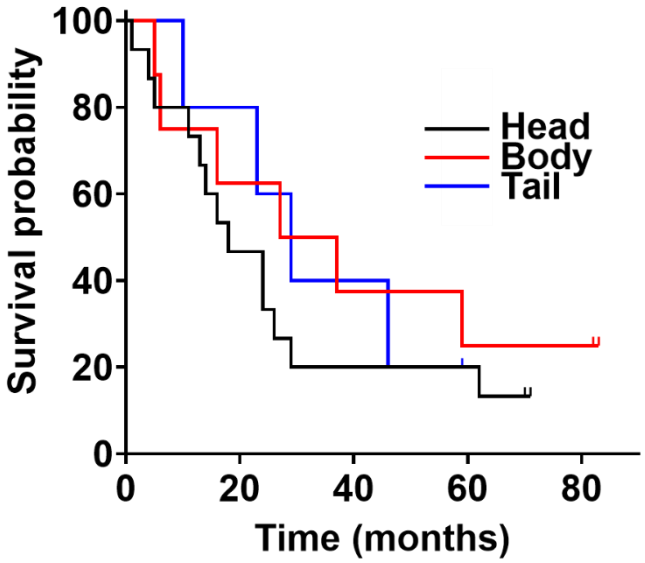

Figure 16. Kaplan-Meier survival analysis of PDAC patients based on tumor localization within the pancreas. *Overall survival of 26 PDAC patients. They were categorized by tumor location within the pancreas: Head (N=14), Body (N=7), and Tail (N=5).*

In summary, our findings reveal that elevated $K_{Ca}3.1$ expression in PDAC patients correlates with poorer overall survival which underscores the clinical relevance of $K_{Ca}3.1$ as a potential therapeutic target in PDAC.

Inhibition of plasma-membrane $K_{Ca}3.1$ decreases tumor node size and reverses gemcitabine-induced fibrosis in KPfC mice

In light of our data showing that elevated $K_{Ca}3.1$ expression correlates with poor survival outcomes in PDAC patients, we sought to evaluate the therapeutic potential of $K_{Ca}3.1$ channel blockers *in vivo*, utilizing the KPfC mouse model of PDAC. This model closely mirrors the pathophysiology, genetic characteristics, and histopathological features of human PDAC (Hingorani et al., 2003; Olive et al., 2004), providing a robust framework for assessing how inhibiting $K_{Ca}3.1$ channels can affect tumor progression and associated fibrotic responses.

Mice were treated with TRAM-34, a potent and selective inhibitor of the $K_{Ca}3.1$ channel (Wulff et al., 2000), administered either alone or in combination with gemcitabine, a standard chemotherapeutic agent commonly used in PDAC treatment (Koltai et al., 2022). This combinatory approach aims to determine if inhibiting $K_{Ca}3.1$ can enhance the effectiveness of gemcitabine, especially in a disease context characterized by its desmoplastic stroma and inherent resistance to conventional therapies. (Provenzano et al., 2012; Tao et al., 2021). Moreover, considering that $K_{Ca}3.1$ channels are not only present on the plasma membrane but also in the mitochondria of PDAC cells (Kovalenko et al., 2016), we aimed to investigate whether the plasma membrane and mitochondrial $K_{Ca}3.1$ channels play distinct roles in cancer progression. Recent findings, including those by Todesca et al., (2024) have shown the importance of mitochondrial $K_{Ca}3.1$ in modulating cancer cell metabolism, oxidative stress, and apoptosis in other cancer types such as non-small cell lung cancer. These mitochondrial channels may influence how cancer cells respond to stress and treatment, providing an additional layer of regulation beyond plasma membrane $K_{Ca}3.1$ activity. This raises the question of whether targeting mitochondrial $K_{Ca}3.1$ could enhance therapeutic outcomes in PDAC, where treatment resistance is a major challenge. To achieve this, we employed maurotoxin, a peptide specifically targeting plasma membrane $K_{Ca}3.1$ channels (Castle et al., 2003). Thus, by comparing the effects of maurotoxin with those of the membrane-permeable TRAM-34, we were able to differentiate the contributions of plasma membrane $K_{Ca}3.1$ from those of mitochondrial $K_{Ca}3.1$ channels in cancer progression.

To reflect the typical clinical landscape of PDAC, where diagnosis and treatment occur at an advanced stage, we began drug administration when the mice were 20 weeks old, a point at which they typically exhibit noticeable symptoms of PDAC (Veite-Schmahl et al., 2017). The schedule of administration of the $K_{Ca}3.1$ channel blocker and/or gemcitabine is depicted in Figure 5. This treatment timeline reflects the delayed initiation of therapeutic interventions that is frequently observed in human patients, thus enhancing the translational relevance of our study.

First, we validated $K_{Ca}3.1$ channel expression in the KPfC mouse model using immunohistochemistry. Cancer cells were identified with CK18 while PSCs surrounding the tumor nodes were marked with α-SMA (Figure 17). $K_{Ca}3.1$ channels were detected in both CK18-positive tumor cells and α-SMA-positive PSCs, confirming their expression within the KPfC mouse tissue (Figure 17, zoomed-in views of the framed cells are presented in the right panels).

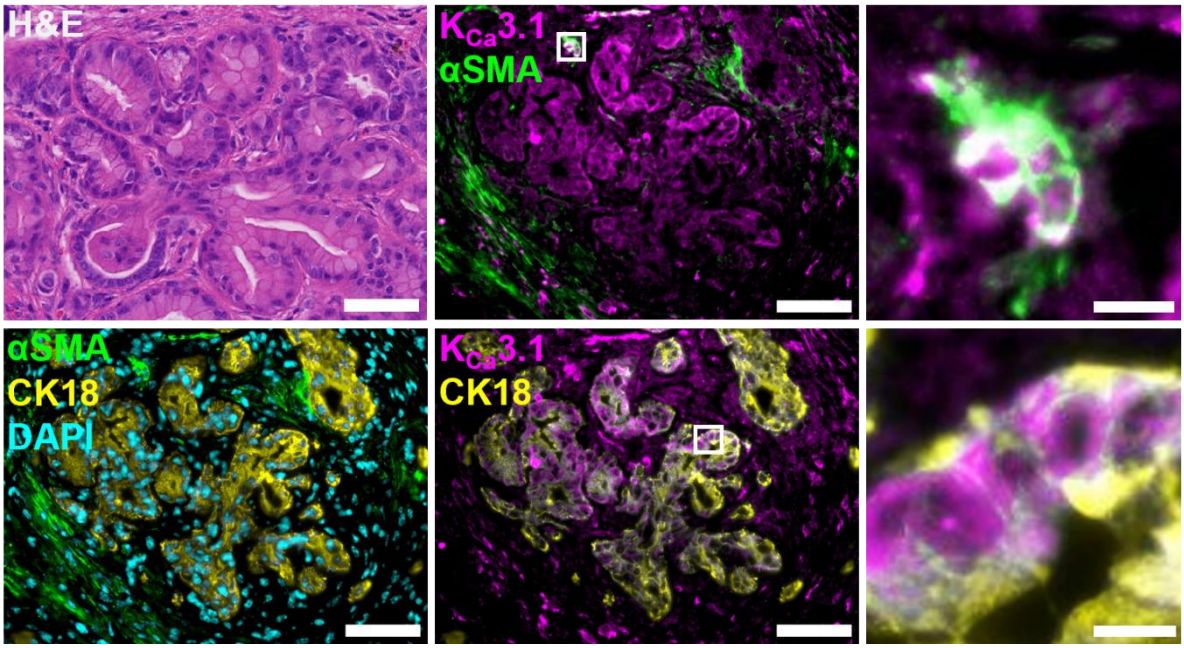

Figure 17. Visualization of K_{Ca}3.1 Expression in KPfC Mouse Tissue. *Representative hematoxylin and eosin (H&E) image of a tumor node, and immunohistochemistry from vehicle-treated mice (N=8), illustrating K_{Ca}3.1 (magenta) localization within the tissue. K_{Ca}3.1 expression is detected in αSMA-positive (green) PSCs (highlighted in the images and zoomed in on the upper right panel) as well as in CK18-positive (yellow) tumorous ducts (highlighted in the images and zoomed in on the lower right panel). Nuclei are stained with DAPI (cyan). Scale bar=50 µm; scale bar in zoomed images=5 µm.*

Then, we analyzed KPfC mouse tissue to evaluate tumor nodes and assess fibrosis levels. Each tumor node was meticulously labeled, and we quantified the extent of fibrosis using Sirius Red staining. A pixel classifier was utilized to distinguish between fibrotic and non-fibrotic areas, facilitating an in-depth investigation of K_{Ca}3.1 expression and its role in tumor progression. The histological analysis of the pancreatic tissue is shown in Figure 18.

The histological examination of pancreatic tissues (Figure 18) from KPfC mice showed no significant macroscopic differences in tumor size across the various treatment protocols (vehicle: 4.95 mm^2, 95% CI, 1.13-19.19 mm^2, N mice=8; TRAM-34: 3.45 mm^2 95% CI, 1.33-31.03 mm^2, N mice=7; maurotoxin (MTX): 12.94 mm^2, 95% CI, 2.40-14.34 mm^2, N mice=3; gemcitabine (GEM): 5.22 mm^2, 95% CI, 1.94-13.93 mm^2, N mice=9; TRAM-34+gemcitabine: 2.45 mm^2, 95% CI, 0.31-7.94 mm^2, N mice=7; maurotoxin+gemcitabine: 5.72mm^2, 95% CI, 2.52- 25.34mm^2, N mice=3) (Figure 19). Additionally, the relative size of the tumor compared to the total tissue area remained unchanged (vehicle: 4.24%, 95% CI, 2,09-23,40%, N mice=8; TRAM-34: 3.72%, 95% CI, 1.85-32.81%, N mice=7; maurotoxin: 12.51%, 95% CI, 4.25-13.12%, N mice=3; gemcitabine: 5.69%, 95% CI, 1.94-14.79%, N mice=9; TRAM-34+gemcitabine: 2.72%, 95% CI, 0.35-8.00%, N mice=7; maurotoxin+gemcitabine: 9.93%, 95% CI, 3.70- 40.21%, N mice=3) (Figure 19).

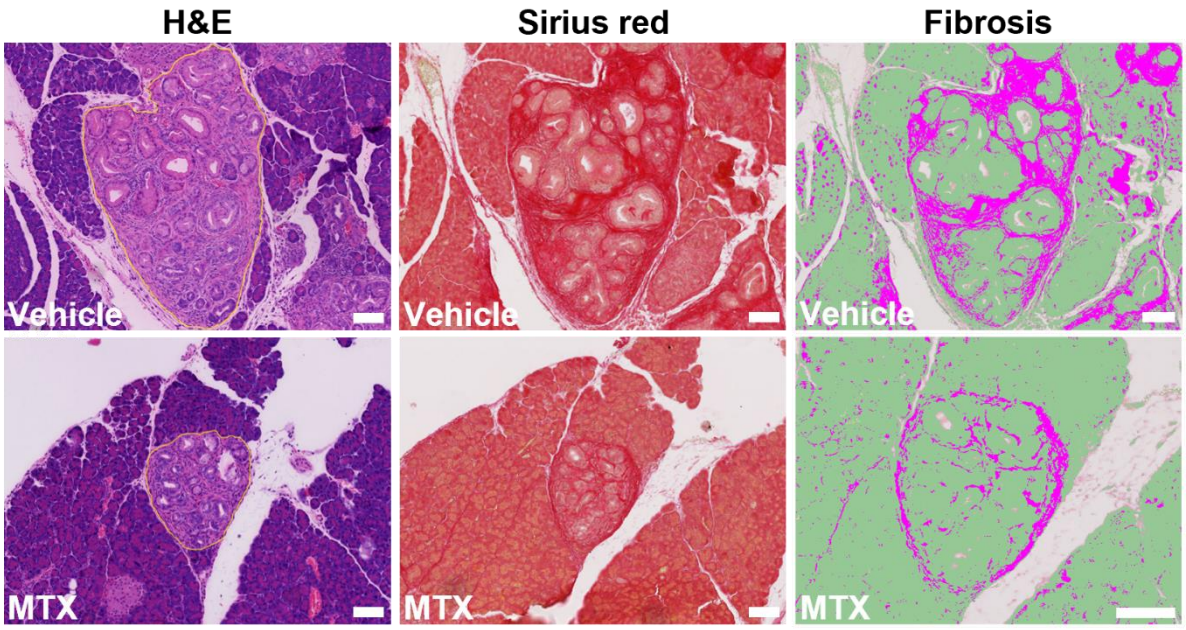

Figure 18. Characterization of PDAC tumor nodes and fibrosis in KPfC mice. *Representative images of PDAC tumor nodes (highlighted in yellow) stained with hematoxylin and eosin (H&E), Sirius Red and labeled using a pixel classifier to assess fibrosis in both vehicle-treated (N=8) and maurotoxin-treated (N=3) mice (MTX). Scale bar = 100 µm.*

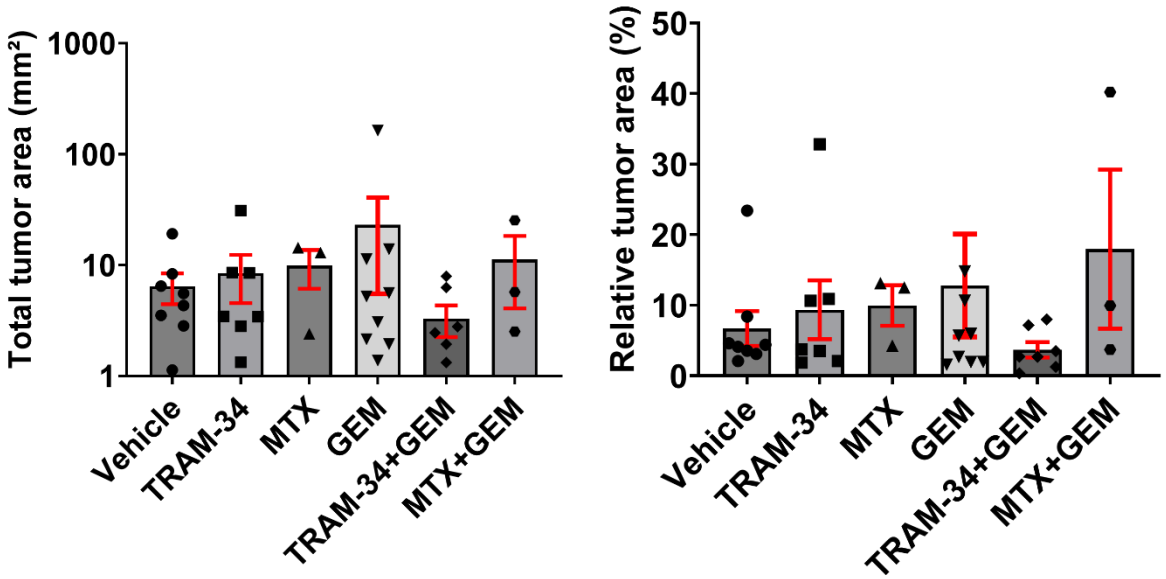

Figure 19. Evaluation of total tumor area (mm²) and relative tumor area (%) in KPfC mice. *Left panel shows the total tumor size across the pancreata of KPfC mice. The area of each tumor node was measured from H&E-stained tissue sections. Right panel illustrates the relative tumor area in histological KPfC tissue sections, calculated by dividing the total tumor area by the total tissue area. In both panel, data points depict individual pancreata (vehicle: N=8; TRAM-34: N=7; MTX: N=3; GEM: N=9; TRAM-34+GEM: N=7; MTX+GEM: N=3).*

However, a closer examination of the microscopic tumor nodes revealed distinct variations within the treatment protocols (Figure 20). By analyzing these nodes individually (n), we observed that treatment with maurotoxin led to a substantial reduction in the mean size of individual tumor nodes compared to the vehicle group (vehicle: 30,269 μm^2, 95% CI, 26,834-34,704 μm^2, n/N=439/8; maurotoxin: 18,604 μm^2, 95% CI, 15,190-24,390 μm^2, n /N=224/3). Furthermore, the combination of maurotoxin with gemcitabine also resulted in a decrease in tumor node size (maurotoxin+gemcitabine: 23,723 μm^2, 95% CI, 17,689- 28,897 μm^2, n/N=250/3). Conversely, other treatment regimens did not produce significant changes in tumor node size. Thus, maurotoxin appears to be a more effective therapeutic option compared to TRAM-34. While the combination of TRAM-34 and gemcitabine seemed more effective than either treatment alone, this reduction in size did not achieve statistical significance compared to the vehicle (TRAM-34: 34,778 μm^2, 95% CI, 28,110-42,608 μm^2, n/N=367/7; gemcitabine: 34,442 μm^2, 95% CI, 31,246-40,048 μm^2, n/N=598/10; TRAM-34+gemcitabine: 24,494, 95% CI, 19,552- 29,262 μm^2, n/N=361/7). These results provide initial evidence supporting the therapeutic potential of maurotoxin, both as a standalone treatment and in conjunction with gemcitabine, for mitigating tumor growth in PDAC.

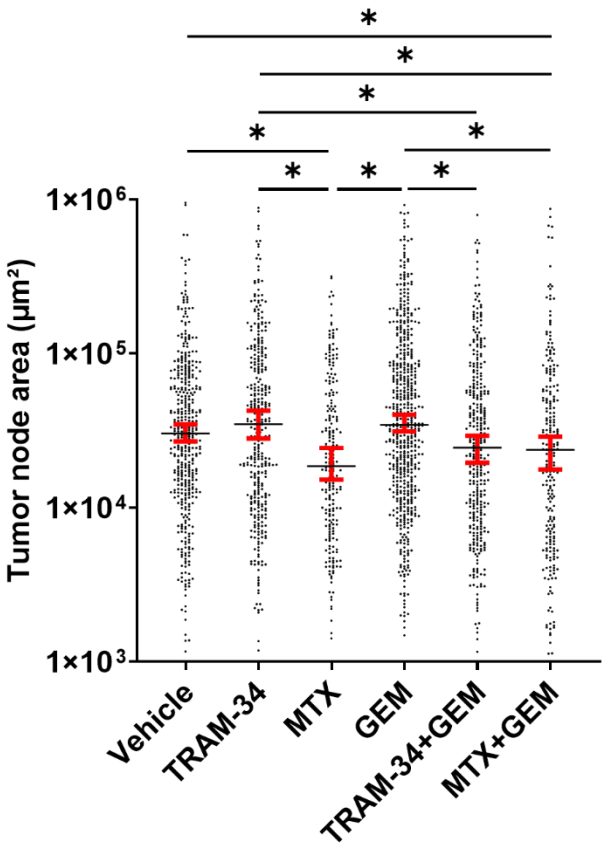

Figure 20. Inhibition of plasma membrane $K_{Ca}3.1$ reduces tumor node size. *Assessment of tumor node size (μm^2) in the pancreata of KPfC mice. The area of each tumor node was determined from H&E-stained tissue sections. Data points represent the sizes of individual tumor nodes (n). Vehicle: n/N=439/8; TRAM-34: n/N=367/7; maurotoxin (MTX): n/N=224/3; gemcitabine (GEM): n/N=598/9; TRAM-34+GEM: n/N=361/7; MTX+GEM: n/N=250/3. The size of the tumor nodes was reduced by 38% in the MTX treatment group compared to the vehicle group, and by 22% in the MTX+GEM group. Statistical comparisons were conducted using the Kruskal-Wallis test followed by Dunn's post hoc test. *p < 0.05.*

These findings also raise an intriguing question: why does inhibiting plasma membrane $K_{Ca}3.1$ channels alone outperform the combined inhibition of both plasma and mitochondrial channels in reducing tumor growth?

We simultaneously evaluated the extent of fibrosis within the tumor nodes by quantifying the Sirius Red-stained area in each node (Figure 21). Gemcitabine treatment induced considerable increase in matrix production compared to the vehicle, almost doubling the amount of fibrosis in the tumor nodes (vehicle: 5,380 μm^2, 95% CI, 4,305-6,728 μm^2, n /N = 439/8; gemcitabine: 10,486 μm^2, 95% CI, 8,528-11,913 μm^2, n/N=598/10), while no other treatment showed a similar effect on fibrosis. The substantially enhanced matrix deposition underscores a critical gap in our understanding of how gemcitabine influences the tumor microenvironment and its potential role in promoting fibrosis. Nevertheless, these results support the idea that combining $K_{Ca}3.1$ inhibitors with gemcitabine could improve therapeutic outcomes by preventing gemcitabine-induced fibrosis, which may help reduce its treatment failures.

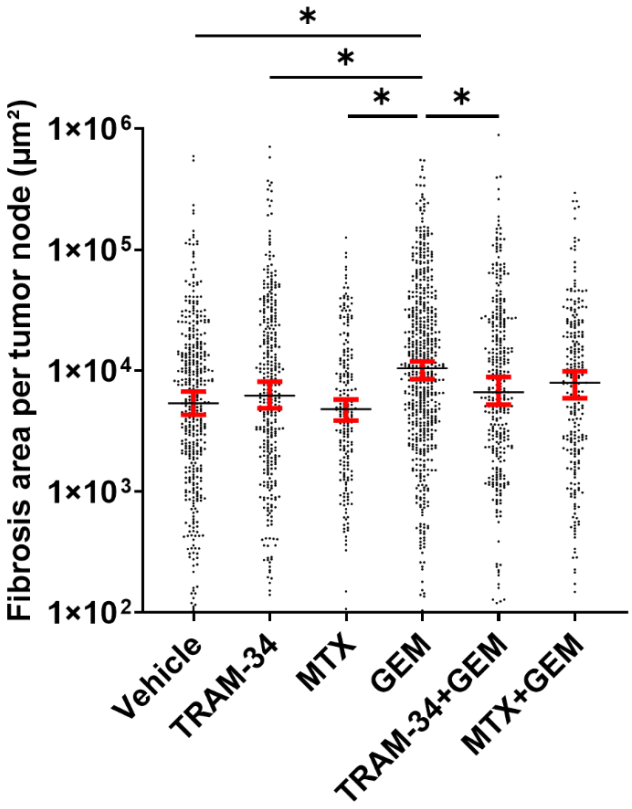

Figure 21. $K_{Ca}3.1$ inhibition reverses gemcitabine-induced fibrosis in KPfC mice. *Assessment of the fibrosis area per tumor node (μm^2) in the pancreata of KPfC mice. The fibrosis area was quantified in tissue sections from KPfC mice using a pixel classifier (illustrated in Figure 18) to differentiate and measure Sirius Red-positive fibrotic tissue from non-fibrotic areas. Each data point represents the fibrosis area within an individual tumor node (n). Vehicle: n/N=439/8; TRAM-34: n/N=367/7; maurotoxin (MTX): n/N=224/3; gemcitabine (GEM): n/N=598/9; TRAM-34+GEM: n/N=361/7; MTX+GEM: n/N=250/3. Gemcitabine induced a 95% increase in matrix production. Statistical comparisons were conducted using the Kruskal-Wallis test followed by Dunn's post hoc test. *p < 0.05.*

Building on these promising *in vivo* results, we recognize the necessity of transitioning to *in vitro* studies to better understand the mechanisms by which tumor growth is impaired.

Characterization of $K_{Ca}3.1$ expression in PDAC and PSC cell lines for spheroid development

To effectively replicate the tumor and its microenvironment, we aimed to establish an *in vitro* 3D-spheroid model utilizing co-cultured human pancreatic cancer cell lines (either PANC-1 or BxPC-3) mixed with the human pancreatic stellate cell line (PS-1). This model is designed to provide a more physiologically relevant system for investigation. To validate this model, we employed RT-qPCR and Western blotting to analyze the expression of $K_{Ca}3.1$ channels in these cell lines.

The RT-qPCR analysis revealed a distinct expression profile, with BxPC-3 cells exhibiting approximately threefold higher mRNA levels of $K_{Ca}3.1$ compared to PANC-1 cells, while PS-1 cells demonstrated lower expression levels (BxPC-3: 6.88, 95% CI, 6.29-7.46, n/N=9/3; PANC-1: 1.97, 95% CI, 1.57-2.85, n/N=12/4; PS-1: 0.08, 95% CI, 0.07-0.16, n/N=9/3) (Figure 22).

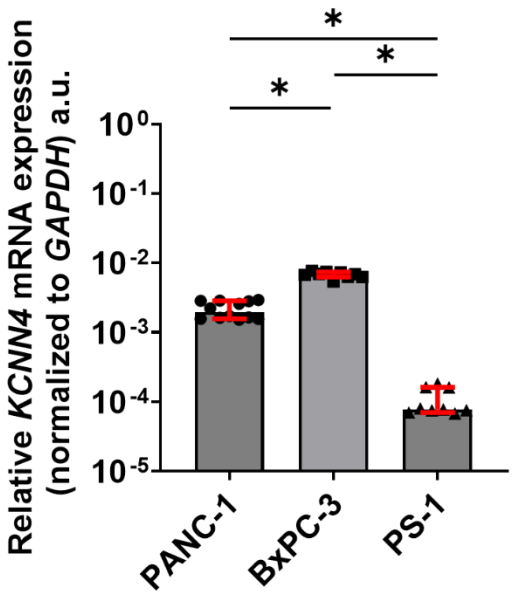

Figure 22. Quantification of KCNN4 ($K_{Ca}3.1$) mRNA expression levels in PDAC and PSC cell lines. *mRNA expression levels of KCNN4 were quantified using quantitative PCR with the $2^{-\Delta CT}$ method, normalized to the housekeeping gene GAPDH. Individual data points represent the expression levels of separate biological replicates from PANC-1 (n/N=12/4), BxPC-3 (n/N=9/3), and PS-1 cells (n/N=9/3). Statistical analysis was performed using the Kruskal-Wallis test with Dunn's post hoc test, *p < 0.05 indicates statistical significance.*

Western blotting further confirmed the presence of $K_{Ca}3.1$ in all tested cell lines, with protein bands detected at the expected molecular weight of 48 kDa (Figure 23)

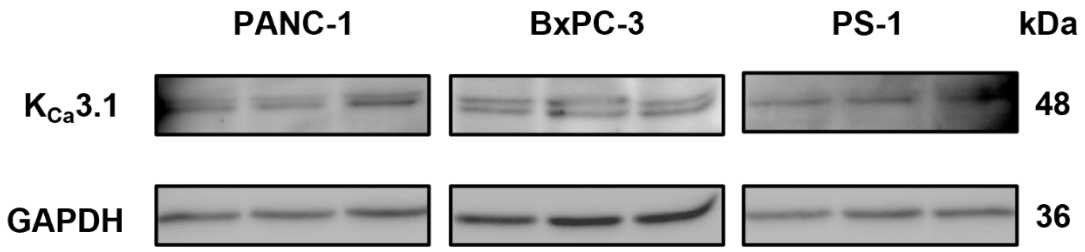

Figure 23. Western blot analysis of of $K_{Ca}3.1$ expression in PDAC and PSC cell lines. *Representative Western blot image showing specific bands for $K_{Ca}3.1$ at 48 kDa and GAPDH at 36 kDa, which serves as a loading control. The image highlights the expression of $K_{Ca}3.1$ in PANC-1, PS-1, and BxPC-3 cell lines.*

Although PANC-1 cells exhibited a trend towards higher $K_{Ca}3.1$ expression levels compared to PS-1 and BxPC-3 cells (Figure 24), these differences did not achieve statistical significance (PANC-1: 2.83, 95% CI, 1.070-5.706, N=6; BxPC-3: 1.43, 95% CI, 0.78-2.30, N=3; PS-1: 1.73, 95% CI, 1.25-1.75, N=3).

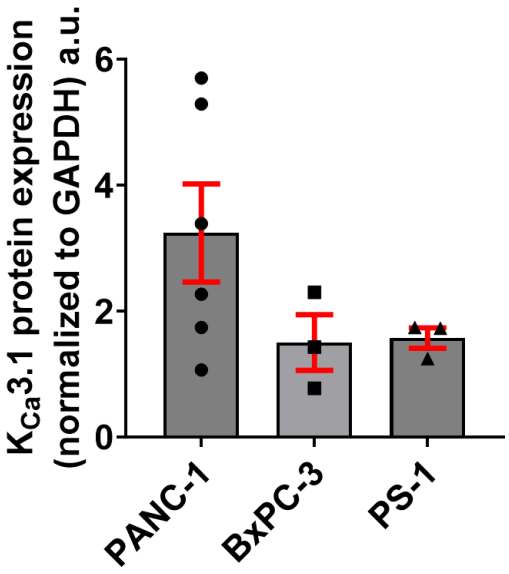

Figure 24. Protein expression levels of $K_{Ca}3.1$ relative to GAPDH. *The bar graph illustrates the relative protein expression levels of $K_{Ca}3.1$, normalized to GAPDH. Individual data points represent the expression levels of separate biological replicates fromPANC-1: n/N=6; BxPC-3: n/N=3/3; and PS-1 cells (n/N=9/3).*

To investigate the subcellular localization of $K_{Ca}3.1$, we performed immunocytochemistry on PANC-1, PS-1, and BxPC-3 cell lines, which revealed a characteristic punctate staining pattern, which is indicative of ion channels (Storck et al., 2017) (Figure 25). This staining was predominantly localized to the plasma membrane, particularly concentrated in the lamellipodia. The presence of the channels in these structures suggests an important role for $K_{Ca}3.1$ in cellular motility and interaction with the extracellular matrix. Together, these findings validate the expression and typical subcellular localization of $K_{Ca}3.1$ channels, reinforcing the suitability of PANC-1, BxPC-3, and PS-1 cell lines for exploring the mechanisms underlying tumor growth and progression in a spheroid model of PDAC.

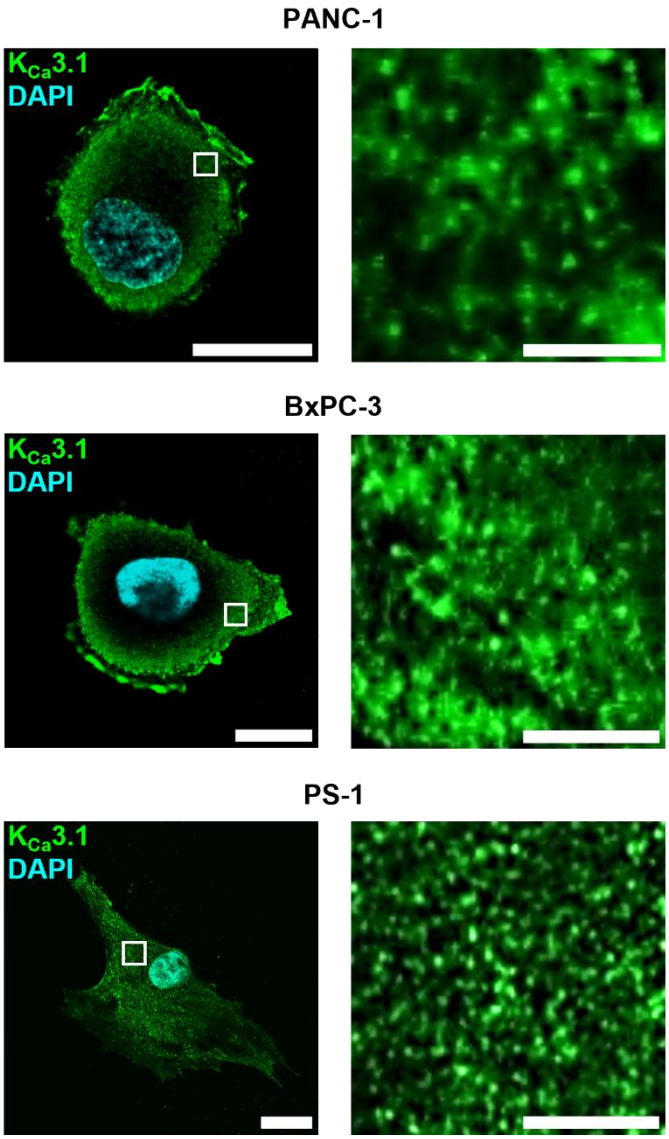

Figure 25 Immunofluorescence imaging of $K_{Ca}3.1$ localization in PDAC and PSC cells. *Representative immunofluorescence images illustrating the localization of $K_{Ca}3.1$ channels in PANC-1, BxPC-3 and PS-1 cells. $K_{Ca}3.1$ is stained in green, while DAPI (nuclear stain) is depicted in cyan. The right panel (zoom on the labelled zone) emphasizes the characteristic punctate staining pattern of the $K_{Ca}3.1$ channel. Scale bar in the left panel=20 µm; scale bar in the right panel=5 µm.*

The expression of $K_{Ca}3.1$ in patient samples, along with its presence in tumor cells and PSCs within the KPfC mouse model, underscores the relevance of using PANC-1, BxPC-3, and PS-1 cell lines for our spheroid model, as these cell lines effectively replicate the $K_{Ca}3.1$ expression profile seen in actual tumors. Using the Cell3iMager Estier, we assessed the three-dimensional architecture of our co-cultured spheroids (described in Figure 7), validating their structural integrity and confirming their appropriateness for subsequent experimental investigations.

Our 3D spheroid model is embedded within a collagen matrix to closely simulate the extracellular matrix (ECM) of pancreatic tissue. This ECM simulation is crucial for maintaining both the structural integrity and the biological functions of pancreatic ductal adenocarcinoma (PDAC)

(Rodrigues et al., 2024; T. Zhang et al., 2024). By using a collagen-based matrix, we aim to replicate key features of the tumor microenvironment, such as cell-matrix interactions and the mechanical properties that are critical for tumor cell survival, proliferation, and migration (Curvello et al., 2021; Rodrigues et al., 2024). This approach provides a more physiologically relevant environment, allowing us to study PDAC behavior *in vitro* with greater accuracy, as collagen-rich ECMs are a hallmark of the pancreatic cancer stroma (Curvello et al., 2021; Norberg et al., 2020).

Loss of $K_{Ca}3.1$ alters key pathways in PDAC

To investigate the mechanism by which $K_{Ca}3.1$ inhibition affects PDAC progression, we developed a knockout model of $K_{Ca}3.1$ in PANC-1 cells, referred to as PANC-1-$K_{Ca}3.1^{-/-}$, by using CRISPR/Cas9 gene editing technology. qPCR was performed to validate the successful knockout of $K_{Ca}3.1$ in our model. The analysis confirmed the complete absence of $K_{Ca}3.1$ mRNA expression in the knock-out cells compared to the parental PANC-1 cells. (PANC-1: 0.00197, 95% CI, 0.00157-0.00285, n/N=12/4; PANC-1-$K_{Ca}3.1^{-/-}$: undetected, n/N=9/3) (Figure 26).

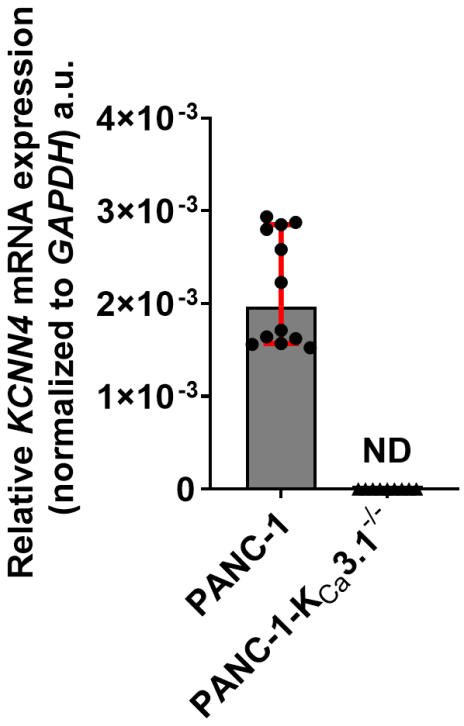

Figure 26. Validation of $K_{Ca}3.1$ (KCNN4) gene knockout in PANC-1-$K_{Ca}3.1^{-/-}$ cells. *Validation of KCNN4 gene knockout in PANC-1-$K_{Ca}3.1^{-/-}$ cells (n/N=9/3) confirmed by qPCR, using the $2^{-\Delta CT}$ method and normalized to the housekeeping gene GAPDH. Parental PANC-1 cells (n/N=12/4) served as the control group. Individual data points represent the expression levels of separate biological replicates.*

This validation step was crucial before proceeding with further experiments. We generated both PANC-1/PS-1 spheroids and PANC-1-$K_{Ca}3.1^{-/-}$/PS-1 spheroids, mimicking the pancreatic tumor microenvironment by embedding them in a PDAC-like matrix for 48 hours. After incubation and retrieval, RNA sequencing was performed to capture gene expression profiles across the two conditions.

Our RNA-seq analysis (GEO: GSE279207) revealed 3,991 differentially expressed genes between PANC-1/PS-1 and PANC-1-$K_{Ca}3.1^{-/-}$/PS-1 spheroids (Figure 27).

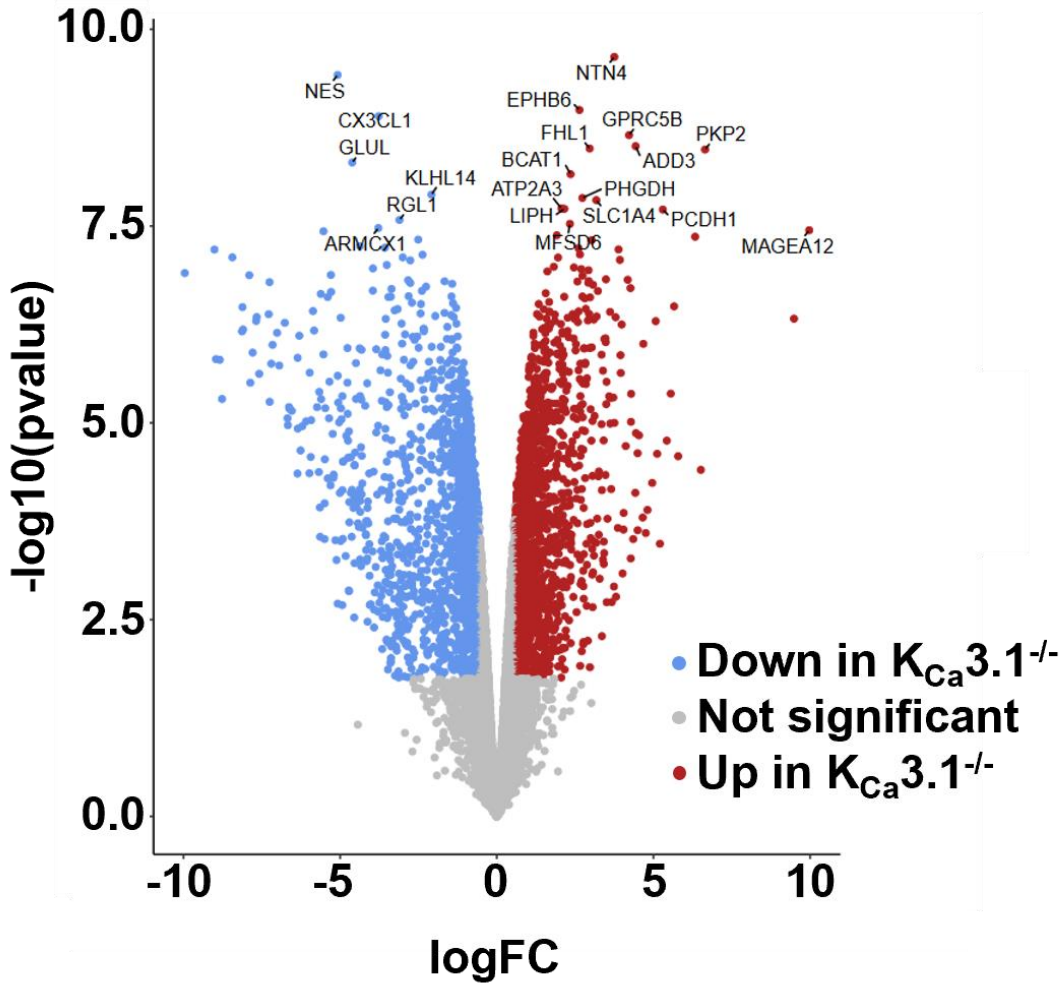

Figure 27. Differential gene expression between PANC-1-$K_{Ca}3.1^{-/-}$/PS-1 and PANC-1/PS-1 spheroids. *Volcano plot depicting differentially expressed genes between PANC-1-$K_{Ca}3.1^{-/-}$/PS-1 (N=3) and PANC-1/PS-1 spheroids (N=3) (GEO: GSE279207). Genes downregulated in PANC-1-$K_{Ca}3.1^{-/-}$/PS-1 are shown in blue (n=1,991), while upregulated genes are shown in red (n=2,000). The top 20 differentially expressed genes are labelled.*

Notably, four critical biological pathways were significantly downregulated in the $K_{Ca}3.1$ knockout spheroids: IFN-α response, IFN-γ response, G2-M checkpoint, and epithelial-mesenchymal transition (EMT) (Figure 28). Although the estrogen response pathway was also affected, we found no sex-related differences in PDAC patients or in any treatment groups of KPfC mice. Additionally, the upregulation of *SLC1A4*, a selective alanine transporter, was observed in PANC-1-$K_{Ca}3.1^{-/-}$/PS-1, suggesting a possible $K_{Ca}3.1$-dependent metabolic link (Parker et al., 2020). Therefore, we focused our investigation on the aforementioned pathways in the KPfC mouse model using immunohistochemistry (IHC).

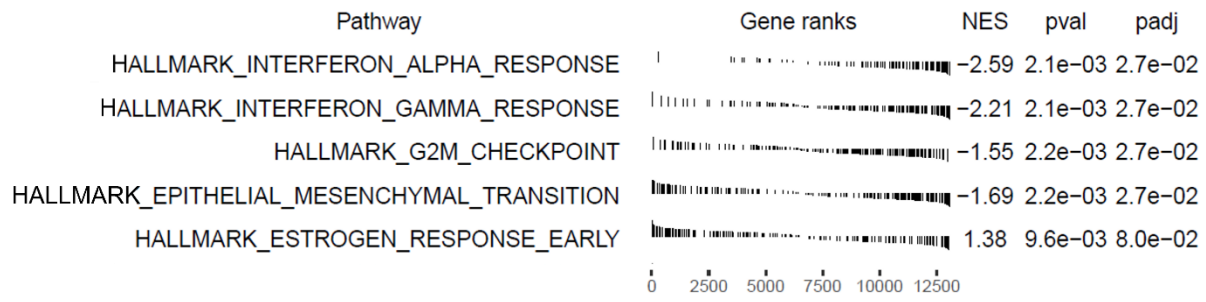

Figure 28. Significantly downregulated biological pathways in PANC-1-$K_{Ca}3.1^{-/-}$/PS-1 spheroids.

$K_{Ca}3.1$ inhibition leads to decreased T-cell exhaustion in tumor-infiltrating immune cells.

Since no immune cells are present in our spheroid model, pancreatic cancer cells and PSCs are the sources of IFN-α and IFN-γ responses in our model. This finding aligns with recent research suggesting that cancer cells can intrinsically mimic aspects of immune signaling, thus affecting the interplay between the tumor and its microenvironment (Gao et al., 2021). Among the 54 IFN-α and 78 IFN-γ-related genes that exhibited significant expression changes (Figure 29-30), most were involved in T-cell regulation.

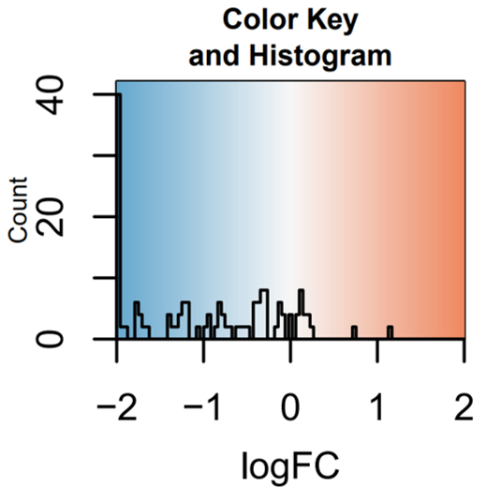

MVB12A
IL4R
MOV10
CASP8
RIPK2
TXNIP
NUB1
IFI35
TRAFD1
TRIM14
IRF7

TDRD7
LY6E
HELZ2
HLA−C
PARP12
TMEM140
PSMB8
TRIM5
IRF2
ELF1
NMI
CSF1
CD47
TRIM21
DDX60
IFIH1
TENT5A
RSAD2
IFITM1
IL7
C1S
EPSTI1
GMPR
SAMD9L
MX1
PARP9
PSMB9
GBP4
HERC6
LPAR6
LGALS3BP
UBE2L6
IFITM3
RTP4
GBP2
LAMP3
CD74
IFI44
IL15
PARP14
SAMD9
IFITM2
DHX58

Figure 29. Differentially expressed genes in the IFN-α response pathway between PANC-1/PS-1 and PANC1-$K_{Ca}3.1^{-/-}$/PS-1. *False Discovery Rate (FDR) < 0.05.*

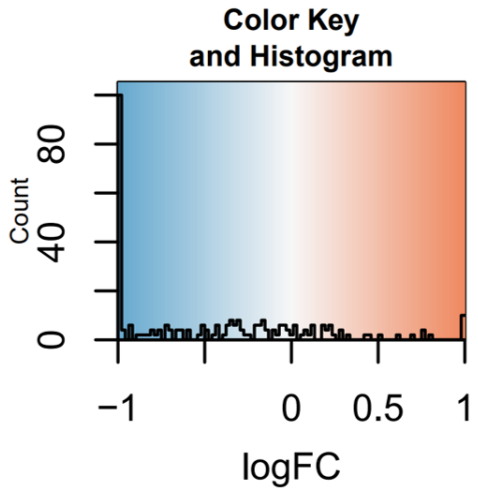

FPR1
PDE4B
PELI1
CCL2
GCH1
PTPN2
CDKN1A
RBCK1
RIPK1
IL4R
CASP7
CASP8
RSAD2
MX2
XAF1
IL15RA
C1R
PLA2G4A
IL7
C1S
EPSTI1
SAMD9L
AUTS2
SERPING1
MX1
VAMP5
CD74
IFI44
IL15
PARP14
IFITM2
DHX58
OAS2
ST8SIA4

PSMB9
GBP4
HERC6
APOL6
LGALS3BP
UBE2L6
HLA−B
IFITM3
RTP4
OAS3
SECTM1
NMI
NAMPT
IRF2
TRIM21
DDX60
RNF213
BTG1
CD69
IFIH1
TNFSF10
NCOA3
PARP12
PSMB8
CASP3
HELZ2
NLRC5
IRF7
TDRD7
LY6E
SOCS3
RIPK2
STAT3
TXNIP
UPP1
CD40
IFI35
SSPN
LATS2
TRIM14
TRAFD1
CASP4
NFKBIA
NFKB1

Figure 30. Differentially expressed genes in the IFN-γ response pathway between PANC-1/PS-1 and PANC1-$K_{Ca}3.1^{-/-}$/PS-1. *False Discovery Rate (FDR) < 0.05.*

Notably, several of these genes, such as CD47 (IFN-α only), IL4R, CASP8, IRF2, TRAFD1, IFI35, CD69 (IFN-γ only), and STAT3 (IFN-γ only), have been linked to T-cell exhaustion, a dysfunctional state that can impair the immune response to cancer (Edilova et al., 2018; Gong et al., 2023; Koyama-Nasu et al., 2022; M. Li et al., 2023; Liang et al., 2024; Sheikh & Utzschneider, 2022; Stewart et al., 2023; Sun et al., 2023). Recent studies have shown the significant role that PDAC and its surrounding microenvironment play in promoting T-cell exhaustion (Saka et al., 2020). Additionally, $K_{Ca}3.1$ has been linked to the regulation of the T-cell exhaustion (Sharma et al., 2024). Building on these insights, we hypothesize that in our model, tumor cells actively contribute to creating an immunosuppressive environment. As such, silencing $K_{Ca}3.1$ could potentially reverse T-cell exhaustion, restore immune surveillance, and thereby hinder cancer progression. Through meticulous immunohistochemical analysis of antibody-stained KPfC tissue, we observed a lack of immune cell infiltration within the tumor nodes. Instead, immune cells were predominantly localized at the edges of the tumor nodes, near the pancreatic tissue border (Figure 31). Within the tumor nodes themselves, the few immune cells present were primarily CD3-positive but not CD8-positive. This suggests a limited presence of cytotoxic CD8+ T cells, which are crucial for directly targeting and eliminating tumor cells (Kumar et al., 2018). The presence of PD1-positive cells among these indicates T-cell exhaustion, especially in the control and gemcitabine-treated groups (Figure 31). In contrast, immune cells in mice treated with maurotoxin or TRAM-34 showed no signs of exhaustion.

Additionally, we observed a notable increase in CD8-positive immune cells in the treated samples compared to the control group. Although these findings highlight the potential of $K_{Ca}3.1$ inhibition in restoring immune function in PDAC, further research is essential to determine its full efficacy in reducing T-cell exhaustion. Additionally, investigating the link between $K_{Ca}3.1$ targeting and the IFN-α and IFN-γ responses is necessary to better understand and optimize this therapeutic strategy.

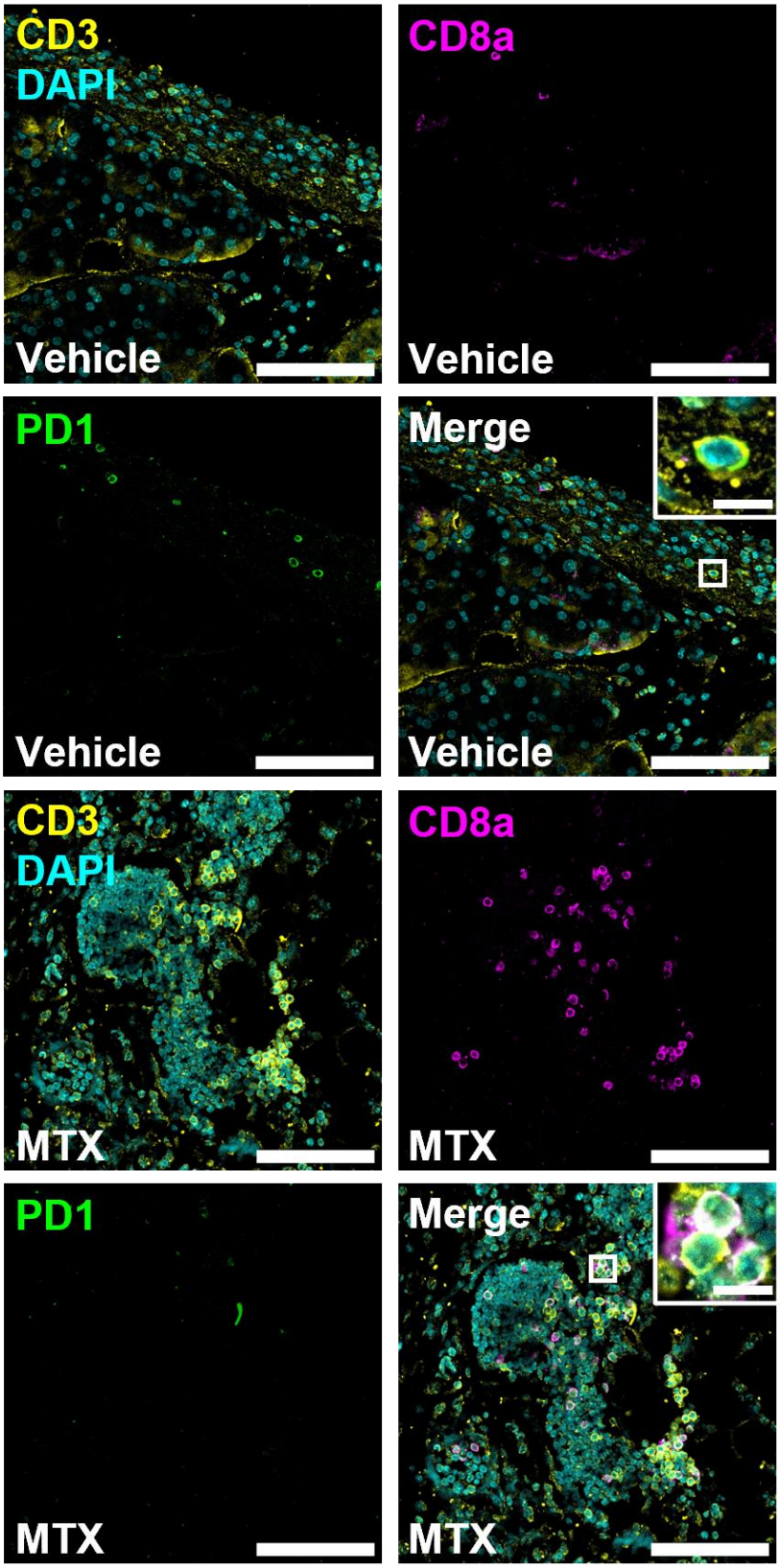

Figure 31. Reduced T-cell exhaustion in tumor-infiltrating immune cells following K_{Ca}3.1 inhibition. *Immunohistochemistry images of tumor-infiltrating immune cells from vehicle-treated (N=8) and maurotoxin (MTX)-treated (N=3) mice, stained for CD3 (yellow) and CD8a (magenta). PD1 (green) highlights T-cell exhaustion. The merged panel shows immune marker co-localization with PD1. Nuclei are stained with DAPI (cyan). Scale bar=100 µm. Scale bar in insets=10 µm.*

$K_{Ca}3.1$ inhibition suppresses EMT in tumor nodes.

The observed downregulation of genes associated with the G2-M checkpoint and EMT in PANC-1-$K_{Ca}3.1^{-/-}$/PS-1 cells suggests a decrease in tumor aggressiveness and could explain our *in vivo* results.

EMT is a key driver of cancer cell invasion and metastasis in PDAC (Palamaris et al., 2021). EMT facilitates the transformation of cancer cells into a more motile and invasive phenotype. Moreover, $K_{Ca}3.1$ has been linked to cellular processes such as migration and invasion (Bonito et al., 2016). This downregulation of genes associated with the EMT pathway upon $K_{Ca}3.1$ inhibition is consistent with the reduction in tumor growth observed in our *in vivo* model and suggests that the channel may contribute directly to EMT in PDAC.

To further validate these findings, we performed immunohistochemical staining for E-cadherin and N-cadherin (Figure 32). The vehicle-treated samples displayed higher N-cadherin positivity within the tumor nodes, indicating a more mesenchymal and invasive phenotype (Figure 32). In contrast, samples treated with the $K_{Ca}3.1$ inhibitors maurotoxin or TRAM-34 showed increased E-cadherin expression, suggesting a shift towards an epithelial phenotype. This shift in cadherin expression patterns supports the hypothesis that inhibiting $K_{Ca}3.1$ promotes a more epithelial-like state in tumor cells, potentially reducing their invasive properties.

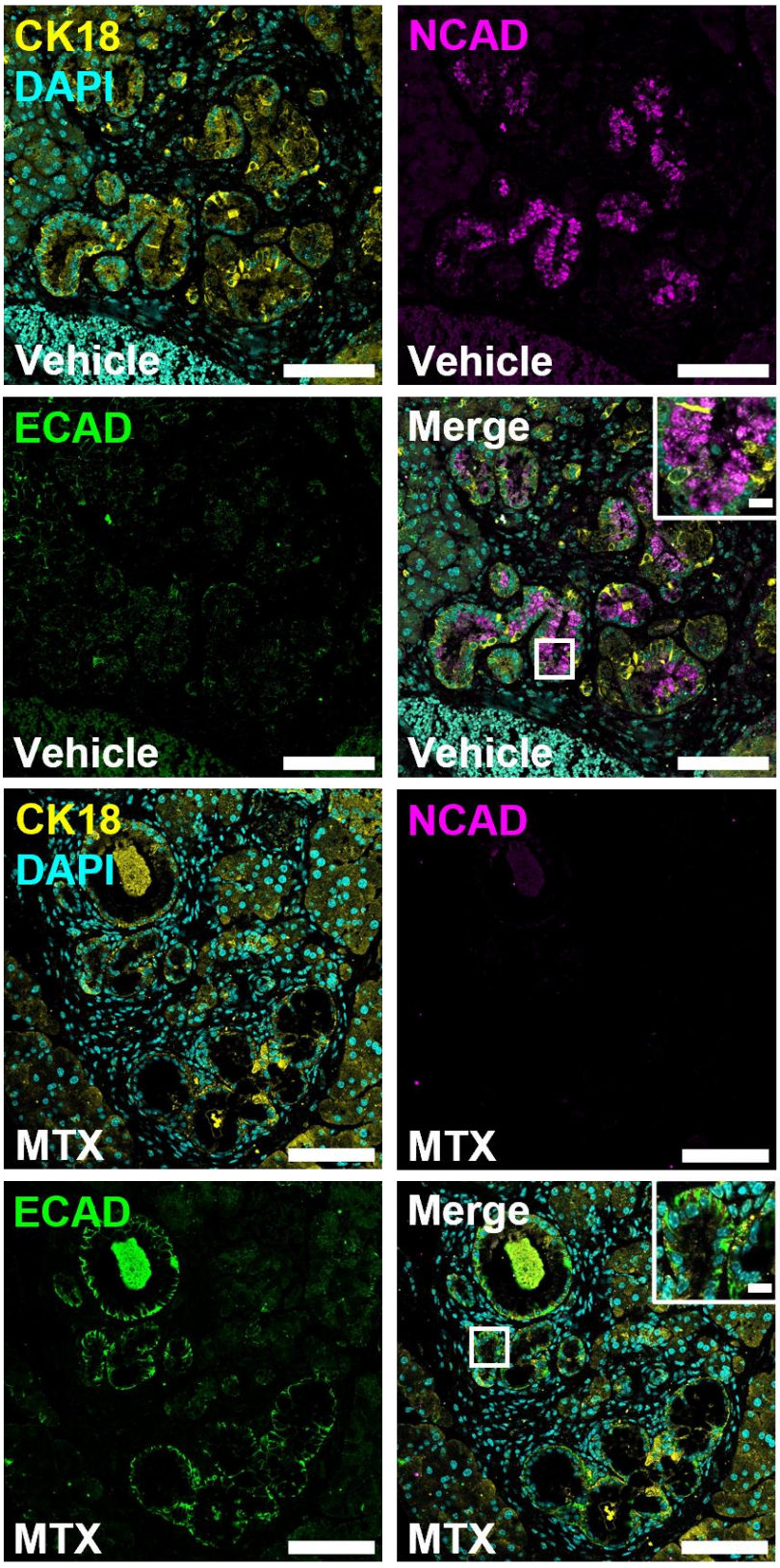

Figure 32. Inhibition of EMT in tumor nodes following $K_{Ca}3.1$ Inhibition. *Immunohistochemistry images of tumor nodes from vehicle-treated (N=8) and maurotoxin (MTX)-treated (N=3) mice, stained for N-cadherin (magenta) and E-cadherin (green), markers of EMT. Both cadherins are localized within CK18-positive (yellow) tumorous ducts, as shown in the insets. Nuclei are counterstained with DAPI (cyan). Scale bar = 100 µm, with inset scale bars=10 µm.*

$K_{Ca}3.1$ inhibition disrupts G2-M checkpoint and induces cell death in PDAC

In PDAC, high expression of G2-M phase-related genes correlates with aggressive tumor behavior and poor patient survival (Oshi et al., 2020). The reduction in G2-M checkpoint gene expression following $K_{Ca}3.1$ knockout, points to a disruption at this critical transition point of the cell cycle. This could prevent cells with DNA damage from progressing into mitosis and effectively limit cell proliferation (Y. Wang et al., 2009). Moreover, $K_{Ca}3.1$ has previously been linked to DNA damage (Ganser et al., 2024; Sevelsted Møller et al., 2016). We propose that inhibiting $K_{Ca}3.1$ induces a malfunction in the G2-M checkpoint. Consequently, cells harboring unrepaired DNA damage are unable to progress through the cell cycle, which precipitates cell death (Y. Wang et al., 2009). To further investigate the impact of $K_{Ca}3.1$ inhibition on tumor cell proliferation and cell death, we performed Ki67/DAB and TUNEL staining on our KPC tissue samples.

No visible differences in proliferation were observed within the tumor nodes between the conditions after staining with Ki67/DAB (Figure 33).

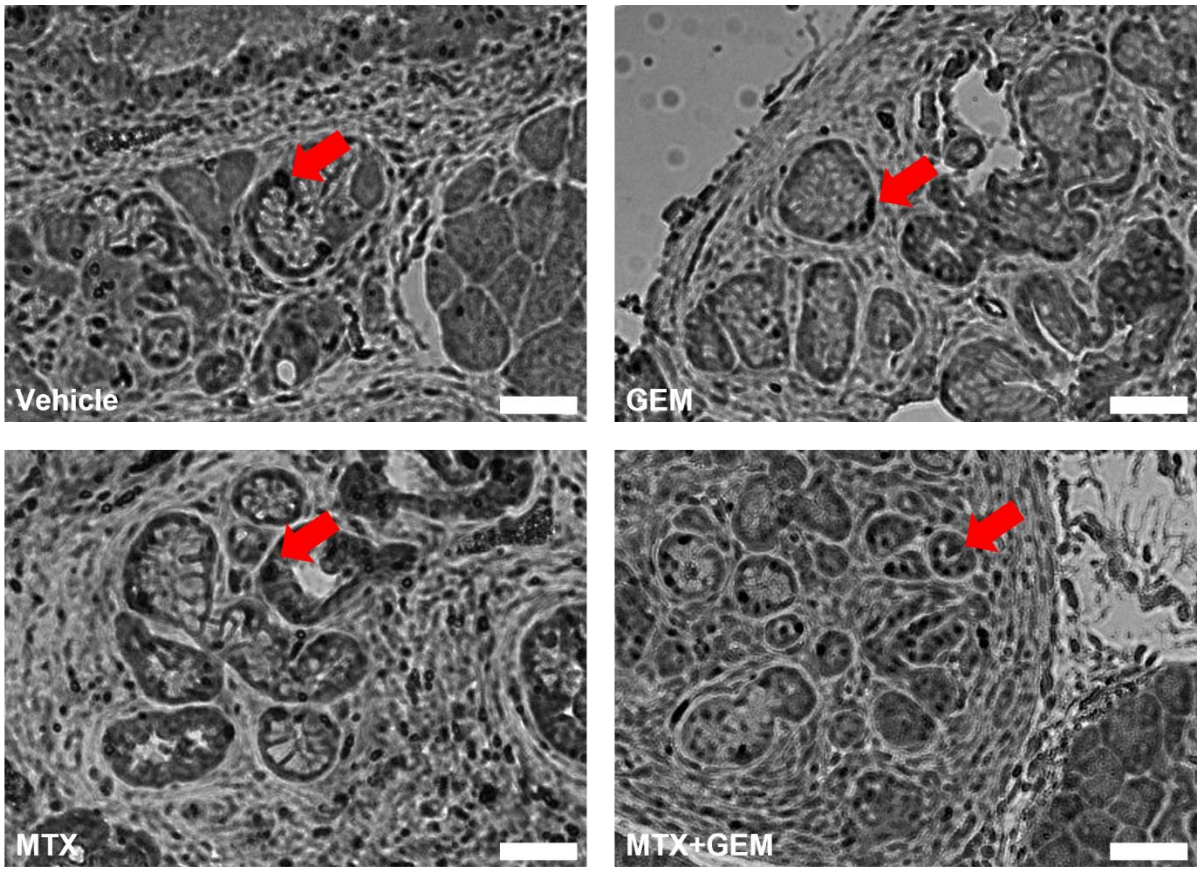

Figure 33. Ki67/DAB staining of tumor tissues in KPfC mice. *Representative Ki67/DAB staining images of tumor nodes in tissues from mice treated with vehicle (N=8), gemcitabine (GEM; N=7), maurotoxin (MTX; N=3), or a combination of MTX and GEM. Ki67 staining marks proliferating cells in the tumor nodes (Red arrows indicate Ki67-positive nuclei, visible as black dots). Scale bar =50 µm.*

In contrast, the TUNEL assay performed on KPfC mouse tissues allowed for a qualitative assessment of cell death across the different treatment conditions (Figure 34). We observed less cell death in the vehicle- and gemcitabine-treated groups than in those treated with maurotoxin,

TRAM-34, or their combination with gemcitabine. The overall number of labeled dead cells was rather low. This finding highlights the protective role of the tumor microenvironment in shielding the tumor core, mirroring the reality of an *in vivo* PDAC model.

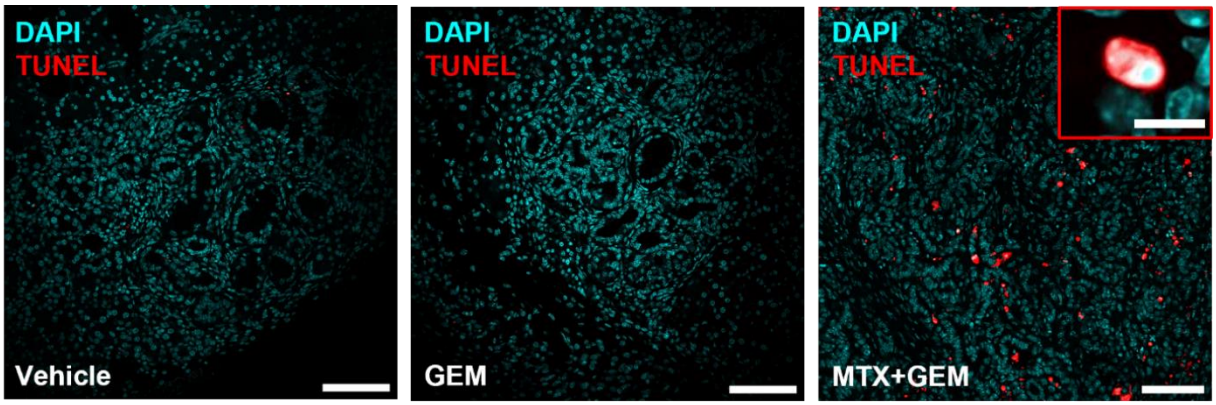

Figure 34. K_{Ca}3.1 inhibition promotes cell death in KPfC tissues. *Representative images of TUNEL staining in KPfC tissue sections from vehicle- (N=8), gemcitabine- (GEM; N=7), and maurotoxin+gemcitabine-treated (MTX+GEM; N=3) groups. Apoptotic cells are marked in red, with nuclei counterstained in cyan (DAPI). The inset highlights a TUNEL-positive cell. Scale bar=100 µm; inset scale bar=10 µm.*

The limited efficacy of gemcitabine in promoting cell death may be attributed to its inability to sufficiently penetrate and reach the tumor nodes. This suggests that while gemcitabine struggles to overcome the protective barriers of the tumor microenvironment, K_{Ca}3.1 inhibition enhances cell death even in the presence of these barriers. However, this experiment did not inform us about a potential additive effect between K_{Ca}3.1 inhibitors and gemcitabine, as no significant differences in cell death were observed between the TRAM-34, maurotoxin, TRAM-34+gemcitabine, or maurotoxin+gemcitabine groups.

Despite the increase in cell death observed with K_{Ca}3.1 inhibition, the Ki67/DAB staining revealed no differences in cell proliferation across treatment groups. These results indicate that K_{Ca}3.1 inhibition primarily induces cell death without affecting tumor cell proliferation. Thus, the therapeutic benefit of K_{Ca}3.1 inhibition previously observed *in vivo* seems to stem from its ability to promote cell death.

The combination of RNA-seq data and immunohistochemical analysis supports the notion that targeting K_{Ca}3.1 contributes to decreased tumor growth in PDAC by downregulating the EMT pathway and promoting cell death. These findings prompted us to further investigate whether K_{Ca}3.1 inhibition affects the invasive potential of PDAC cells in a 3D spheroid model. We assessed spheroid integrity, invasion, and cell death.

Inhibition of plasma membrane K_{Ca}3.1 with maurotoxin decreases more effectively the invasive potential of PDAC spheroids

To investigate whether K_{Ca}3.1 inhibition affects the migratory and invasive potential of PDAC cells, we assessed the impact of K_{Ca}3.1 channel blockers on spheroid invasion in a 3D *in vitro* model. We monitored cell emigration from spheroids over a 48-h period, quantifying the invasive zone on

an hourly basis (described in Figure 10). In the first hours, spheroid cells exerted contractile force and pulled on the surrounding matrix, causing the spheroid to shrink, a crucial step for their migration. This was followed by spheroid expansion and the formation of an invasive front.

Building on our *in vivo* results regarding maurotoxin efficacy over TRAM-34, we compared the specific effect of targeting plasma membrane and mitochondrial $K_{Ca}3.1$ channels on spheroid invasion. The data show that maurotoxin significantly surpassed TRAM-34 in reducing the invasive potential of PANC-1/PS-1 spheroids (control: 282,756 ± 36,394 μm^2, N=4; maurotoxin (MTX): 103,666 ± 44,670 μm^2, N=4; TRAM-34: 223,695 ± 20,953 μm^2, N=4) (Figure 35). Remarkably, when combined with TRAM-34, maurotoxin inhibitory effect was attenuated compared to maurotoxin alone (TRAM-34+maurotoxin: 241,223 ± 28,284 μm^2, N=4). This suggests that maurotoxin inhibits plasma membrane $K_{Ca}3.1$ channels, leading to a reduction in cell invasion. In contrast, broader inhibition by TRAM-34, including mitochondrial $K_{Ca}3.1$ channels, appears to play a protective role in PDAC cells. This mitochondrial protection could be essential for cell survival or adaptation in the invasive process, and its inhibition may inadvertently counterbalance the positive effects of plasma membrane $K_{Ca}3.1$ blockade and reduce the overall effectiveness of the treatment. These findings reveal a novel complexity in targeting $K_{Ca}3.1$ channels for cancer therapy, where inhibiting different subtypes can have opposing effects on treatment outcomes.

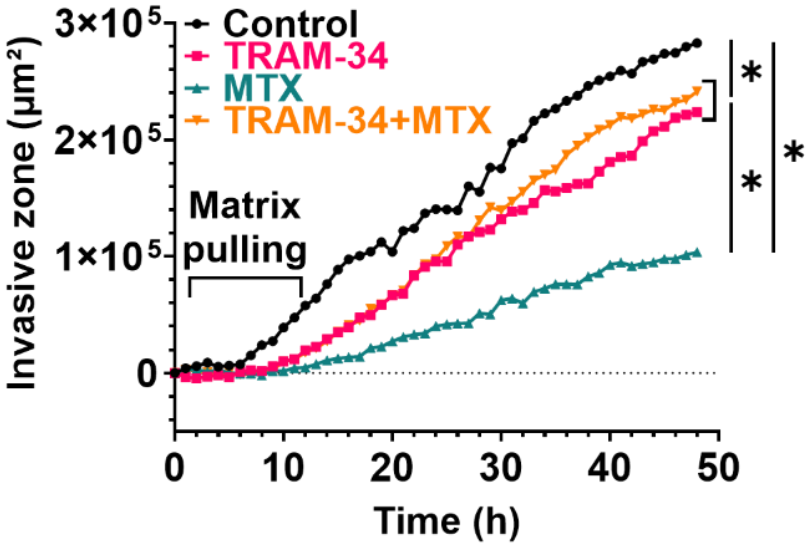

Figure 35. Maurotoxin more effectively reduces the invasive potential of PANC-1/PS-1 spheroids compared to TRAM-34. *Quantification of the invasive zones over a 48-h period in PANC-1/PS-1 spheroids treated with DMSO (Control, N=4), TRAM-34 (N=4), maurotoxin (MTX, N=4), or a combination of both (TRAM-34+MTX, N=4). The data represent mean values from all spheroids analyzed. Statistical analysis was performed using two-way ANOVA with Tukey's multiple comparison test. *p < 0.05.*

$K_{Ca}3.1$ inhibition impacts the morphology of the migrating cells

Following the approach of our *in vivo* experiments, we treated PANC-1/PS-1 and BxPC-3/PS-1 spheroids with TRAM-34 or maurotoxin either alone or in combination with gemcitabine. $K_{Ca}3.1$ inhibition led to a shift in the migration patterns of single cells emerging from the spheroids (Figures 36-37). In the vehicle-treated PANC-1/PS-1 spheroids, cells migrated collectively, with a

spindle-shaped morphology, creating a cohesive migration front, forming spindle-shaped structures that moved in a coordinated fashion. However, treatment with $K_{Ca}3.1$ inhibitors disrupted this behavior, with cells migrating predominantly as single round-shaped cells rather than in a collective manner (Figure 36).

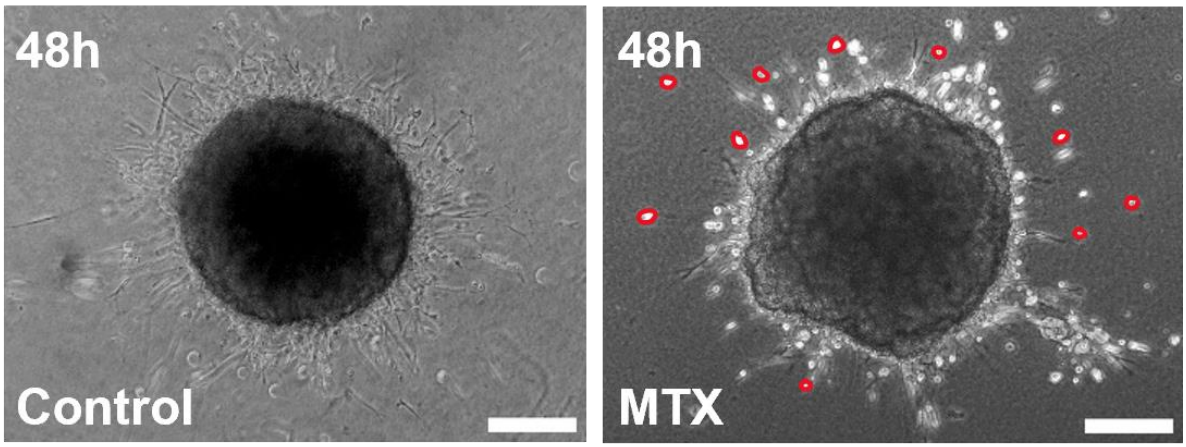

Figure 36. Representative images depicting the migration patterns of PANC-1/PS-1 and BxPC-3/PS-1 spheroids treated with DMSO (control) or maurotoxin (MTX). *Individual cells are highlighted in red. Scale bar=200 µm.*

Similarly, in BxPC-3/PS-1 spheroids, both maurotoxin and TRAM-34 induced a distinct migration pattern, showing enhanced single-cell movement and a reduction in spindle-shaped collective structures (Figure 37).

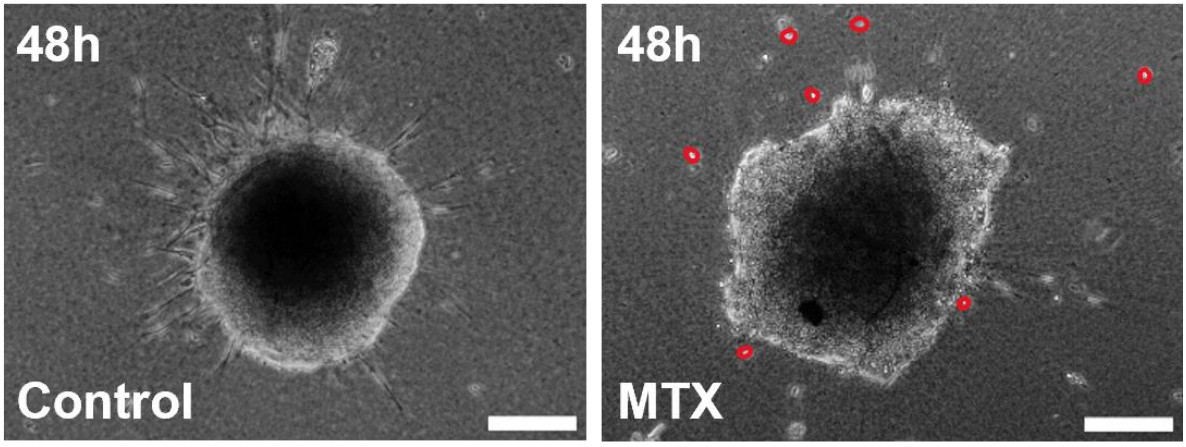

Figure 37. Representative images depicting the migration patterns of BxPC-3/PS-1 and BxPC-3/PS-1 spheroids treated with DMSO (control) or maurotoxin (MTX). *Individual cells are highlighted in red. Scale bar = 200 µm.*

These changes suggest that targeting $K_{Ca}3.1$ channels disrupts cell-cell adhesion within the spheroids, potentially weakening the cohesion between cells and promoting a more dispersed migration mode. Additionally, we observed that cells from both PANC-1/PS-1 and BxPC-3/PS-1 spheroids required a lag period of up to 10 h before initiating migration. During this time, cells pulled matrix fibers towards the spheroid, possibly remodeling the extracellular matrix to facilitate

invasion. Notably, spheroids treated with maurotoxin, gemcitabine, or their combination experienced a significantly prolonged lag period before cell emigration initiated (Figures 38-39). This delay in migration suggests that $K_{Ca}3.1$ inhibition impairs the ability of the cells to efficiently interact with the surrounding matrix. These findings indicate that $K_{Ca}3.1$ inhibition not only alters migration patterns but may also impact matrix interactions and the timing of cell emigration.

Plasma membrane $K_{Ca}3.1$ inhibition decreases the invasive potential of mixed spheroids

Our emigration results showed that both maurotoxin alone and its combination with gemcitabine reduced the invasiveness of PANC-1/PS-1 and BxPC-3/PS-1 spheroids (PANC-1/PS-1 control: 217,262 ± 27,894 μm^2, N=14; PANC-1/PS-1 maurotoxin: 89,658 ± 20,281 μm^2, N=10; PANC-1/PS-1 maurotoxin+gemcitabine: 70,043 ± 15,659 μm^2, N=6; BxPC-3/PS-1 control: 141,332 ± 29,919 μm^2, N=10; BxPC-3/PS-1 maurotoxin: 74,643 ± 12,032 μm^2, N=7; BxPC-3/PS-1 maurotoxin+gemcitabine: 58,847 ± 8,841 μm^2, N=5) (Figures 38-39).

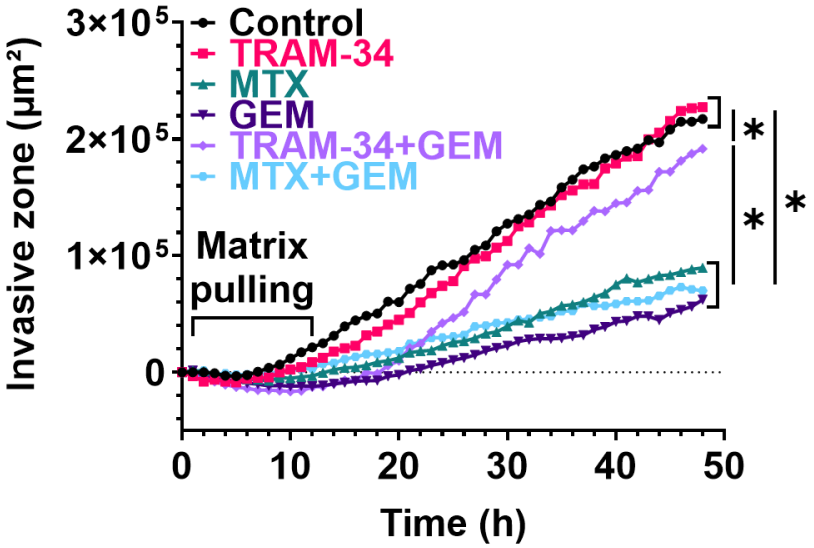

Figure 38: $K_{Ca}3.1$ inhibition with maurotoxin decreases the invasive potential of PANC-1/PS-1 spheroids more efficiently than TRAM-34. *Quantification of the invasive potential of PANC-1/PS-1 spheroids following treatment with DMSO (Control, N=14), TRAM-34 (N=8), maurotoxin (MTX, N=10), gemcitabine (GEM, N=10), or a combination of gemcitabine with either inhibitor (TRAM-34+GEM, N=4; MTX+GEM, N=6). Data represent the mean values. Statistical significance was determined using two-way ANOVA followed by Tukey's multiple comparison test. *p < 0.05.*

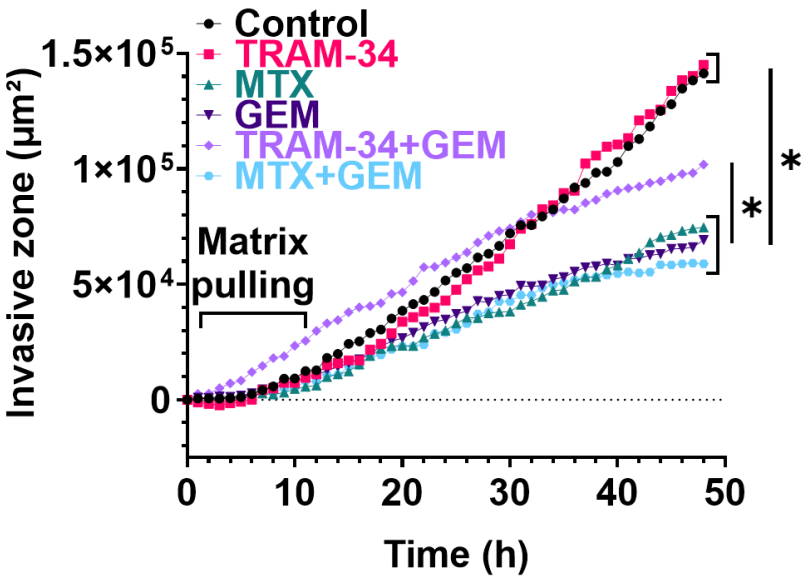

Figure 39. Inhibition of $K_{Ca}3.1$ with maurotoxin decreases the invasive potential of BxPC-3/PS-1 spheroids more efficiently than TRAM-34. *The invasive potential of BxPC-3/PS-1 spheroids was evaluated following treatment with DMSO (Control, N=10), TRAM-34 (N=5) maurotoxin (MTX, N=7), gemcitabine (GEM, N=8) or a combination of either inhibitor with gemcitabine (TRAM-34+GEM, N=5; MTX+GEM, N=5). Data represent the mean values. Statistical significance was determined using two-way ANOVA followed by Tukey's multiple comparison test. *p < 0.05.*

In both spheroid models, the combination of maurotoxin and gemcitabine was slightly more effective. Nevertheless, no significant additive effects were observed. Notably, gemcitabine alone was just as effective as maurotoxin and its combination in both PANC-1/PS-1 and BxPC-3/PS-1 spheroids (PANC-1/PS-1 gemcitabine: 62,324 ± 14,405 µm^2, N=10; BxPC-3/PS-1 gemcitabine: 69,180 ± 9,449 µm^2, N=8). This outcome is quite surprising given that in our *in vivo* experiments, gemcitabine had little to no effect on tumor growth. In PANC-1/PS-1 spheroids, TRAM-34 combined with gemcitabine also reduced the invasive potential of the spheroids (PANC-1/PS-1 TRAM-34+gemcitabine: 191,631± 31,698 µm^2, N=4) (Figure 38) but significantly less than maurotoxin. Unexpectedly, this combination was less effective than gemcitabine alone, indicating that TRAM-34 may hinder the full therapeutic efficacy of gemcitabine. Nevertheless, maurotoxin consistently outperformed both TRAM-34 and its combination with gemcitabine (PANC-1/PS-1 TRAM-34: 227,268 ± 30,217 µm^2, N=8; BxPC-3/PS-1 TRAM-34: 145,034 ± 37,945 µm^2, N=5; BxPC-3/PS-1 TRAM-34+gemcitabine: 101,862 ± 34,131 µm^2, N=5) (Figures 38-39). These findings further confirm our *in vivo* data and align with our RNA-seq results, showing that $K_{Ca}3.1$ inhibition decreases EMT, leading to reduced invasiveness in these spheroid models. Yet again, maurotoxin stands out as the most effective treatment in this study, underlining its potential as a key therapeutic option.

$K_V1.3$ channel activity is not detected in PANC-1 cells

To ensure that the observed effects in our spheroid experiments were not due to off-target actions of maurotoxin, we investigated the potential involvement of the $K_V1.3$ channel in PANC-1 cells, as maurotoxin is known to also inhibit $K_V1.3$ (Castle et al., 2003). Our patch-clamp experiments showed no maurotoxin-sensitive voltage-gated K^+ currents in these cells, indicating that $K_V1.3$

channels are not expressed in the plasma membrane of PANC-1 cells. Therefore, the effects of maurotoxin on the spheroids are specifically attributed to $K_{Ca}3.1$ inhibition (Figure 40).

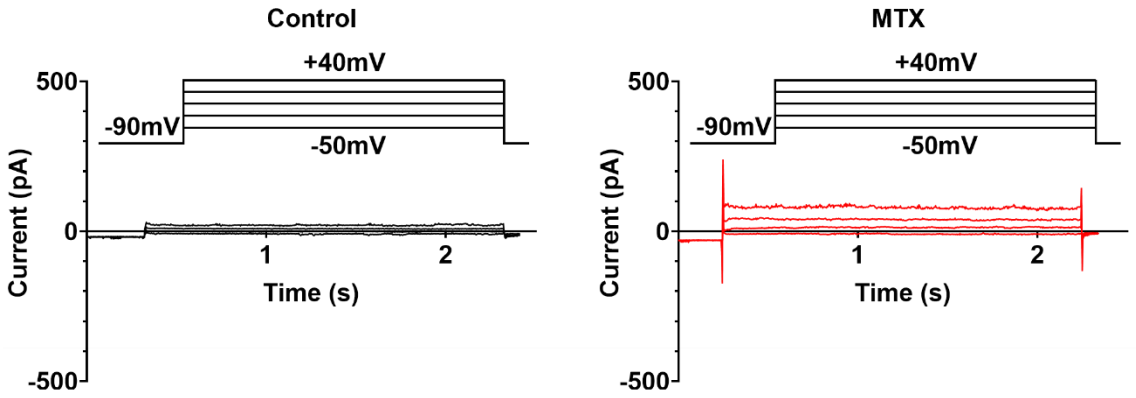

Figure 40. $K_v1.3$ channel activity Is absent in PANC-1 cells. *Representative whole-cell patch-clamp recordings of PANC-1 cells under control conditions (left) and in the presence of 20 nM maurotoxin (MTX) (right). Voltage pulses were applied between −90 and +40 Mv.*

Inhibiting mitochondrial $K_{Ca}3.1$ does not diminish the invasive potential of PANC-1/PS-1 spheroids.

Finally, to verify our hypothesis regarding the differential effects of $K_{Ca}3.1$ based on its localization, we focused on targeting mitochondrial $K_{Ca}3.1$. Using mitochondrially targeted forms of senicapoc (WMS – 98 02, 30 µM and WMS – 98 03, 30 µM) (Figures 8-9) in PANC-1/PS-1 spheroids, we found no difference between the mitochondrial inhibitor-treated spheroids and the control group (control: 241,256 ± 97,363 μm^2, N=5; mito-senicapoc 02: 215,440 ± 92,176 μm^2, N=5; mito-senicapoc 03: 221,660 ± 17,893 μm^2, N=5; negative control 04: 199,941 ± 96,332 μm^2, N=4) (Figure 41), suggesting that the effects we observed *in vitro* are linked to plasma membrane $K_{Ca}3.1$ rather than mitochondrial $K_{Ca}3.1$. This reinforces the idea that plasma membrane $K_{Ca}3.1$ plays a more critical role in the cellular processes in PDAC and further solidifies maurotoxin as a potential therapeutic agent.

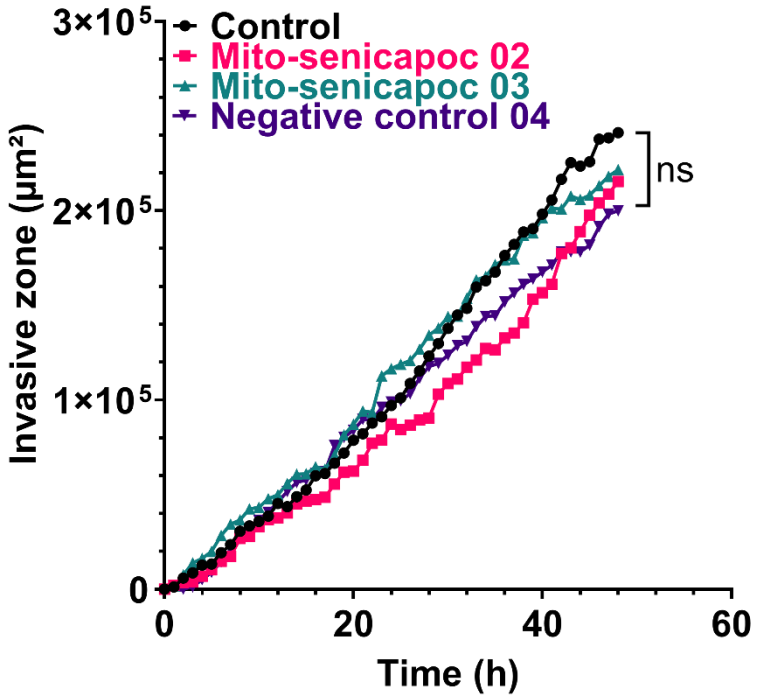

Figure 41. Inhibition of mitochondrial $K_{Ca}3.1$ does not reduce the invasive potential of PANC-1/PS-1 spheroids. *quantification of the invasive potential of PANC-1/PS-1 spheroids was evaluated following treatment with DMSO (control, N=5); mito-senicapoc 02: (WMS – 98 02, N=5); mito-senicapoc 03: (WMS – 98 03, N=5); negative control 04: (WMS – 98 04, N=4).*

PS-1-only spheroids are highly sensitive to gemcitabine

To better understand the variable efficacy of gemcitabine *in vivo* versus *in vitro*, we produced single-cell spheroids composed exclusively of either PANC-1 or PS-1 cells. This strategy enabled us to examine the response of each cell line to gemcitabine in a precise, controlled manner without interference from other cell types.

Our results indicated a trend toward an additive effect of TRAM-34 and gemcitabine on spheroids formed from PANC-1 cells (PANC-1 control: 64,075 ± 11,238 µm^2, N=5; PANC-1 TRAM-34+gemcitabine: 26,674 ± 14,547 µm^2, N=5). However, this effect was not statistically significant (p= 0.3481), implying that while there may be some influence of the drug combination on PANC-1 spheroids, the interaction was not robust enough to confirm a definitive additive or synergistic relationship in this context (Figure 42).

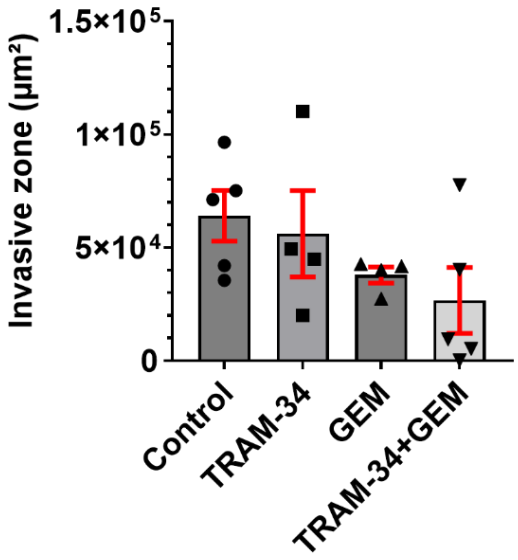

Figure 42. PANC-1-only spheroids show a trend towards additive effects of K_{Ca}3.1 inhibition in combination with gemcitabine on its invasive potential. *Quantification of invasive zones at 48 h in PANC-1-only spheroids treated with DMSO (Control, N=5), TRAM-34 (N=4), gemcitabine (GEM, N=4), or a combination of TRAM-34 and gemcitabine (TRAM-34+GEM, N=5). Data points represent individual spheroid invasive zones.*

In contrast, PS-1 spheroids exhibited an exceptional sensitivity to gemcitabine (Figure 43), leading to a marked reduction in their invasive capacity (PS-1 control: 52,374 ± 27,991 µm^2, N=6; PS-1 gemcitabine: -6,007 ± 3,064 µm^2, N=6) (Figure 44). However, when combined with TRAM-34, the decrease in invasive potential was notably lessened (PS-1 TRAM-34+gemcitabine: 30,826 ± 18,764 µm^2, N=6), suggesting that K_{Ca}3.1 inhibition may interfere with the ability of gemcitabine to limit invasion in PS-1 cells. These observations imply that gemcitabine predominantly targets PSCs in our model, while TRAM-34 seems to be more effective on cancer cells, revealing a complex interplay between the two cell types within the tumor microenvironment.

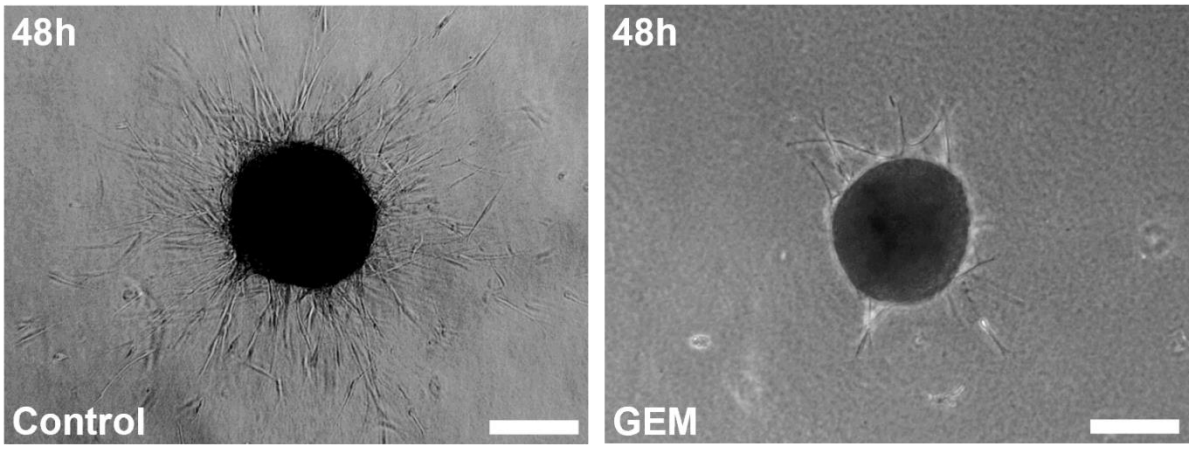

Figure 43. Gemcitabine reduces invasive capacity in PS-1 spheroids. *Representative images illustrating the migration patterns of PS-1-only spheroids treated with either DMSO (control, N=7) or gemcitabine (GEM, N=7). Scale bar=200 µm.*

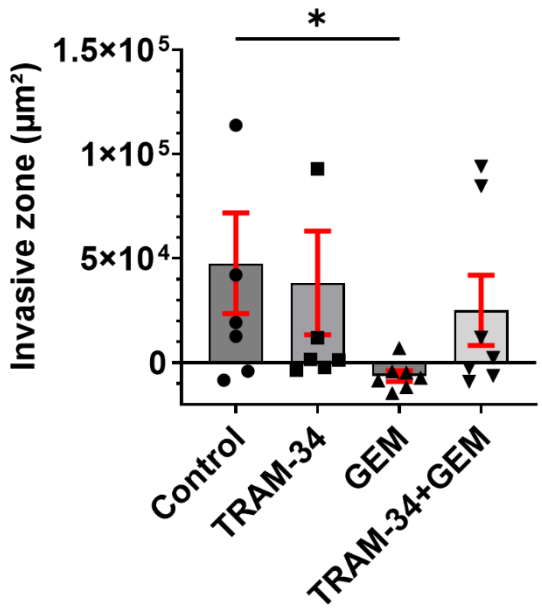

Figure 44. PS-1-only spheroids exhibit strong sensitivity to gemcitabine. *Assessment of invasive zones at 48 hours in PS-1-only spheroids treated with DMSO (control, N=7), TRAM-34 (N=7), gemcitabine (GEM, N=7), or a combination of TRAM-34 and gemcitabine (TRAM-34+GEM, N=7). Data points represent individual spheroid invasive zones. Statistical analysis was performed using a Kruskal-Wallis test with Dunn's post hoc test. *p < 0.05.*

Although PS-1 cells exhibited increased sensitivity to gemcitabine in our *in vitro* models, this does not correlate with our *in vivo* findings where fibrosis increased in tumor nodes following gemcitabine treatment. Given that PSCs should be highly responsive to gemcitabine, we would expect a reduction in fibrosis, not an increase. This paradox suggests that gemcitabine, by altering the PDAC microenvironment (Principe et al., 2020), may trigger a resistance mechanism *in vivo*, leading to enhanced extracellular matrix production as a protective response. This upregulation of matrix synthesis could contribute to the observed increase in desmoplasia. Furthermore, this mechanism might explain the impaired migration of PS-1 spheroids, as the cells appear to prioritize matrix production over motility.

To explore this hypothesis, we quantified the extracellular matrix produced by PANC-1 and PS-1 cells after vitamin C and TGF-β1, in conjunction with our various treatments. This approach allowed us to assess whether gemcitabine could influence matrix production and contribute to the altered migratory behavior observed in PS1 spheroids. Representative images of PS-1 matrix production are shown in Figure 45, highlighting the extent of extracellular matrix deposition in response to the various treatments.

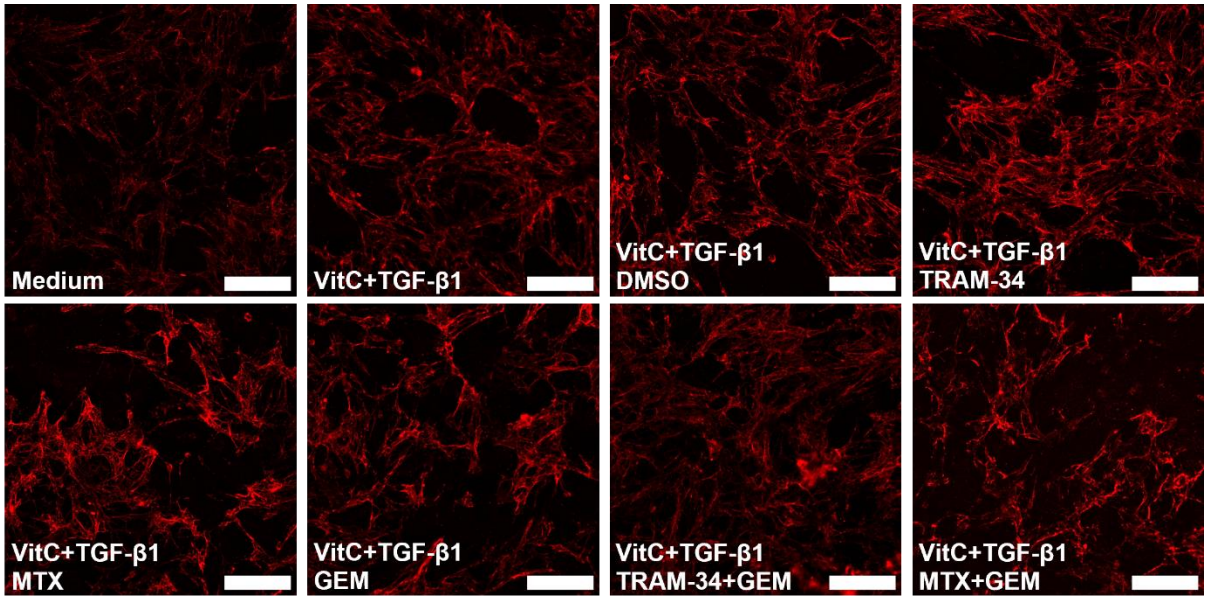

Figure 45. PSC-derived matrix quantity remains unchanged by gemcitabine. *Representative fluorescence images of CNA-35-tdTomato-labeled extracellular collagen (red) in PS-1 cells stimulated with vitamin C (VitC) and TGF-β1. The following treatment conditions are displayed: control (Medium), VitC+TGF-β1, DMSO, TRAM-34, maurotoxin (MTX), gemcitabine (GEM), and combinations of gemcitabine with either inhibitor (TRAM-34+GEM; MTX+GEM). Scale bar=200 µm.*

Our experiments revealed no difference in matrix production when comparing the different treatments within each cell type. In PS-1 cells, matrix production remained consistent across all treatment conditions (medium: 0.29 ± 0.09 a.u., n/N=11/4; VitC+TGF-β1: 0.61 ± 0.10 a.u., n/N=12/4; DMSO: 0,76 ± 0,09 a.u., n/N=12/4; TRAM-34: 0.67 ± 0.13 a.u., n/N=12/; MTX: 0.62 ± 0.11 a.u., n/N=12/; GEM: 0.58 ± 0.07 a.u., n/N=12/; TRAM-34+GEM: 0.46 ± 0.07 a.u., n/N=12/4; MTX+GEM: 0.69 ± 0.18 a.u., n/N=8/4), and similarly, PANC-1 cells showed no variation in matrix production between treatments (medium: 0.11, 95% CI, 0.01-0.23 a.u., n/N=5/4; VitC+TGF-β1: 0.14, 95% CI, 0.02-0.26 a.u., n/N=5/4; DMSO: 0.42, 95% CI, 0.01-1.2 a.u., n/N=5/4; TRAM-34: 0.18, 95% CI, 0.02-0.3 a.u., n/N=5/4; MTX: 0.40, 95% CI, 0.01-0.71 a.u., n/N=5/4; GEM: 0.30, 95% CI, 0.01-1.22 a.u., n/N=5/4; TRAM-34+GEM: 0.27, 95% CI, 0.01-0.66 a.u., n/N=5/4; MTX+GEM: 0,31, 95% CI, 0.01-0.69 a.u., n/N=5/4) (Figure 46).

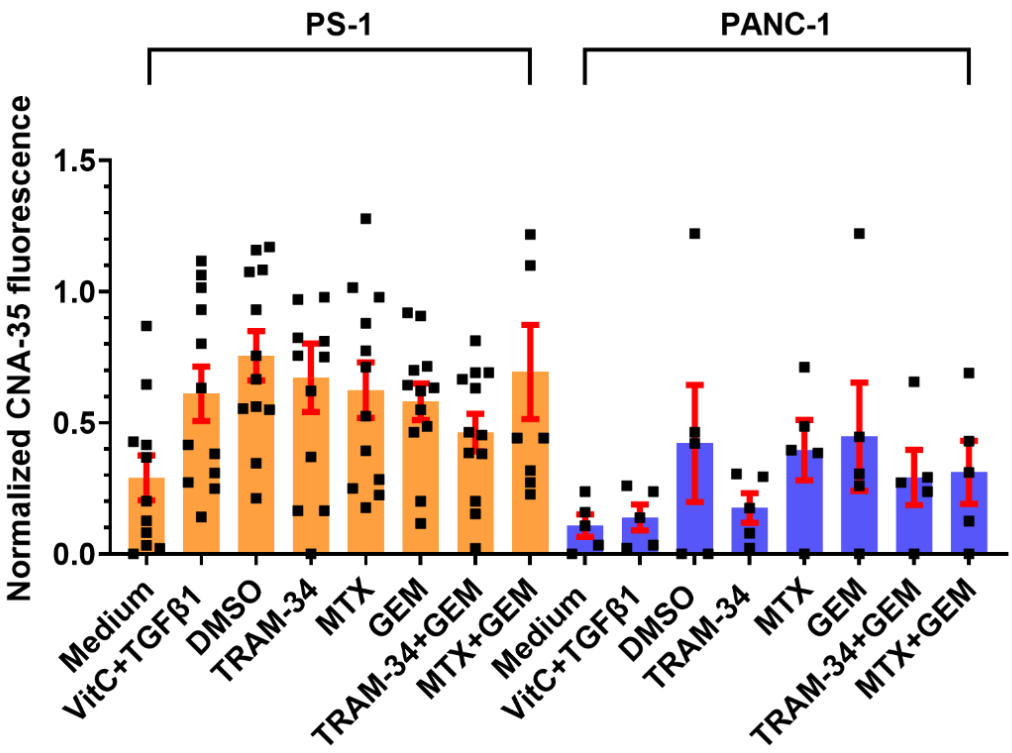

Figure 46. Targeting $K_{Ca}3.1$ and gemcitabine does not alter matrix quantity in PSC- and PDAC-derived cultures. *Quantification of CNA-35-tdTomato fluorescence intensity in PS-1 and PANC-1 cells following stimulation with VitC and TGF-β. medium (PS-1: n/N=11/4; PANC-1: n/N=5/4); VitC+TGF-β (PS-1: n/N=12/4; PANC-1: n/N=5/4), DMSO (PS-1: n/N=12/4; PANC-1: n/N=5/4), TRAM-34 (PS-1: n/N=12/4; PANC-1: n/N=5/4), maurotoxin (MTX: PS-1: n/N=12/4; PANC-1: n/N=5/4), gemcitabine (GEM: PS-1: n/N=12/4; PANC-1: n/N=5/4); TRAM-34+GEM (PS-1: n/N=12/4; PANC-1: n/N=5/4); MTX+GEM (PS-1: n/N=12/4; PANC-1: n/N=5/4). Each data point represents an individual replicate (n).*

Initially, we expected that cancer cells would not produce any matrix, and that the various treatments would therefore have no effect. It was therefore surprising that there was no change at all in matrix production following treatment in PS-1 cells. This might be attributed to the fact that the experiment was conducted in a 2D monolayer setting, where matrix production could differ from what occurs in a 3D environment. Additionally, in a spheroid *in vitro* setup, gemcitabine may have easier access to the cells, whereas *in vivo*, the protective desmoplastic core of the tumor microenvironment could shield spheroids from treatment.

PANC-1-$K_{Ca}3.1^{-/-}$/PS-1 spheroids display diminished cell-cell adhesion

With the new insights we gained regarding the inhibition of $K_{Ca}3.1$ in wild-type PANC-1/PS-1 spheroids, our next step was to compare the behavior of PANC-1-$K_{Ca}3.1^{-/-}$/PS-1 spheroids with that of wild-type PANC-1/PS-1 spheroids and to assess their response to the various treatments we have outlined above.

The PANC-1-$K_{Ca}3.1^{-/-}$/PS-1 spheroids displayed minimal matrix pulling and a loss of spheroid integrity, with cells dispersing from the core and causing the spheroid to nearly collapse (Figure 47).

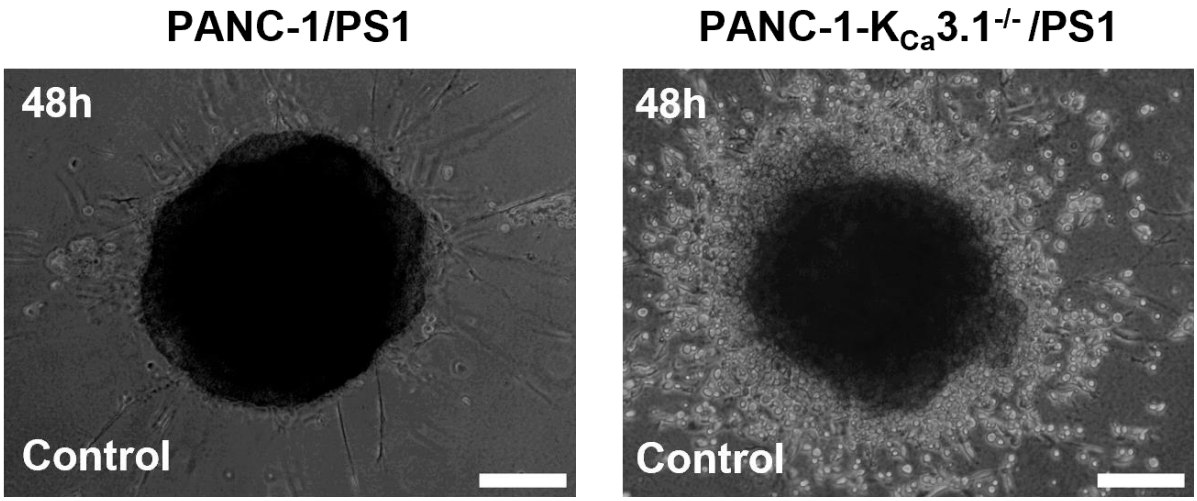

Figure 47. PANC-1-$K_{Ca}3.1^{-/-}$/PS-1 spheroids exhibit reduced cell-cell adhesion. *Representative images showing the migration patterns of PANC-1/PS-1 (N=7) spheroids compared to PANC-1-$K_{Ca}3.1^{-/-}$/PS-1 spheroids (N=14)., both treated with DMSO (Control). Scale bar = 200 µm.*

Unexpectedly, the PANC-1-$K_{Ca}3.1^{-/-}$/PS-1 spheroids were noticeably more invasive than their wild-type counterparts (PANC-1-$K_{Ca}3.1^{-/-}$/PS-1: 270,337 ± 50,459 µm^2, N=14; PANC-1/PS-1: 125,625 ± 17,779 µm^2, N=7) (Figure 48). These observations suggest that $K_{Ca}3.1$ channels may play a crucial role in maintaining cell-cell adhesion and regulating the dynamic behavior of cells within the spheroid. Notably, this mirrors the shifts in migration patterns seen when spheroids were treated with $K_{Ca}3.1$ inhibitors (Figures 36-37).

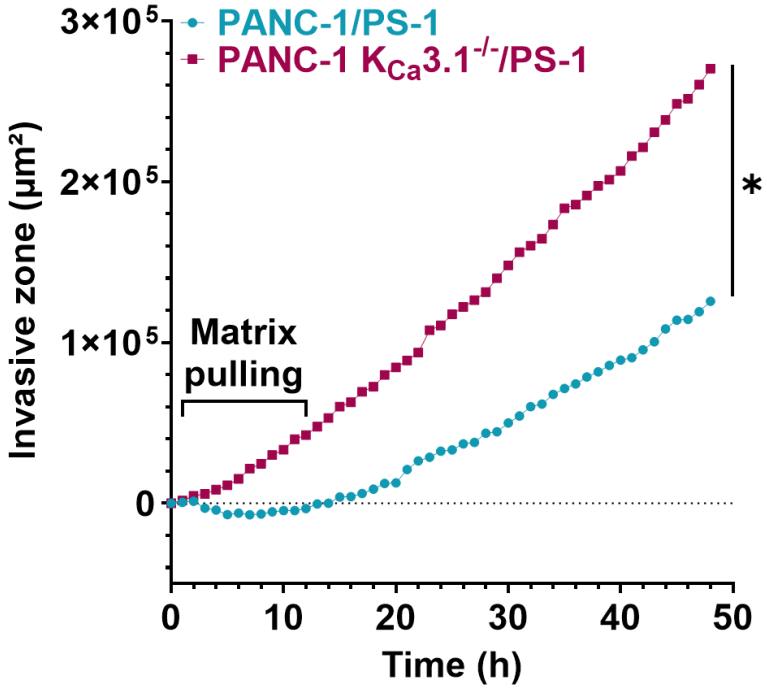

Figure 48. PANC-1-$K_{Ca}3.1^{-/-}$/PS-1 spheroids display greater invasiveness compared to WT PANC-1/PS-1 spheroids. *Comparison of invasive zones between WT PANC-1/PS-1 spheroids (N=7) and PANC-1-$K_{Ca}3.1^{-/-}$/PS-1 spheroids (N=14). Statistical analysis was performed using two-way ANOVA followed by Tukey's multiple comparison test. *p < 0.05.*

Moreover, PANC-1-$K_{Ca}3.1^{-/-}$/PS-1 spheroids showed no response to $K_{Ca}3.1$ inhibitors (Figure 49), whether used alone or in combination with gemcitabine. The only notable effect was attributed to gemcitabine itself, which significantly reduced the invasive potential of spheroids. (control: 341,269 ± 67,874 µm^2, N=10; gemcitabine: 164,226 ± 60,640 µm^2, N=11) (Figure 50). These results align with our previous findings showing that PSCs remain largely unaffected by $K_{Ca}3.1$ inhibition. Furthermore, this lack of response in the knockout model further confirms the specificity of these inhibitors for the $K_{Ca}3.1$ channel and highlights its critical role in cancer cell behavior.

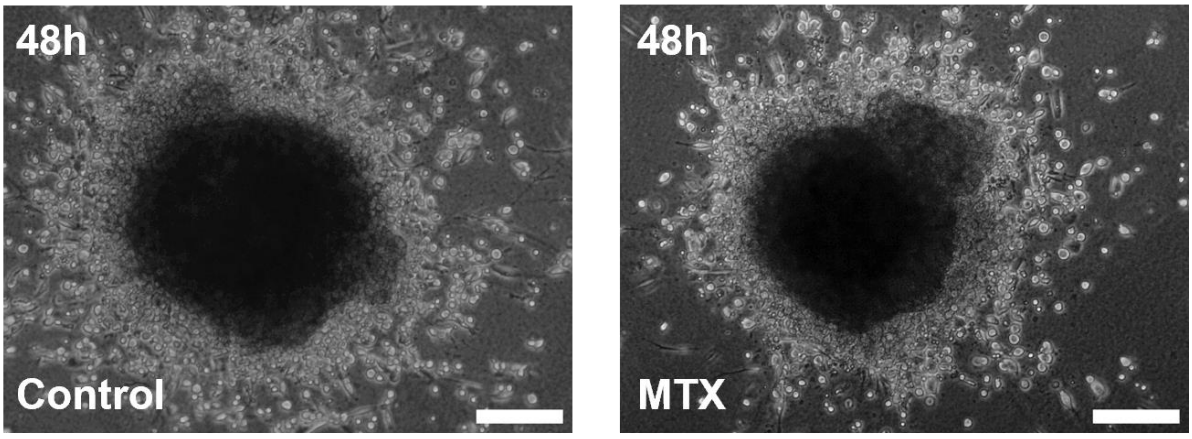

***Figure* 49. Maurotoxin does not alter migration in PANC-1-$K_{Ca}3.1^{-/-}$/PS-1 spheroids.** Representative images showing the migration patterns of PANC-1-$K_{Ca}3.1^{-/-}$/PS-1 spheroids treated with either DMSO (Control, N=10) or maurotoxin (MTX, N=5). Scale bar = 200 µm.

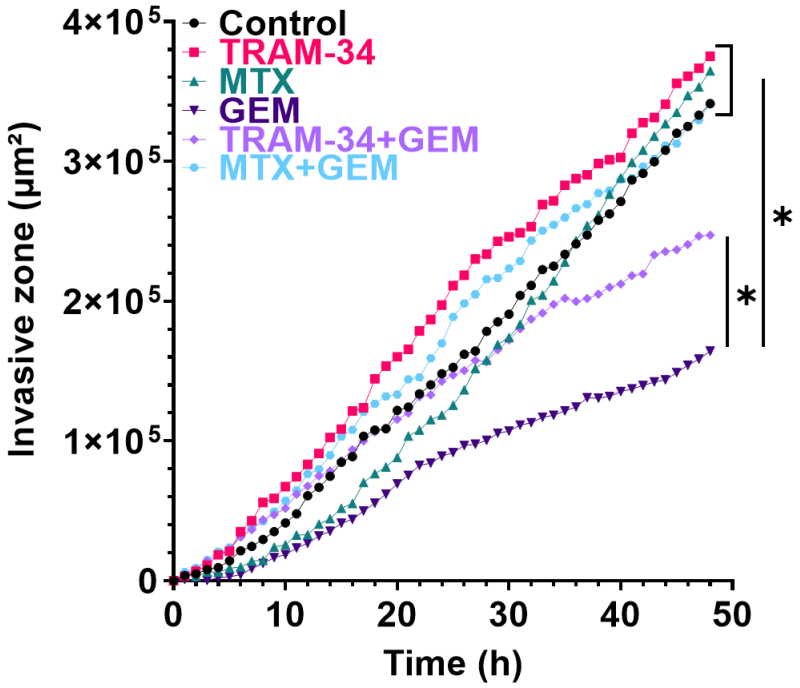

Figure 50. Gemcitabine reduces the invasive potential of PANC-1-$K_{Ca}3.1^{-/-}$/PS-1 spheroids, while $K_{Ca}3.1$ inhibitors show no additional effect. *Assessment of the invasive potential of PANC-1-$K_{Ca}3.1^{-/-}$/PS-1 spheroids following treatment with DMSO (Control, N=10), TRAM-34 (N=6), maurotoxin (MTX, N=5), gemcitabine (GEM, N=11), or a combination of either inhibitor with gemcitabine (TRAM-34+GEM, N=7; MTX+GEM, N=5). Statistical analysis was performed using two-way ANOVA followed by Tukey's multiple comparison test. *$p < 0.05$.*

Inhibition of plasma membrane $K_{Ca}3.1$ with maurotoxin induces cell death

Based on our RNA-seq and immunohistochemistry findings, we shifted our focus to cell death as a potential explanation to correlate the decreased tumor node size observed *in vivo* and the reduced invasiveness of treated spheroids.

PANC-1/PS-1 spheroids were stained with Annexin-V following a 24-h treatment period (Figure 51).

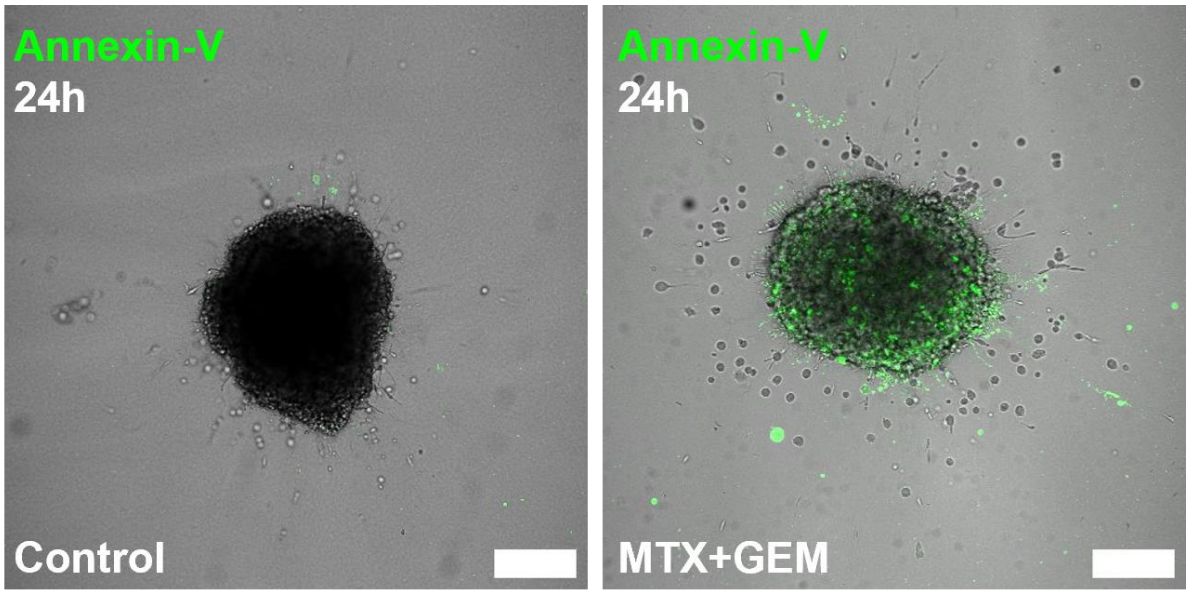

Figure 51. Representative images showing of Annexin-V staining in PANC-1/PS-1 spheroids following 24 h of treatment. *The figure compares a control spheroid (N=8) with one treated with maurotoxin and gemcitabine (MTX+GEM, N=6). Scale bar = 250 µm.*

Maurotoxin treatment resulted in a substantial increase in cell death within the spheroids (control: 1% ± 0.4%, N=8; maurotoxin: 17.3% ± 1.9%, N=10) (Figure 52). When combined with gemcitabine (maurotoxin+gemcitabine: 28.4% ± 4,4%, N=6), this effect became even more pronounced, offering insight into the molecular mechanisms responsible for the observed decrease in spheroid invasiveness. These findings suggest that the enhanced cell death may play a key role in limiting the invasive potential of the treated spheroids.

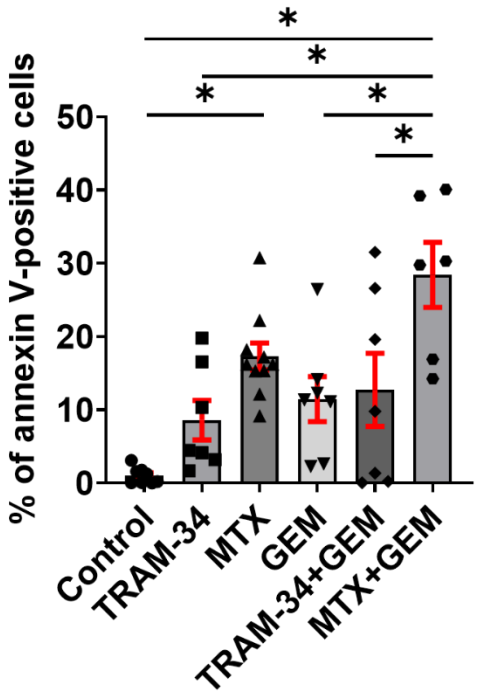

Figure 52. The inhibition of plasma membrane $K_{Ca}3.1$ with maurotoxin, combined with gemcitabine, induces cell death. *Evaluation of Annexin V-positive cells in spheroids following 24 h of treatment (Control: N=8; TRAM-34: N=7; MTX: N=10; GEM: N=7; TRAM-34+GEM: N=7; MTX+GEM: N=6). Data points represent individual spheroids. Statistical analysis was carried out using one-way ANOVA with Tukey's multiple comparison test. *p < 0.05.*

Additional assays, including the CellTox™ Green Cytotoxicity Assay and RealTime-Glo™ MT Cell Viability Assay, confirmed the superior effectiveness of combining maurotoxin with gemcitabine. These experiments revealed an increase in cytotoxicity and a corresponding drop in cell viability when spheroids were treated with the combination treatment (Figure 53-54). Notably, the combination of maurotoxin and gemcitabine was more effective than either treatment alone, and surpassed the effect of TRAM-34 combined with gemcitabine (Cytotoxicity: control: 189 ± 28 a.u., N=5; maurotoxin+gemcitabine: 380 ± 51 a.u., N=5 ; TRAM-34+gemcitabine: 206 ± 38 a.u., N=5; Viability: control: 105,860 ± 8,702 a.u. , N=5; maurotoxin+gemcitabine: 6,110 ± 3,736 a.u., N=5 ; TRAM-34+gemcitabine: 37,780 ±10,792 a.u. N=5). These results suggest maurotoxin as a promising complementary adjunct to chemotherapy in PDAC, explaining its stronger impact on spheroid invasiveness compared to TRAM-34.

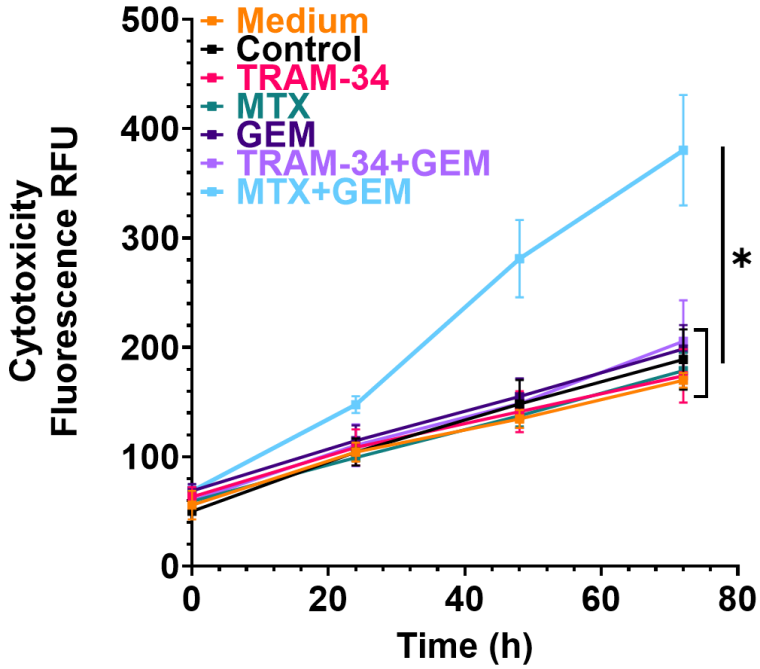

Figure 53. Inhibition of $K_{Ca}3.1$ with maurotoxin and its combination with gemcitabine increase cytotoxicity in PANC-1/PS-1 spheroids. *Cytotoxicity was quantified over a 72h period using the CellTox™ Green assay, where fluorescence intensity (RFU) served as an indicator of cell death in PANC-1/PS-1 spheroids. Treatments included DMSO (Control, N=3), TRAM-34 (N=4), maurotoxin (MTX, N=5), gemcitabine (GEM, N=5 and the combination of TRAM-34 or maurotoxin with gemcitabine (TRAM-34+GEM: N=5; MTX+GEM: N=5). The "Medium" condition represented untreated spheroids assessed with CellTox Green. Statistical significance was determined by two-way ANOVA followed by Tukey's multiple comparison test. *p < 0.05.*

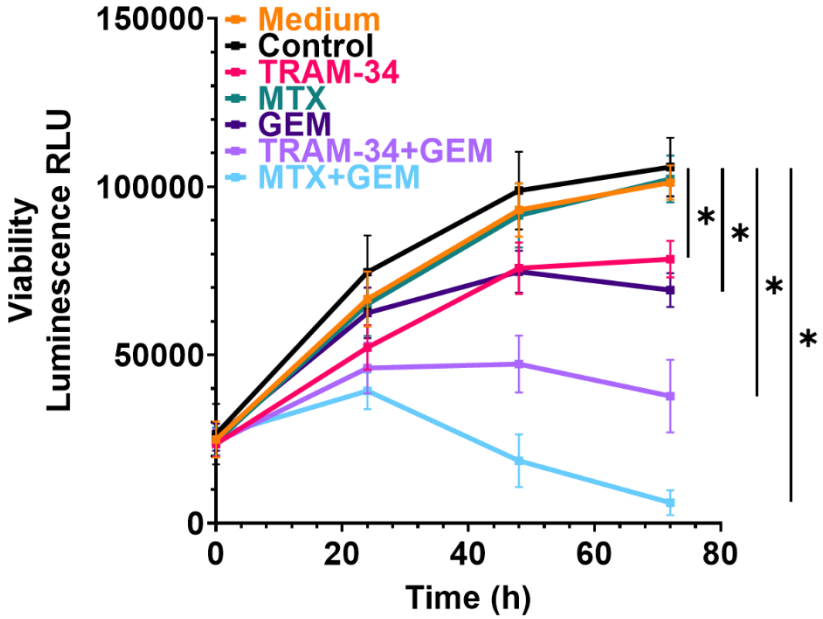

Figure 54. Inhibition of $K_{Ca}3.1$ with maurotoxin and its combination with gemcitabine decrease the viability of the cells in PANC-1/PS-1 spheroids. *Spheroid viability was assessed over a 72h period using the CellTiter-Glo assay across different treatment conditions: Control (N=3), TRAM-34 (N=4), maurotoxin (MTX, N=4), gemcitabine (GEM, N=5), TRAM-34 combined with gemcitabine (TRAM-34+GEM, N=5), and maurotoxin combined with gemcitabine (MTX+GEM, N=5). Luminescence (RLU) values represent metabolic activity, serving as a proxy for cell viability. The "Medium" condition refers to spheroids assessed with CellTiter-Glo without additional treatments. Statistical significance was determined using two-way ANOVA followed by Tukey's multiple comparison test. *p < 0.05.*

These findings align with our previous cell death experiments in KPfC tissue, further highlighting the role of the tumor microenvironment in mitigating the effects of gemcitabine. Collectively, these results indicate that the cytotoxic effect of $K_{Ca}3.1$ channel inhibition is primarily due to the targeting of plasma membrane $K_{Ca}3.1$ activity. Importantly, by enhancing gemcitabine-induced cytotoxicity, maurotoxin emerges as a promising candidate in potentially impairing tumor progression and improving treatment outcomes in PDAC.

DISCUSSION

PDAC remains one of the most lethal cancers (Park et al., 2021; Tirpe et al., 2024), primarily due to its resistance to conventional treatments such as gemcitabine (Koltai et al., 2022). The tumor microenvironment in PDAC is particularly hostile (Blaszczak & Swietach, 2021; S. F. Pedersen et al., 2017), characterized by extensive fibrosis, hypoxia, and poor vascularization, all of which contribute to treatment failure (Provenzano et al., 2012; Sperb et al., 2020; Tao et al., 2021). In this context, a promising novel approach is targeting ion channels (Kischel et al., 2019; M. Li et al., 2023). In PDAC, the calcium-activated potassium channel $K_{Ca}3.1$ has gained attention for its role in various aspects of tumor biology, including cell proliferation, migration, and apoptosis resistance (Bonito et al., 2016; Jäger et al., 2004; Mo et al., 2022).

The aim of our study was to investigate the therapeutic potential of $K_{Ca}3.1$ inhibition in PDAC by combining *in vitro* and *in vivo* models to better reflect the complexity of the tumor microenvironment. Specifically, we explored how inhibiting $K_{Ca}3.1$, both alone and in combination with gemcitabine, affected tumor growth, cell death, migration, and fibrosis. So far, most studies, have focused almost exclusively on $K_{Ca}3.1$ in PDAC from a narrow, two-dimensional viewpoint, centering primarily on cancer cells (Bonito et al., 2016; Jäger et al., 2004). However, the broader and more intricate dynamics involving other $K_{Ca}3.1$-expressing cells, such as PSCs and immune cells, which play a crucial role in driving tumor progression, have been largely overlooked. The novelty of our study lies in the use of an immunocompetent genetically engineered mouse model (KPfC) (Hingorani et al., 2003; Olive et al., 2004), which closely resembles the human PDAC, as well as the development of a three-dimensional (3D) *in vitro* co-culture spheroid model embedded in a collagen matrix that simulates the pancreatic ECM. Both models mimicked important features of the complex interactions of the tumor cells with their microenvironment. This approach allowed us to examine not only the effects on tumor cells but also the interplay between cancer cells and other $K_{Ca}3.1$-expressing cells in the tumor microenvironment, such as fibrosis-producing pancreatic stellate cells (PSCs) and immune cells.

Targeting plasma membrane $K_{Ca}3.1$ in PDAC impairs cancer progression

Our data revealed new insights into the effect of $K_{Ca}3.1$ inhibition in PDAC. The potential prognostic significance of $K_{Ca}3.1$ expression in PDAC was first explored through survival analysis using the Kaplan-Meier Plotter tool. Drawing on large-scale RNA-seq datasets from sources like GEO, EGA, and TCGA, the Kaplan-Meier survival analysis revealed a significant correlation between high $K_{Ca}3.1$ expression and reduced overall survival. Patients in the high-expression group had notably poorer survival outcomes compared to those with lower $K_{Ca}3.1$ expression. Building upon this, we further analyzed $K_{Ca}3.1$ expression in our own cohort of PDAC patients using qPCR. When the cohort was dichotomized into high- and low-expression groups based, we observed a trend suggesting that patients with higher $K_{Ca}3.1$ expression had also a shorter overall survival. This trend was consistent with the Kaplan-Meier Plotter results and with previous studies (S. Jiang et al., 2017), reinforcing the potential role of $K_{Ca}3.1$ as a prognostic indicator in PDAC.

Exploring the inhibition of $K_{Ca}3.1$ channels, both as a stand-alone and in combination with gemcitabine, delivered promising results in both *in vivo* and *in vitro* settings. We targeted $K_{Ca}3.1$ using two specific $K_{Ca}3.1$ inhibitors: TRAM-34 and maurotoxin. TRAM-34 is a selective small molecule inhibitor of the $K_{Ca}3.1$ channel (Wulff et al., 2000) which blocks both plasma membrane and mitochondrial $K_{Ca}3.1$ channels. Maurotoxin, a peptide inhibitor, was used to specifically target $K_{Ca}3.1$ channels located in the plasma membrane of cells (Castle et al., 2003).

The inhibition of $K_{Ca}3.1$ resulted in a substantial reduction in tumor size *in vivo* and impaired cancer cell migration *in vitro*. Notably, maurotoxin stood out in this study showing superior efficacy over TRAM-34 in both *in vitro* and *in vivo* settings underscoring its potential as a stronger therapeutic option for PDAC. This finding is particularly novel, as previous studies have typically reported only limited effects of maurotoxin in targeting $K_{Ca}3.1$ channels (Bulk et al., 2022; Todesca et al., 2024). Maurotoxin monotherapy, as well as its combination with gemcitabine, effectively reduced the size of tumor nodes and induced cell death *in vivo* suggesting that it disrupts essential tumor survival mechanisms. Moreover, the combination treatment significantly mitigated gemcitabine-induced fibrosis. *In vitro*, inhibiting $K_{Ca}3.1$ with maurotoxin, both alone and in combination with gemcitabine, led to impaired cancer cell migration and further promoted cell death in the co-culture spheroid model.

We gained further insight into the underlying mechanisms of $K_{Ca}3.1$ inhibition by comparing spheroids composed of $K_{Ca}3.1^{-/-}$ PDAC cells co-cultured PSCs to those containing wild-type PDAC cells and PSCs. This approach allowed us to closely examine the molecular alterations resulting from $K_{Ca}3.1$ deletion. Through RNA sequencing analysis (GEO: GSE279207), we identified four key pathways that were significantly affected: IFN-α and IFN-γ signaling, G2-M checkpoint regulation, and epithelial-mesenchymal transition (EMT). These findings provided important clues as to why $K_{Ca}3.1$ inhibition effectively reduced tumor nodes size. The downregulation of the G2/M checkpoint, a critical regulator of cell cycle progression (de Gooijer et al., 2017), indicates that $K_{Ca}3.1$ inhibition may impair the ability of cancer cells to successfully transition from the G2 phase to mitosis. This disruption of cell cycle progression can lead to mitotic catastrophe, a mechanism of cell death triggered by improper cell division (Mc Gee, 2015). When cells fail to properly pass the G2/M checkpoint, they accumulate DNA damage and are more likely to undergo apoptosis or other forms of cell death. Additionally, the downregulation of EMT likely contributed to reduced cancer cell migration and metastatic potential (S. Wang et al., 2017). Together, these effects provide a mechanistic explanation for the improved therapeutic outcomes observed with $K_{Ca}3.1$ inhibition, highlighting both its direct impact on tumor cells and its broader effects on the tumor microenvironment, including reduced cell migration and enhanced susceptibility to cell death.

Our findings suggest that $K_{Ca}3.1$ inhibition, particularly with maurotoxin, offers a promising therapeutic strategy for PDAC.

Figure 55 illustrates the specific effects of plasma membrane $K_{Ca}3.1$ inhibition on tumor progression, highlighting how this targeted approach leads to reduced tumor size, impaired cell invasion, and enhanced cell death in PDAC.

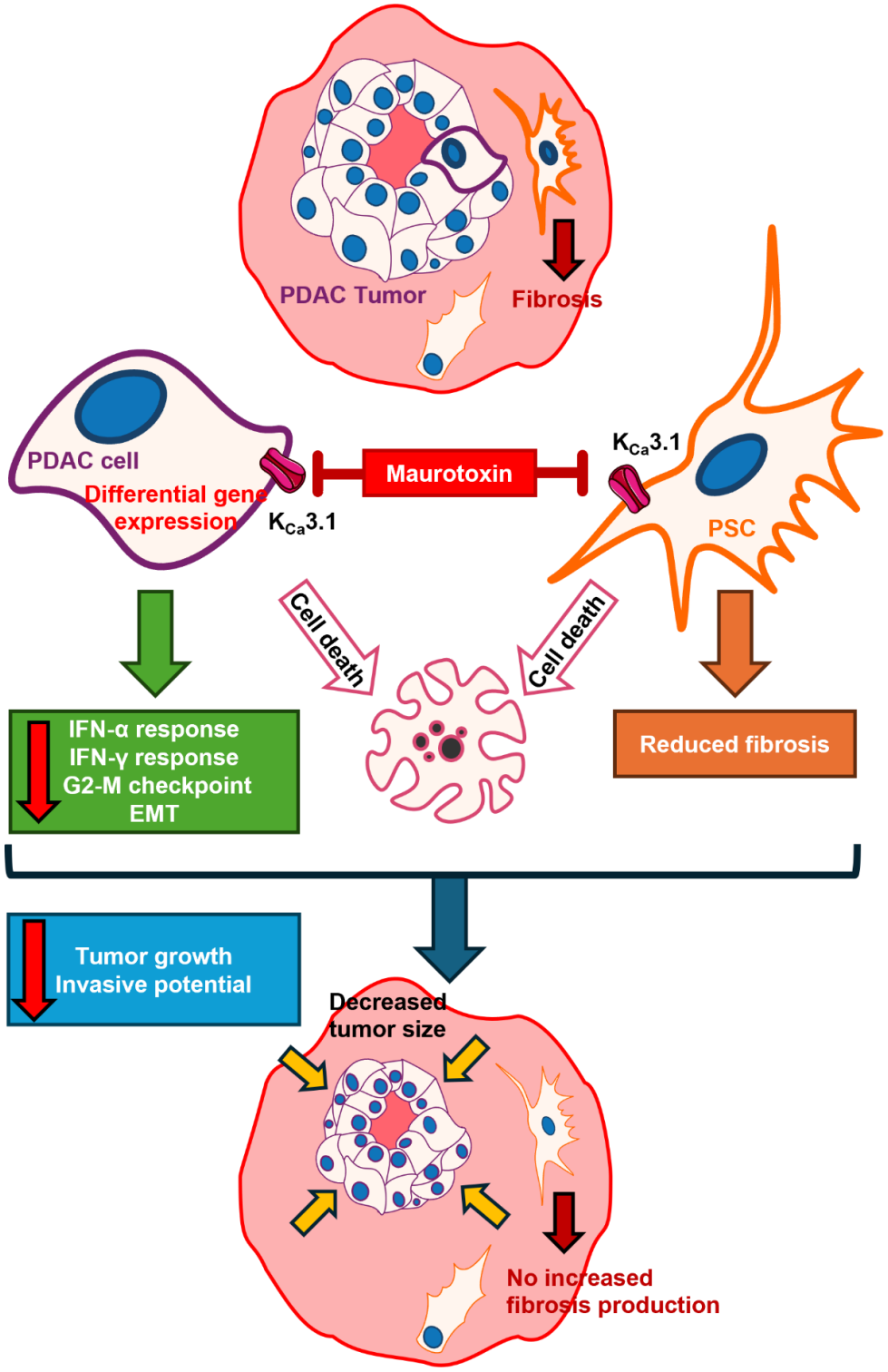

Figure 55. Inhibition of plasma membrane $K_{Ca}3.1$ channels in PDAC reduces tumor growth and promotes cell death. *This figure illustrates the impact of targeting plasma membrane $K_{Ca}3.1$ channels PDAC and PSCs using maurotoxin. PDAC tumor nodes are typically encapsulated within a dense fibrotic stroma, largely driven by PSCs. Maurotoxin, by targeting plasma membrane $K_{Ca}3.1$ channels in both PDAC cells and PSCs, induces significant gene expression changes in the tumor cells, leading to a marked reduction in their invasive potential. Additionally, this inhibition reduces fibrosis and induces cell death in both PDAC cells and PSCs. As a result, tumor growth is decreased without triggering desmoplasia. The figure includes elements created using Servier Medical Art, licensed under Creative Commons Attribution 3.0 unported.*

Mitochondrial $K_{Ca}3.1$ plays a limited role in PDAC progression

Our results suggested that $K_{Ca}3.1$ may have distinct functions depending on its subcellular localization. *In vitro*, inhibiting plasma membrane $K_{Ca}3.1$ with maurotoxin significantly reduced the invasiveness of PDAC spheroids, outperforming TRAM-34, which inhibits $K_{Ca}3.1$ in both the plasma membrane and in the inner membrane of mitochondria (Bulk et al., 2022). Inhibiting mitochondrial $K_{Ca}3.1$ channels appears to counteract the effects of blocking those in the plasma membrane. In contrast, in non-small cell lung cancer (NSCLC), only mitochondrial $K_{Ca}3.1$ inhibition contributes to overcome resistance to therapy resistance (Todesca et al., 2024). This suggests a tumor-specific function for $K_{Ca}3.1$.

To clarify the differential effects based on $K_{Ca}3.1$ localization, we investigated mitochondrial $K_{Ca}3.1$ using mitochondrially targeted forms of senicapoc (WMS-98 02 and WMS-98 03) in PANC-1/PS-1 spheroids. Our results showed no significant differences between mitochondrial inhibitor-treated spheroids and the control group, suggesting that the effects we observed *in vitro* were not linked to mitochondrial $K_{Ca}3.1$ but rather to the plasma membrane form of $K_{Ca}3.1$. This reinforces the notion that plasma membrane $K_{Ca}3.1$ plays a critical role in the cellular processes driving PDAC progression, particularly regarding tumor invasiveness, cell death, and the modulation of the tumor microenvironment.

Furthermore, this observation strengthens the hypothesis that the effects of maurotoxin are predominantly due to its inhibition of plasma membrane $K_{Ca}3.1$, rather than its impact on other ion channels like $K_V1.3$. Knowing that maurotoxin also inhibits $K_V1.3$ channels, which have been proposed as a therapeutic target in pancreatic cancer (Patel et al., 2023), we initially considered whether this could explain the effects we observed. However, previous studies have shown that the impact of $K_V1.3$ in PDAC is largely linked to its mitochondrial form (Patel et al., 2023). Maurotoxin specifically blocks plasma membrane channels (Todesca et al., 2024). Therefore, it seems unlikely that $K_V1.3$ inhibition alone accounts for the benefits observed in our study. Moreover, our patch clamp experiment showed no evidence of maurotoxin-sensitive voltage-gated K^+ currents in PANC-1 cells.

Our findings, therefore, indicate that plasma membrane $K_{Ca}3.1$ inhibition is the primary driver of the outcomes seen in our study. Consequently, targeting $K_{Ca}3.1$ channels in the plasma membrane with maurotoxin appears to be a promising therapeutic strategy for PDAC. In contrast, mitochondrial $K_{Ca}3.1$ channels have a less dominant role in PDAC.

$K_{Ca}3.1$ inhibition restores T-cell functions

$K_{Ca}3.1$ is expressed in the plasma membranes of lymphocytes, and plays a critical role in the immune response (Cahalan & Chandy, 2009; Feske et al., 2015). Despite the expectation that inhibiting the channel might suppress the anti-tumor immune response, we unexpectedly found a greater immune cell infiltration in tumors treated with maurotoxin. Furthermore, $K_{Ca}3.1$ inhibition appeared to restore T-cell function; this paradox might be explained by two potential mechanisms. First, the reduction in tumor fibrosis, due to $K_{Ca}3.1$ inhibition, may have enhanced immune cell access to the tumor microenvironment (Pethő et al., 2023; Renkawitz et al., 2019).

Second, $K_{Ca}3.1$ inhibition might have influenced the expression of genes associated with T-cell exhaustion, as suggested by our RNAseq data and supported by recent findings (Gawali et al., 2021; Sharma et al., 2024). This restoration of T-cell activity could explain the enhanced anti-tumor effects seen in both monotherapy and combination treatments. More research is needed to explore how $K_{Ca}3.1$ inhibition affects immune regulation, particularly in relation to T-cell exhaustion and its interaction with IFN-α and IFN-γ signaling pathways.

Gemcitabine shows variable efficacy across models

One of the unexpected findings of our study was the differential response of cells to gemcitabine *in vitro* versus *in vivo*. *In vitro*, gemcitabine alone exhibited a strong inhibitory effect on the invasive potential of the mixed spheroids, but this effect was diminished when combined with TRAM-34. This suggests that the efficacy of the treatment is likely cell context dependent. In particular, PS-1 only spheroids showed heightened sensitivity to gemcitabine, indicating that the drug was primarily affecting PSCs. Conversely, TRAM-34 primarily impacted cancer cells suggesting that each treatment influences different cellular components within the tumor. This interplay points to the complexity of the microenvironment of PDAC, where both stromal and cancer cell interactions shape the therapeutic outcome.

However, these *in vitro* results were not mirrored *in vivo*, where gemcitabine had no discernible impact on tumor size in KPfC mice. A plausible explanation for this discrepancy is the absence of fibrosis *in vitro*, which may have allowed gemcitabine to act more directly on the cells. *In vivo*, the dense fibrotic stroma likely acted as a barrier, shielding the tumor from the drug and leading to treatment failure (Provenzano et al., 2012). In the KPfC mice, we observed gemcitabine-induced matrix production, a known mechanism of resistance in PDAC (Principe et al., 2020). Additionally, gemcitabine resistance is often linked to EMT (Koltai et al., 2022). Our study showed that $K_{Ca}3.1$ inhibition not only reduced fibrosis but also inhibited EMT, suggesting that targeting $K_{Ca}3.1$ could mitigate two major contributors to gemcitabine resistance. Therefore, targeting $K_{Ca}3.1$ offers a promising strategy not only to enhance the effects of chemotherapy but also to address potential mechanisms of treatment resistance in PDAC.

Investigating the effects of treatment on matrix production, we aimed to understand whether gemcitabine or $K_{Ca}3.1$ inhibitors could alter the deposition of extracellular matrix in cancer cells and PSCs. Based on the established view that pancreatic cancer cells typically rely on PSCs for matrix production, we initially expected that matrix production would be affected only in the stromal cells by these treatments, and that cancer cells would remain unaffected. Contrary to our expectations, no changes in matrix production were observed in PSCs cells after treatment, indicating that neither gemcitabine nor $K_{Ca}3.1$ inhibition had an impact on matrix deposition *in vitro*.

This lack of effect *in vitro* highlights a fundamental difference between the cellular environment of our *in vitro* models and the more complex tumor microenvironment seen *in vivo*. Our *in vivo* results clearly showed that gemcitabine induced matrix production. The discrepancy between *in vitro* and *in vivo* findings underscores the complexity of the PDAC microenvironment in modulating drug response. Without the fibrotic barrier present *in vitro*, gemcitabine acted directly on the cells, thus explaining the stronger inhibitory effects observed and the lack of neo-synthesized matrix. Furthermore, although our complex matrix was designed to closely resemble the PDAC microenvironment, we acknowledge that it may not fully capture the intricacies of the

in vivo tumor stroma. Factors such as the degree of collagen cross-linking and the density of the collagen network may differ in vivo, affecting drug delivery and therapeutic outcomes in ways that are challenging to replicate *in vitro (Song et al., 2022)*. Thus, while the *in vitro* models provide valuable insights, these results emphasize the need to account for tumor-stromal interactions in therapeutic strategies in PDAC.

$K_{Ca}3.1$ inhibition alters cell-cell adhesion in PDAC

The loss of cell-cell adhesion observed in PANC-1- $K_{Ca}3.1^{-/-}$/PS-1 spheroids highlights the crucial role of this channel in maintaining cellular interactions within the PDAC tumor microenvironment. When treated with $K_{Ca}3.1$ inhibitors, the wild-type mixed spheroids displayed changes in cell migration patterns, with more rounded cells emerging from the spheroids instead of the typical spindle-shaped, mesenchymal-like cells. This shift suggests that $K_{Ca}3.1$ inhibition disrupts cell-cell adhesion, which may alter the invasive behavior of tumor cells. The roundish morphology observed could indicate a transition to a more epithelial-like state, which contrasts with the elongated, migratory form typically associated with invasive mesenchymal cells. This aligns with our RNA-seq data, which shows a reduction in EMT.

Interestingly, these findings differ from previous observations in non-small cell lung cancer (NSCLC), where $K_{Ca}3.1$ inhibition increased cell-matrix adhesion and reduced tumor cell migration (Todesca et al., 2024). This contrast suggests that $K_{Ca}3.1$ inhibition likely triggers distinct intracellular signaling pathways in PDAC compared to NSCLC. In NSCLC, mitochondrial ROS plays a central role in $K_{Ca}3.1$-dependent signaling. In PDAC the disruption of intracellular Ca^{2+} homeostasis might be the key intermediary when $K_{Ca}3.1$ channels are blocked in the plasma membrane. This difference in signaling cascades may explain why $K_{Ca}3.1$ inhibition affects cell behavior differently across these two tumor types, reinforcing the idea that $K_{Ca}3.1$ functions in a tumor-specific manner.

While the disruption of cell-cell adhesion *in vitro* raises questions about its implications *in vivo*, our data show that it did not lead to increased metastasis or a higher number of tumor nodes in KPfC mice. None of the mice treated with $K_{Ca}3.1$ inhibitors exhibited metastasis, and the number of tumor nodes remained comparable between treated and untreated groups. This suggests that while $K_{Ca}3.1$ inhibition alters cellular adhesion and migration patterns *in vitro*, these changes do not necessarily translate into more aggressive or metastatic behavior *in vivo*.

One possible explanation for this is that the looser adhesion observed in treated cells may have allowed better penetration of gemcitabine into the tumor tissue, potentially enhancing its efficacy. The disruption of cell-cell adhesion might facilitate greater drug access to the tumor core (Khalili & Ahmad, 2015). Alternatively, the weakening of cell-cell interactions could also increase cell susceptibility to cell death mechanisms, such as anoikis (Y. N. Kim et al., 2012), which occurs when cells detach from their neighbors and the extracellular matrix. Thus, while disruption of cell-cell adhesion is often linked to processes like EMT and metastasis, it could also expose vulnerabilities in tumor cells that can be exploited by treatments like gemcitabine.

Further research is needed to fully understand how $K_{Ca}3.1$ inhibition modulates intracellular signaling in PDAC and its impact on treatment response.

Strengths and limitations of our model

One of the key strengths of this study lies in the innovative model systems we employed. The 3D spheroid model, embedded in a collagen matrix is a significant improvement over traditional 2D models, which fail to capture the complexity of the PDAC tumor microenvironment. Similarly, the KPfC mouse model, which is immunocompetent and replicates the human PDAC microenvironment, enabled us to assess the effects of $K_{Ca}3.1$ inhibition in a more clinically relevant setting. Importantly, this study provides novel *in vivo* data on $K_{Ca}3.1$ targeting in PDAC which represents a significant advancement in understanding its therapeutic potential. However, while our 3D *in vitro* models provide valuable insights into ECM interactions, it lacks important physiological components, such as immune responses. One way to enhance the relevance of our 3D models would be the introduction of immune cells. This would allow us to better simulate the immune-tumor interactions that occur *in vivo* and provide a better understanding of how $K_{Ca}3.1$ targeting affects both cancer cells and immune dynamics. This improvement could help bridge the gap between *in vitro* and *in vivo* studies and improve the translational relevance of our findings.

Relevance of the study

This study is the first to show the efficacy of maurotoxin in targeting $K_{Ca}3.1$ channels in PDAC *in vivo*, highlighting its therapeutic potential in a clinically relevant setting. Many previous investigations on $K_{Ca}3.1$ inhibition in PDAC were limited to *in vitro* studies, without addressing the subcellular localization of the channel. By specifically targeting plasma membrane $K_{Ca}3.1$ channels with maurotoxin, our study provides novel insights into the distinct roles of channel localization in PDAC progression and offers a promising avenue for therapeutic intervention.

Moreover, our work introduces mechanistic insights that have not been explored before. Through RNA sequencing analysis, we identified novel gene regulatory pathways that are modulated upon $K_{Ca}3.1$ inhibition. These discoveries offer a deeper understanding of the molecular mechanisms underpinning PDAC and highlight the specific gene networks that may contribute to tumor progression when $K_{Ca}3.1$ channels are blocked.

We also evaluated the effects of a mitochondrially targeted senicapoc, specifically designed to inhibit mitochondrial $K_{Ca}3.1$ channels, in PDAC cells. Despite this targeted approach, we observed no significant impact on PDAC progression in the spheroid model, indicating that mitochondrial $K_{Ca}3.1$ is not a key driver in this cancer. While being in line with our other results, this observation contrasts with findings in other cancers, such as non-small cell lung cancer (Todesca et al., 2024), where mitochondrial $K_{Ca}3.1$ has been implicated in tumor growth and survival. These results underscore the importance of focusing on plasma membrane $K_{Ca}3.1$ channels in PDAC, a strategy that is unprecedented in the context of this malignancy.

Despite these advances, there are uncertainties regarding the clinical application of maurotoxin in patients. Its safety, pharmacokinetics, and optimal delivery methods remain untested in human trials. In contrast, senicapoc, a highly potent and selective inhibitor of $K_{Ca}3.1$ channels,

has been tested in humans in a phase III clinical trials for the treatment of sickle cell anemia (Ataga et al., 2008). The drug has been considered for repurposing in other conditions, including non-small cell lung cancer (NSCLC). While this is still in early phases of research, senicapoc represents the most advanced $K_{Ca}3.1$ blocker for clinical adaptation. Nevertheless, to be relevant to our research in PDAC, senicapoc would require modifications to specifically target only plasma membrane-localized $K_{Ca}3.1$ channels, similar to the strategies used for developing mitochondrially targeted versions of senicapoc. Such refinements are essential to ensure that senicapoc can be repurposed for effective and selective treatment of PDAC, avoiding its broad inhibition of both plasma membrane and mitochondrial $K_{Ca}3.1$ channels. This targeted approach would align better with the therapeutic needs identified in our study, making it a more viable option for clinical application in PDAC.

Consequently, this study paves the way for future investigations into refining $K_{Ca}3.1$ channel inhibitors for targeted therapy in PDAC, with the potential to improve treatment outcomes in this highly aggressive cancer.

CONCLUSION

This thesis underscores the therapeutic potential of targeting $K_{Ca}3.1$ in PDAC, providing a new avenue in the fight against one of the most lethal cancers. By showing that $K_{Ca}3.1$ inhibition, particularly with maurotoxin, can reduce tumor growth, invasiveness, and fibrosis while enhancing cell death, this research highlights the importance of subcellular targeting in cancer therapy. The findings not only expand our understanding of ion channel biology in cancer but also propose $K_{Ca}3.1$ as a viable target for overcoming the limitations of conventional therapies.

Crucially, the study shows that manipulating the tumor microenvironment and cellular processes via ion channels can yield meaningful therapeutic results. While the mechanistic insights provided by RNA sequencing are promising, they open the door to more comprehensive exploration of the role of $K_{Ca}3.1$ in regulating key pathways that affect tumor survival, immune interactions, and motility of the cancer cells.

However, this research also highlights the complexities of the PDAC microenvironment and the challenges that remain in translating these findings into clinical practice. Future work will need to bridge the gap between preclinical results and patient outcomes, with an emphasis on refining $K_{Ca}3.1$ inhibitors and evaluating their safety and efficacy in human trials.

Consequently, $K_{Ca}3.1$ inhibition emerges as a compelling strategy for PDAC treatment, with the potential to complement existing therapies and mitigate some of the disease most challenging features. This study paves the way for new, targeted approaches in the battle against PDAC, offering hope for improved survival outcomes in this devastating cancer.

REFERENCES

Afgan, E., Baker, D., Batut, B., Van Den Beek, M., Bouvier, D., Ech, M., Chilton, J., Clements, D., Coraor, N., Grüning, B. A., Guerler, A., Hillman-Jackson, J., Hiltemann, S., Jalili, V., Rasche, H., Soranzo, N., Goecks, J., Taylor, J., Nekrutenko, A., & Blankenberg, D. (2018). The Galaxy platform for accessible, reproducible and collaborative biomedical analyses: 2018 update. *Nucleic Acids Research*, *46*(W1), W537–W544. https://doi.org/10.1093/NAR/GKY379

Aguilera, K. Y., Huang, H., Du, W., Hagopian, M. M., Wang, Z., Hinz, S., Hwang, T. H., Wang, H., Fleming, J. B., Castrillon, D. H., Ren, X., Ding, K., & Brekken, R. A. (2017). Inhibition of Discoidin Domain Receptor 1 Reduces Collagen-mediated Tumorigenicity in Pancreatic Ductal Adenocarcinoma. *Molecular Cancer Therapeutics*, *16*(11), 2473–2485. https://doi.org/10.1158/1535-7163.MCT-16-0834

Aguilera, K. Y., Rivera, L. B., Hur, H., Carbon, J. G., Toombs, J. E., Goldstein, C. D., Dellinger, M. T., Castrillon, D. H., & Brekken, R. A. (2014). Collagen signaling enhances tumor progression after anti-VEGF therapy in a murine model of pancreatic ductal adenocarcinoma. *Cancer Research*, *74*(4), 1032–1044. https://doi.org/10.1158/0008-5472.CAN-13-2800

Alhamdoosh, M., Ng, M., Wilson, N. J., Sheridan, J. M., Huynh, H., Wilson, M. J., & Ritchie, M. E. (2017). Combining multiple tools outperforms individual methods in gene set enrichment analyses. *Bioinformatics (Oxford, England)*, *33*(3), 414–424. https://doi.org/10.1093/BIOINFORMATICS/BTW623

Aper, S. J. A., Van Spreeuwel, A. C. C., Van Turnhout, M. C., Van Der Linden, A. J., Pieters, P. A., Van Der Zon, N. L. L., De La Rambelje, S. L., Bouten, C. V. C., & Merkx, M. (2014). Colorful protein-based fluorescent probes for collagen imaging. *PloS One*, *9*(12). https://doi.org/10.1371/JOURNAL.PONE.0114983

Apte, M. V., Pirola, R. C., & Wilson, J. S. (2012). Pancreatic stellate cells: a starring role in normal and diseased pancreas. *Frontiers in Physiology*, *3*. https://doi.org/10.3389/FPHYS.2012.00344

Ataga, K. I., Smith, W. R., De Castro, L. M., Swerdlow, P., Saunthararajah, Y., Castro, O., Vichinsky, E., Kutlar, A., Orringer, E. P., Rigdon, G. C., & Stacker, J. W. (2008). Efficacy and safety of the Gardos channel blocker, senicapoc (ICA-17043), in patients with sickle cell anemia. *Blood*, *111*(8), 3991–3997. https://doi.org/10.1182/BLOOD-2007-08-110098

Bachmann, M., Rossa, A., Varanita, T., Fioretti, B., Biasutto, L., Milenkovic, S., Checchetto, V., Peruzzo, R., Ahmad, S. A., Patel, S. H., Lukowski, R., Edwards, M. J., Ceccarelli, M., Gulbins, E., Zoratti, M., Mattarei, A., & Szabo, I. (2022). Pharmacological targeting of the mitochondrial calcium-dependent potassium channel KCa3.1 triggers cell death and reduces tumor growth and metastasis in vivo. *Cell Death & Disease 2022 13:12*, *13*(12), 1–19. https://doi.org/10.1038/s41419-022-05463-8

Bailey, P., Chang, D. K., Nones, K., Johns, A. L., Patch, A. M., Gingras, M. C., Miller, D. K., Christ, A. N., Bruxner, T. J. C., Quinn, M. C., Nourse, C., Murtaugh, L. C., Harliwong, I.,

Idrisoglu, S., Manning, S., Nourbakhsh, E., Wani, S., Fink, L., Holmes, O., … Grimmond, S. M. (2016). Genomic analyses identify molecular subtypes of pancreatic cancer. *Nature*, *531*(7592), 47–52. https://doi.org/10.1038/NATURE16965

Bankhead, P., Loughrey, M. B., Fernández, J. A., Dombrowski, Y., McArt, D. G., Dunne, P. D., McQuaid, S., Gray, R. T., Murray, L. J., Coleman, H. G., James, J. A., Salto-Tellez, M., & Hamilton, P. W. (2017). QuPath: Open source software for digital pathology image analysis. *Scientific Reports*, *7*(1). https://doi.org/10.1038/S41598-017-17204-5

Becker, A. E., Hernandez, Y. G., Frucht, H., & Lucas, A. L. (2014). Pancreatic ductal adenocarcinoma: risk factors, screening, and early detection. *World Journal of Gastroenterology*, *20*(32), 11182–11198. https://doi.org/10.3748/WJG.V20.I32.11182

Biffi, G., Oni, T. E., Spielman, B., Hao, Y., Elyada, E., Park, Y., Preall, J., & Tuveson, D. A. (2019). IL1-Induced JAK/STAT Signaling Is Antagonized by TGFβ to Shape CAF Heterogeneity in Pancreatic Ductal Adenocarcinoma. *Cancer Discovery*, *9*(2), 282–301. https://doi.org/10.1158/2159-8290.CD-18-0710

Blaszczak, W., & Swietach, P. (2021). What do cellular responses to acidity tell us about cancer? *Cancer and Metastasis Reviews*, *40*(4), 1159–1176. https://doi.org/10.1007/s10555-021-10005-3

Bonito, B., Sauter, D. R. P., Schwab, A., Djamgoz, M. B. A., & Novak, I. (2016). KCa3.1 (IK) modulates pancreatic cancer cell migration, invasion and proliferation: anomalous effects on TRAM-34. *Pflugers Archiv European Journal of Physiology*, *468*(11–12), 1865–1875. https://doi.org/10.1007/S00424-016-1891-9/METRICS

Brown, B. M., Pressley, B., & Wulff, H. (2018). KCa3.1 Channel Modulators as Potential Therapeutic Compounds for Glioblastoma. *Current Neuropharmacology*, *16*(5). https://doi.org/10.2174/1570159X15666170630164226

Bulk, E., Todesca, L. M., Bachmann, M., Szabo, I., Rieke, M., & Schwab, A. (2022). Functional expression of mitochondrial KCa3.1 channels in non-small cell lung cancer cells. *Pflugers Archiv*, *474*(11), 1147. https://doi.org/10.1007/S00424-022-02748-X

Cahalan, M. D., & Chandy, K. G. (2009). The functional network of ion channels in T lymphocytes. *Immunological Reviews*, *231*(1), 59. https://doi.org/10.1111/J.1600-065X.2009.00816.X

Castle, N. A., London, D. O., Creech, C., Fajloun, Z., Stocker, J. W., & Sabatier, J. M. (2003). Maurotoxin: a potent inhibitor of intermediate conductance Ca2+-activated potassium channels. *Molecular Pharmacology*, *63*(2), 409–418. https://doi.org/10.1124/MOL.63.2.409

Celià-Terrassa, T., & Kang, Y. (2024). How important is EMT for cancer metastasis? *PLOS Biology*, *22*(2), e3002487. https://doi.org/10.1371/JOURNAL.PBIO.3002487

Chang, D. T., Schellenberg, D., Shen, J., Kim, J., Goodman, K. A., Fisher, G. A., Ford, J. M., Desser, T., Quon, A., & Koong, A. C. (2009). Stereotactic radiotherapy for unresectable adenocarcinoma of the pancreas. *Cancer*, *115*(3), 665–672. https://doi.org/10.1002/CNCR.24059

Chen, Y. J., Raman, G., Bodendiek, S., O'Donnell, M. E., & Wulff, H. (2011). The KCa3.1 blocker TRAM-34 reduces infarction and neurological deficit in a rat model of ischemia/reperfusion stroke. *Journal of Cerebral Blood Flow & Metabolism*, *31*(12), 2363. https://doi.org/10.1038/JCBFM.2011.101

Chimote, A. A., Balajthy, A., Arnold, M. J., Newton, H. S., Hajdu, P., Qualtieri, J., Wise-Draper, T., & Conforti, L. (2018). A defect in KCa3.1 channel activity limits the ability of CD8+ T cells from cancer patients to infiltrate an adenosine-rich microenvironment. *Science Signaling*, *11*(527). https://doi.org/10.1126/SCISIGNAL.AAQ1616

Chou, C. C., Lunn, C. A., & Murgolo, N. J. (2008). KCa3.1: target and marker for cancer, autoimmune disorder and vascular inflammation? *Expert Review of Molecular Diagnostics*, *8*(2), 179–187. https://doi.org/10.1586/14737159.8.2.179

Clark, C. E., Hingorani, S. R., Mick, R., Combs, C., Tuveson, D. A., & Vonderheide, R. H. (2007). Dynamics of the immune reaction to pancreatic cancer from inception to invasion. *Cancer Research*, *67*(19), 9518–9527. https://doi.org/10.1158/0008-5472.CAN-07-0175

Conroy, T., Desseigne, F., Ychou, M., Bouché, O., Guimbaud, R., Bécouarn, Y., Adenis, A., Raoul, J.-L., Gourgou-Bourgade, S., de la Fouchardière, C., Bennouna, J., Bachet, J.-B., Khemissa-Akouz, F., Péré-Vergé, D., Delbaldo, C., Assenat, E., Chauffert, B., Michel, P., Montoto-Grillot, C., & Ducreux, M. (2011). FOLFIRINOX versus gemcitabine for metastatic pancreatic cancer. *The New England Journal of Medicine*, *364*(19), 1817–1825. https://doi.org/10.1056/NEJMOA1011923

Coradini, D., Casarsa, C., & Oriana, S. (2011). Epithelial cell polarity and tumorigenesis: new perspectives for cancer detection and treatment. *Acta Pharmacologica Sinica*, *32*(5), 552–564. https://doi.org/10.1038/APS.2011.20

Cozzolino, M., & Panyi, G. (2024). Intracellular acidity impedes KCa3.1 activation by Riluzole and SKA-31. *Frontiers in Pharmacology*, *15*. https://doi.org/10.3389/FPHAR.2024.1380655

Curvello, R., Kast, V., Abuwarwar, M. H., Fletcher, A. L., Garnier, G., & Loessner, D. (2021). 3D Collagen-Nanocellulose Matrices Model the Tumour Microenvironment of Pancreatic Cancer. *Frontiers in Digital Health*, *3*, 704584. https://doi.org/10.3389/FDGTH.2021.704584/BIBTEX

Daniel, S. K., Sullivan, K. M., Labadie, K. P., & Pillarisetty, V. G. (2019). Hypoxia as a barrier to immunotherapy in pancreatic adenocarcinoma. *Clinical and Translational Medicine*, *8*(1). https://doi.org/10.1186/S40169-019-0226-9

de Gooijer, M. C., van den Top, A., Bockaj, I., Beijnen, J. H., Würdinger, T., & van Tellingen, O. (2017). The G2 checkpoint—a node-based molecular switch. *FEBS Open Bio*, *7*(4), 439. https://doi.org/10.1002/2211-5463.12206

Djamgoz, M. B. A., Coombes, R. C., & Schwab, A. (2014). Ion transport and cancer: from initiation to metastasis. *Philosophical Transactions of the Royal Society of London. Series B, Biological Sciences*, *369*(1638). https://doi.org/10.1098/RSTB.2013.0092

Dougan, S. K. (2017). The Pancreatic Cancer Microenvironment. *Cancer Journal (Sudbury, Mass.)*, *23*(6), 321–325. https://doi.org/10.1097/PPO.0000000000000288

Edilova, M. I., Abdul-Sater, A. A., & Watts, T. H. (2018). TRAF1 Signaling in Human Health and Disease. *Frontiers in Immunology*, *9*, 422468. https://doi.org/10.3389/FIMMU.2018.02969/BIBTEX

Ene-Obong, A., Clear, A. J., Watt, J., Wang, J., Fatah, R., Riches, J. C., Marshall, J. F., Chin-Aleong, J., Chelala, C., Gribben, J. G., Ramsay, A. G., & Kocher, H. M. (2013). Activated pancreatic stellate cells sequester CD8+ T cells to reduce their infiltration of the juxtatumoral compartment of pancreatic ductal adenocarcinoma. *Gastroenterology*, *145*(5), 1121–1132. https://doi.org/10.1053/J.GASTRO.2013.07.025

Erkan, M., Kurtoglu, M., & Kleeff, J. (2016). The role of hypoxia in pancreatic cancer: a potential therapeutic target? *Expert Review of Gastroenterology & Hepatology*, *10*(3), 301–316. https://doi.org/10.1586/17474124.2016.1117386

Estes, D. J., Memarsadeghi, S., Lundy, S. K., Marti, F., Mikol, D. D., Fox, D. A., & Mayer, M. (2008). High-throughput profiling of ion channel activity in primary human lymphocytes. *Analytical Chemistry*, *80*(10), 3728–3735. https://doi.org/10.1021/AC800164V

Fanger, C. M., Ghanshani, S., Logsdon, N. J., Rauer, H., Kalman, K., Zhou, J., Beckingham, K., Chandy, K. G., Cahalan, M. D., & Aiyar, J. (1999). Calmodulin Mediates Calcium-dependent Activation of the Intermediate Conductance KCa Channel,IKCa1. *Journal of Biological Chemistry*, *274*(9), 5746–5754. https://doi.org/10.1074/jbc.274.9.5746

Feske, S., Wulff, H., & Skolnik, E. Y. (2015). Ion Channels in Innate and Adaptive Immunity. *Annual Review of Immunology*, *33*, 291. https://doi.org/10.1146/ANNUREV-IMMUNOL-032414-112212

Froeling, F. E. M., Mirza, T. A., Feakins, R. M., Seedhar, A., Elia, G., Hart, I. R., & Kocher, H. M. (2009). Organotypic Culture Model of Pancreatic Cancer Demonstrates that Stromal Cells Modulate E-Cadherin, β-Catenin, and Ezrin Expression in Tumor Cells. *The American Journal of Pathology*, *175*(2), 636. https://doi.org/10.2353/AJPATH.2009.090131

Gannon, M., Herrera, P.-L., & Wright, C. V. E. (2000). *Mosaic Cre-Mediated Recombination in Pancreas Using the pdx-1 Enhancer/Promoter*. https://doi.org/10.1002/(SICI)1526-968X(200002)26:2

Ganser, K., Stransky, N., Abed, T., Quintanilla-Martinez, L., Gonzalez-Menendez, I., Naumann, U., Koch, P., Krueger, M., Ruth, P., Huber, S. M., & Eckert, F. (2024). KCa channel targeting impairs DNA repair and invasiveness of patient-derived glioblastoma stem cells in culture and orthotopic mouse xenografts which only in part is predictable by KCa expression levels. *International Journal of Cancer*. https://doi.org/10.1002/IJC.35064

Gao, R., He, B., Huang, Q., Wang, Z., Yan, M., Lam, E. W. F., Lin, S., Wang, B., & Liu, Q. (2021). Cancer cell immune mimicry delineates onco-immunologic modulation. *IScience*, *24*(10), 103133. https://doi.org/10.1016/J.ISCI.2021.103133

Garg, B., Giri, B., Modi, S., Sethi, V., Castro, I., Umland, O., Ban, Y., Lavania, S., Dawra, R., Banerjee, S., Vickers, S., Merchant, N. B., Chen, S. X., Gilboa, E., Ramakrishnan, S., Saluja, A., & Dudeja, V. (2018). NFκB in Pancreatic Stellate Cells Reduces Infiltration

of Tumors by Cytotoxic T Cells and Killing of Cancer Cells, via Up-regulation of CXCL12. *Gastroenterology*, *155*(3), 880-891.e8. https://doi.org/10.1053/J.GASTRO.2018.05.051

Gawali, V. S., Chimote, A. A., Newton, H. S., Feria-Garzón, M. G., Chirra, M., Janssen, E. M., Wise-Draper, T. M., & Conforti, L. (2021). Immune Checkpoint Inhibitors Regulate K+ Channel Activity in Cytotoxic T Lymphocytes of Head and Neck Cancer Patients. *Frontiers in Pharmacology*, *12*, 742862. https://doi.org/10.3389/FPHAR.2021.742862/BIBTEX

Gerlach, A. C., Gangopadhyay, N. N., & Devor, D. C. (2000). Kinase-dependent regulation of the intermediate conductance, calcium-dependent potassium channel, hIK1. *The Journal of Biological Chemistry*, *275*(1), 585–598. https://doi.org/10.1074/JBC.275.1.585

Ghanshani, S., Wulff, H., Miller, M. J., Rohm, H., Neben, A., Gutman, G. A., Cahalan, M. D., & Chandy, K. G. (2000). *Up-regulation of the IKCa1 Potassium Channel during T-cell Activation MOLECULAR MECHANISM AND FUNCTIONAL CONSEQUENCES**. https://doi.org/10.1074/jbc.M003941200

Gillen, S., Schuster, T., Büschenfelde, C. M. Zum, Friess, H., & Kleeff, J. (2010). Preoperative/neoadjuvant therapy in pancreatic cancer: a systematic review and meta-analysis of response and resection percentages. *PLoS Medicine*, *7*(4). https://doi.org/10.1371/JOURNAL.PMED.1000267

Glaser, F., Hundehege, P., Bulk, E., Todesca, L. M., Schimmelpfennig, S., Nass, E., Budde, T., Meuth, S. G., & Schwab, A. (2021). KCa channel blockers increase effectiveness of the EGF receptor TK inhibitor erlotinib in non-small cell lung cancer cells (A549). *Scientific Reports*, *11*(1). https://doi.org/10.1038/S41598-021-97406-0

Gong, Z., Jia, Q., Guo, J., Li, C., Xu, S., Jin, Z., Chu, H., Wan, Y. Y., Zhu, B., & Zhou, Y. (2023). Caspase-8 contributes to an immuno-hot microenvironment by promoting phagocytosis via an ecto-calreticulin-dependent mechanism. *Experimental Hematology and Oncology*, *12*(1), 1–14. https://doi.org/10.1186/S40164-022-00371-1/FIGURES/6

Gouaux, E., & MacKinnon, R. (2005). Principles of selective ion transport in channels and pumps. *Science (New York, N.Y.)*, *310*(5753), 1461–1465. https://doi.org/10.1126/SCIENCE.1113666

Grasso, C., Jansen, G., & Giovannetti, E. (2017). Drug resistance in pancreatic cancer: Impact of altered energy metabolism. *Critical Reviews in Oncology/Hematology*, *114*, 139–152. https://doi.org/10.1016/J.CRITREVONC.2017.03.026

Grgic, I., Eichler, I., Heinau, P., Si, H., Brakemeier, S., Hoyer, J., & Köhler, R. (2005). Selective blockade of the intermediate-conductance Ca2+-activated K+ channel suppresses proliferation of microvascular and macrovascular endothelial cells and angiogenesis in vivo. *Arteriosclerosis, Thrombosis, and Vascular Biology*, *25*(4), 704–709. https://doi.org/10.1161/01.ATV.0000156399.12787.5C

Groot, V. P., Rezaee, N., Wu, W., Cameron, J. L., Fishman, E. K., Hruban, R. H., Weiss, M. J., Zheng, L., Wolfgang, C. L., & He, J. (2018). Patterns, Timing, and Predictors of

Recurrence Following Pancreatectomy for Pancreatic Ductal Adenocarcinoma. *Annals of Surgery*, *267*(5), 936–945. https://doi.org/10.1097/SLA.0000000000002234

Győrffy, B. (2024). Integrated analysis of public datasets for the discovery and validation of survival-associated genes in solid tumors. *Innovation (Cambridge (Mass.))*, *5*(3). https://doi.org/10.1016/J.XINN.2024.100625

Halbrook, C. J., Lyssiotis, C. A., Pasca di Magliano, M., & Maitra, A. (2023). Pancreatic Cancer: Advances and Challenges. *Cell*, *186*(8), 1729. https://doi.org/10.1016/J.CELL.2023.02.014

Hartupee, C., Nagalo, B. M., Chabu, C. Y., Tesfay, M. Z., Coleman-Barnett, J., West, J. T., & Moaven, O. (2024). Pancreatic cancer tumor microenvironment is a major therapeutic barrier and target. *Frontiers in Immunology*, *15*, 1287459. https://doi.org/10.3389/FIMMU.2024.1287459/BIBTEX

Hayashi, M., & Novak, I. (2013). Molecular basis of potassium channels in pancreatic duct epithelial cells. *Channels*, *7*(6), 432. https://doi.org/10.4161/CHAN.26100

Hayashi, M., Wang, J., Hede, S. E., & Novak, I. (2012). An intermediate-conductance Ca 2-activated K channel is important for secretion in pancreatic duct cells. *Am J Physiol Cell Physiol*, *303*, 151–159. https://doi.org/10.1152/ajpcell.00089.2012

Henley, S. J., Ward, E. M., Scott, S., Ma, J., Anderson, R. N., Firth, A. U., Thomas, C. C., Islami, F., Weir, H. K., Lewis, D. R., Sherman, R. L., Wu, M., Benard, V. B., Richardson, L. C., Jemal, A., Cronin, K., & Kohler, B. A. (2020). Annual report to the nation on the status of cancer, part I: National cancer statistics. *Cancer*, *126*(10), 2225–2249. https://doi.org/10.1002/cncr.32802

Henríquez, C., Riquelme, T. T., Vera, D., Julio-Kalajzić, F., Ehrenfeld, P., Melvin, J. E., Figueroa, C. D., Sarmiento, J., & Flores, C. A. (2016). The calcium-activated potassium channel KCa3.1 plays a central role in the chemotactic response of mammalian neutrophils. *Acta Physiologica (Oxford, England)*, *216*(1), 132–145. https://doi.org/10.1111/APHA.12548

Hessmann, E., Buchholz, S. M., Demir, I. E., Singh, S. K., Gress, T. M., Ellenrieder, V., Neesse, A., Hessmann, E., Buchholz, S. M., Demir, I. E., Singh, S. K., Gress, T. M., Ellenrieder, V., & Neesse, A. (2020). Microenvironmental Determinants of Pancreatic Cancer. *Physiological Reviews*, *100*(4), 1707–1751. https://doi.org/10.1152/PHYSREV.00042.2019

Hingorani, S. R., Petricoin, E. F., Maitra, A., Rajapakse, V., King, C., Jacobetz, M. A., Ross, S., Conrads, T. P., Veenstra, T. D., Hitt, B. A., Kawaguchi, Y., Johann, D., Liotta, L. A., Crawford, H. C., Putt, M. E., Jacks, T., Wright, C. V. E., Hruban, R. H., Lowy, A. M., & Tuveson, D. A. (2003). Preinvasive and invasive ductal pancreatic cancer and its early detection in the mouse. *Cancer Cell*, *4*(6), 437–450. https://doi.org/10.1016/S1535-6108(03)00309-X

Hofschröer, V., Najder, K., Rugi, M., Bouazzi, R., Cozzolino, M., Arcangeli, A., Panyi, G., & Schwab, A. (2021). Ion Channels Orchestrate Pancreatic Ductal Adenocarcinoma Progression and Therapy. *Frontiers in Pharmacology*, *11*. https://doi.org/10.3389/FPHAR.2020.586599

Hosein, A. N., Brekken, R. A., & Maitra, A. (2020). Pancreatic cancer stroma: an update on therapeutic targeting strategies. *Nature Reviews. Gastroenterology & Hepatology*, *17*(8), 487–505. https://doi.org/10.1038/S41575-020-0300-1

Hu, J. X., Lin, Y. Y., Zhao, C. F., Chen, W. B., Liu, Q. C., Li, Q. W., & Gao, F. (2021). Pancreatic cancer: A review of epidemiology, trend, and risk factors. *World Journal of Gastroenterology*, *27*(27), 4298. https://doi.org/10.3748/WJG.V27.I27.4298

Imamura, T., Iguchi, H., Manabe, T., Ohshio, G., Yoshimura, T., Wang, Z. H., Suwa, H., Ishigami, S., & Imamura, M. (1995). Quantitative analysis of collagen and collagen subtypes I, III, and V in human pancreatic cancer, tumor-associated chronic pancreatitis, and alcoholic chronic pancreatitis. *Pancreas*, *11*(4), 357–364. https://doi.org/10.1097/00006676-199511000-00007

Ishiguro, H., Yamamoto, A., Nakakuki, M., Yi, L., Ishiguro, M., Yamaguchi, M., Kondo, S., & Mochimaru, Y. (2012). PHYSIOLOGY AND PATHOPHYSIOLOGY OF BICARBONATE SECRETION BY PANCREATIC DUCT EPITHELIUM. *Nagoya Journal of Medical Science*, *74*(1–2), 1. https://pmc.ncbi.nlm.nih.gov/articles/PMC4831246/

Ishii, T. M., Silvia, C., Hirschberg, B., Bond, C. T., Adelman, J. P., & Maylie, J. (1997). A human intermediate conductance calcium-activated potassium channel. *Proceedings of the National Academy of Sciences of the United States of America*, *94*(21), 11651–11656. https://doi.org/10.1073/PNAS.94.21.11651

Jacobetz, M. A., Chan, D. S., Neesse, A., Bapiro, T. E., Cook, N., Frese, K. K., Feig, C., Nakagawa, T., Caldwell, M. E., Zecchini, H. I., Lolkema, M. P., Jiang, P., Kultti, A., Thompson, C. B., Maneval, D. C., Jodrell, D. I., Frost, G. I., Shepard, H. M., Skepper, J. N., & Tuveson, D. A. (2013). Hyaluronan impairs vascular function and drug delivery in a mouse model of pancreatic cancer. *Gut*, *62*(1), 112–120. https://doi.org/10.1136/GUTJNL-2012-302529

Jäger, H., Dreker, T., Buck, A., Giehl, K., Gress, T., & Grissmer, S. (2004). Blockage of Intermediate-Conductance Ca^{2+} -Activated K^{+} Channels Inhibit Human Pancreatic Cancer Cell Growth in Vitro. *Molecular Pharmacology*, *65*(3), 630–638. https://doi.org/10.1124/mol.65.3.630

Jang, S. H., Choi, S. Y., Ryu, P. D., & Lee, S. Y. (2011). Anti-proliferative effect of Kv1.3 blockers in A549 human lung adenocarcinoma in vitro and in vivo. *European Journal of Pharmacology*, *651*(1–3), 26–32. https://doi.org/10.1016/J.EJPHAR.2010.10.066

Jiang, H., Hegde, S., Knolhoff, B. L., Zhu, Y., Herndon, J. M., Meyer, M. A., Nywening, T. M., Hawkins, W. G., Shapiro, I. M., Weaver, D. T., Pachter, J. A., Wang-Gillam, A., & DeNardo, D. G. (2016). Targeting focal adhesion kinase renders pancreatic cancers responsive to checkpoint immunotherapy. *Nature Medicine*, *22*(8), 851–860. https://doi.org/10.1038/NM.4123

Jiang, S. H., Zhu, L. L., Zhang, M., Li, R. K., Yang, Q., Yan, J. Y., Zhang, C., Yang, J. Y., Dong, F. Y., Dai, M., Hu, L. P., Li, J., Li, Q., Wang, Y. H., Yang, X. M., Zhang, Y. L., Nie, H. Z., Zhu, L., Zhang, X. L., … Zhang, Z. G. (2019). GABRP regulates chemokine signalling, macrophage recruitment and tumour progression in pancreatic cancer through tuning KCNN4-mediated Ca2+ signalling in a GABA-independent manner. *Gut*, *68*(11), 1994–2006. https://doi.org/10.1136/GUTJNL-2018-317479

Jiang, S., Zhu, L., Yang, J., Hu, L., Gu, J., Xing, X., Sun, Y., & Zhang, Z. (2017). Integrated expression profiling of potassium channels identifys KCNN4 as a prognostic biomarker of pancreatic cancer. *Biochemical and Biophysical Research Communications*, *494*(1–2), 113–119. https://doi.org/10.1016/J.BBRC.2017.10.072

Jin, G., Hong, W., Guo, Y., Bai, Y., & Chen, B. (2020). Molecular Mechanism of Pancreatic Stellate Cells Activation in Chronic Pancreatitis and Pancreatic Cancer. *Journal of Cancer*, *11*(6), 1505. https://doi.org/10.7150/JCA.38616

Jin, L. W., Lucente, J. Di, Nguyen, H. M., Singh, V., Singh, L., Chavez, M., Bushong, T., Wulff, H., & Maezawa, I. (2019). Repurposing the KCa3.1 inhibitor senicapoc for Alzheimer's disease. *Annals of Clinical and Translational Neurology*, *6*(4), 723. https://doi.org/10.1002/ACN3.754

Joiner, W. J., Khanna, R., Schlichter, L. C., & Kaczmarek, L. K. (2001). Calmodulin Regulates Assembly and Trafficking of SK4/IK1 Ca 2+-activated K+ Channels. *Journal of Biological Chemistry*, *276*(41), 37980–37985. https://doi.org/10.1074/jbc.m104965200

Jones, S., Zhang, X., Parsons, D. W., Lin, J. C. H., Leary, R. J., Angenendt, P., Mankoo, P., Carter, H., Kamiyama, H., Jimeno, A., Hong, S. M., Fu, B., Lin, M. T., Calhoun, E. S., Kamiyama, M., Walter, K., Nikolskaya, T., Nikolsky, Y., Hartigan, J., … Kinzler, K. W. (2008). Core signaling pathways in human pancreatic cancers revealed by global genomic analyses. *Science (New York, N.Y.)*, *321*(5897), 1801–1806. https://doi.org/10.1126/SCIENCE.1164368

Jung, S. R., Kim, K., Hille, B., Nguyen, T. D., & Koh, D. S. (2006). Pattern of Ca2+ increase determines the type of secretory mechanism activated in dog pancreatic duct epithelial cells. *The Journal of Physiology*, *576*(Pt 1), 163. https://doi.org/10.1113/JPHYSIOL.2006.114876

Kanda, M., Matthaei, H., Wu, J., Hong, S. M., Yu, J., Borges, M., Hruban, R. H., Maitra, A., Kinzler, K., Vogelstein, B., & Goggins, M. (2012). Presence of somatic mutations in most early-stage pancreatic intraepithelial neoplasia. *Gastroenterology*, *142*(4). https://doi.org/10.1053/J.GASTRO.2011.12.042

Karatug Kacar, A. (2020). Indomethacin decreases insulin secretion by reducing KCa3.1 as a biomarker of pancreatic tumor and causes apoptotic cell death. *Journal of Biochemical and Molecular Toxicology*, *34*(7). https://doi.org/10.1002/JBT.22488

Khalili, A. A., & Ahmad, M. R. (2015). A Review of Cell Adhesion Studies for Biomedical and Biological Applications. *International Journal of Molecular Sciences*, *16*(8), 18149–18184. https://doi.org/10.3390/IJMS160818149

Kim, D., Langmead, B., & Salzberg, S. L. (2015). HISAT: a fast spliced aligner with low memory requirements. *Nature Methods*, *12*(4), 357–360. https://doi.org/10.1038/NMETH.3317

Kim, Y. N., Koo, K. H., Sung, J. Y., Yun, U. J., & Kim, H. (2012). Anoikis resistance: an essential prerequisite for tumor metastasis. *International Journal of Cell Biology*, *2012*. https://doi.org/10.1155/2012/306879

Kischel, P., Girault, A., Rodat-Despoix, L., Chamlali, M., Radoslavova, S., Daya, H. A., Lefebvre, T., Foulon, A., Rybarczyk, P., Hague, F., Dhennin-Duthille, I., Gautier, M., & Ouadid-Ahidouch, H. (2019). Ion Channels: New Actors Playing in Chemotherapeutic Resistance. *Cancers*, *11*(3). https://doi.org/10.3390/CANCERS11030376

Klatte, D. C. F., Clift, K. E., Mantia, S. K., Millares, L., Hoogenboom, S. A. M., Presutti, R. J., & Wallace, M. B. (2023). Identification of individuals at high-risk for pancreatic cancer using a digital patient-input tool combining family cancer history screening and new-onset diabetes. *Preventive Medicine Reports*, *31*, 102110. https://doi.org/10.1016/J.PMEDR.2023.102110

Kleeff, J., Korc, M., Apte, M., La Vecchia, C., Johnson, C. D., Biankin, A. V., Neale, R. E., Tempero, M., Tuveson, D. A., Hruban, R. H., & Neoptolemos, J. P. (2016). Pancreatic cancer. *Nature Reviews. Disease Primers*, *2*. https://doi.org/10.1038/NRDP.2016.22

Köhler, R., Degenhardt, C., Kühn, M., Runkel, N., Paul, M., & Hoyer, J. (2000). Expression and function of endothelial Ca(2+)-activated K(+) channels in human mesenteric artery: A single-cell reverse transcriptase-polymerase chain reaction and electrophysiological study in situ. *Circulation Research*, *87*(6), 496–503. https://doi.org/10.1161/01.RES.87.6.496

Köhler, R., Wulff, H., Eichler, I., Kneifel, M., Neumann, D., Knorr, A., Grgic, I., Kämpfe, D., Si, H., Wibawa, J., Real, R., Borner, K., Brakemeier, S., Orzechowski, H. D., Reusch, H. P., Paul, M., Chandy, K. G., & Hoyer, J. (2003). Blockade of the intermediate-conductance calcium-activated potassium channel as a new therapeutic strategy for restenosis. *Circulation*, *108*(9), 1119–1125. https://doi.org/10.1161/01.CIR.0000086464.04719.DD/ASSET/2557048B-D935-43E8-B441-76A1B6B1396A/ASSETS/GRAPHIC/19FF5.JPEG

Koltai, T., Reshkin, S. J., Carvalho, T. M. A., Di Molfetta, D., Greco, M. R., Alfarouk, K. O., & Cardone, R. A. (2022). Resistance to Gemcitabine in Pancreatic Ductal Adenocarcinoma: A Physiopathologic and Pharmacologic Review. *Cancers*, *14*(10). https://doi.org/10.3390/CANCERS14102486

Korotkevich, G., Sukhov, V., Budin, N., Shpak, B., Artyomov, M. N., & Sergushichev, A. (2021). Fast gene set enrichment analysis. *BioRxiv*, 060012. https://doi.org/10.1101/060012

Koshy, S., Wu, D., Hu, X., Tajhya, R. B., Huq, R., Khan, F. S., Pennington, M. W., Wulff, H., Yotnda, P., & Beeton, C. (2013). Blocking KCa3.1 Channels Increases Tumor Cell Killing by a Subpopulation of Human Natural Killer Lymphocytes. *PLOS ONE*, *8*(10), e76740. https://doi.org/10.1371/JOURNAL.PONE.0076740

Kovalenko, I., Glasauer, A., Schöckel, L., Sauter, D. R. P., Ehrmann, A., Sohler, F., Hägebarth, A., Novak, I., & Christian, S. (2016). Identification of KCa3.1 Channel as a Novel Regulator of Oxidative Phosphorylation in a Subset of Pancreatic Carcinoma Cell Lines. *PLOS ONE*, *11*(8), e0160658. https://doi.org/10.1371/journal.pone.0160658

Koyama-Nasu, R., Wang, Y., Hasegawa, I., Endo, Y., Nakayama, T., & Kimura, M. Y. (2022). The cellular and molecular basis of CD69 function in anti-tumor immunity.

International Immunology, *34*(11), 555–561. https://doi.org/10.1093/INTIMM/DXAC024

Kshatri, A. S., Gonzalez-Hernandez, A., & Giraldez, T. (2018). Physiological Roles and Therapeutic Potential of Ca2+ Activated Potassium Channels in the Nervous System. *Frontiers in Molecular Neuroscience*, *11*. https://doi.org/10.3389/FNMOL.2018.00258

Kumar, B. V., Connors, T. J., & Farber, D. L. (2018). Human T cell development, localization, and function throughout life. *Immunity*, *48*(2), 202. https://doi.org/10.1016/J.IMMUNI.2018.01.007

Kurata, N., Fujita, H., Ohuchida, K., Mizumoto, K., Mahawithitwong, P., Sakai, H., Onimaru, M., Manabe, T., Ohtsuka, T., & Tanaka, M. (2011). Predicting the chemosensitivity of pancreatic cancer cells by quantifying the expression levels of genes associated with the metabolism of gemcitabine and 5-fluorouracil. *International Journal of Oncology*, *39*(2), 473–482. https://doi.org/10.3892/IJO.2011.1058

Li, J., Byrne, K. T., Yan, F., Yamazoe, T., Chen, Z., Baslan, T., Richman, L. P., Lin, J. H., Sun, Y. H., Rech, A. J., Balli, D., Hay, C. A., Sela, Y., Merrell, A. J., Liudahl, S. M., Gordon, N., Norgard, R. J., Yuan, S., Yu, S., … Stanger, B. Z. (2018). Tumor Cell-Intrinsic Factors Underlie Heterogeneity of Immune Cell Infiltration and Response to Immunotherapy. *Immunity*, *49*(1), 178-193.e7. https://doi.org/10.1016/J.IMMUNI.2018.06.006

Li, M., Tian, P., Zhao, Q., Ma, X., & Zhang, Y. (2023). Potassium channels: Novel targets for tumor diagnosis and chemoresistance. *Frontiers in Oncology*, *12*, 1074469. https://doi.org/10.3389/FONC.2022.1074469/BIBTEX

Liang, H., Zheng, Y., Huang, Z., Dai, J., Yao, L., Xie, D., Chen, D., Qiu, H., Wang, H., Li, H., Leng, J., Tang, Z., Zhang, D., & Zhou, H. (2024). Pan-cancer analysis for the prognostic and immunological role of CD47: interact with TNFRSF9 inducing CD8 + T cell exhaustion. *Discover Oncology*, *15*(1). https://doi.org/10.1007/S12672-024-00951-Z

Liao, Y., Smyth, G. K., & Shi, W. (2014). featureCounts: an efficient general purpose program for assigning sequence reads to genomic features. *Bioinformatics (Oxford, England)*, *30*(7), 923–930. https://doi.org/10.1093/BIOINFORMATICS/BTT656

Liu, R., Holik, A. Z., Su, S., Jansz, N., Chen, K., Leong, H. S., Blewitt, M. E., Asselin-Labat, M. L., Smyth, G. K., & Ritchie, M. E. (2015). Why weight? Modelling sample and observational level variability improves power in RNA-seq analyses. *Nucleic Acids Research*, *43*(15). https://doi.org/10.1093/NAR/GKV412

Livak, K. J., & Schmittgen, T. D. (2001). Analysis of relative gene expression data using real-time quantitative PCR and the 2(-Delta Delta C(T)) Method. *Methods (San Diego, Calif.)*, *25*(4), 402–408. https://doi.org/10.1006/METH.2001.1262

Maddalena, M., Mallel, G., Nataraj, N. B., Shreberk-Shaked, M., Hassin, O., Mukherjee, S., Arandkar, S., Rotkopf, R., Kapsack, A., Lambiase, G., Pellegrino, B., Ben-Isaac, E., Golani, O., Addadi, Y., Hajaj, E., Eilam, R., Straussman, R., Yarden, Y., Lotem, M., & Oren, M. (2021). TP53 missense mutations in PDAC are associated with enhanced fibrosis and an immunosuppressive microenvironment. *Proceedings of the National Academy of Sciences of the United States of America*, *118*(23), e2025631118.

https://doi.org/10.1073/PNAS.2025631118/SUPPL_FILE/PNAS.2025631118.SD02.CSV

Mahajan, U. M., Langhoff, E., Goni, E., Costello, E., Greenhalf, W., Halloran, C., Ormanns, S., Kruger, S., Boeck, S., Ribback, S., Beyer, G., Dombroswki, F., Weiss, F. U., Neoptolemos, J. P., Werner, J., D'Haese, J. G., Bazhin, A., Peterhansl, J., Pichlmeier, S., … Mayerle, J. (2018). Immune Cell and Stromal Signature Associated With Progression-Free Survival of Patients With Resected Pancreatic Ductal Adenocarcinoma. *Gastroenterology*, *155*(5), 1625-1639.e2. https://doi.org/10.1053/J.GASTRO.2018.08.009

Makohon-Moore, A. P., Matsukuma, K., Zhang, M., Reiter, J. G., Gerold, J. M., Jiao, Y., Sikkema, L., Attiyeh, M. A., Yachida, S., Sandone, C., Hruban, R. H., Klimstra, D. S., Papadopoulos, N., Nowak, M. A., Kinzler, K. W., Vogelstein, B., & Iacobuzio -Donahue, C. A. (2018). Precancerous neoplastic cells can move through the pancreatic ductal system. *Nature*, *561*(7722), 201–205. https://doi.org/10.1038/S41586-018-0481-8

Manji, G. A., Olive, K. P., Saenger, Y. M., & Oberstein, P. (2017). Current and Emerging Therapies in Metastatic Pancreatic Cancer. *Clinical Cancer Research : An Official Journal of the American Association for Cancer Research*, *23*(7), 1670–1678. https://doi.org/10.1158/1078-0432.CCR-16-2319

Mathews, L. A., Cabarcas, S. M., Hurt, E. M., Zhang, X., Jaffee, E. M., & Farrar, W. L. (2011). Increased expression of DNA repair genes in invasive human pancreatic cancer cells. *Pancreas*, *40*(5), 730–739. https://doi.org/10.1097/MPA.0B013E31821AE25B

Mato, E., Lucas, M., Petriz, J., Gomis, R., & Novials, A. (2009). Identification of a pancreatic stellate cell population with properties of progenitor cells: new role for stellate cells in the pancreas. *The Biochemical Journal*, *421*(2), 181–191. https://doi.org/10.1042/BJ20081466

Mavros, M. N., Moris, Di., Karanicolas, P. J., Katz, M. H. G., O'Reilly, E. M., & Pawlik, T. M. (2021). Clinical Trials of Systemic Chemotherapy for Resectable Pancreatic Cancer: A Review. *JAMA Surgery*, *156*(7), 663–672. https://doi.org/10.1001/JAMASURG.2021.0149

Maylie, J., Bond, C. T., Herson, P. S., Lee, W.-S., & Adelman, J. P. (2004). Small conductance Ca^{2+} -activated K^{+} channels and calmodulin. *The Journal of Physiology*, *554*(2), 255–261. https://doi.org/10.1113/jphysiol.2003.049072

Mc Gee, M. M. (2015). Targeting the Mitotic Catastrophe Signaling Pathway in Cancer. *Mediators of Inflammation*, *2015*, 146282. https://doi.org/10.1155/2015/146282

McFerrin, M. B., Turner, K. L., Cuddapah, V. A., & Sontheimer, H. (2012). Differential role of IK and BK potassium channels as mediators of intrinsic and extrinsic apoptotic cell death. *American Journal of Physiology - Cell Physiology*, *303*(10), C1070. https://doi.org/10.1152/AJPCELL.00040.2012

Melstrom, L. G., Salazar, M. D., & Diamond, D. J. (2017). The pancreatic cancer microenvironment: A true double agent. *Journal of Surgical Oncology*, *116*(1), 7–15. https://doi.org/10.1002/JSO.24643

Mo, X., Zhang, C. fei, Xu, P., Ding, M., Ma, Z. jie, Sun, Q., Liu, Y., Bi, H. kai, Guo, X., Abdelatty, A., Hu, C., Xu, H. jun, Zhou, G. ren, Jia, Y. liang, & Xia, H. ping. (2022). KCNN4-mediated Ca2+/MET/AKT axis is promising for targeted therapy of pancreatic ductal adenocarcinoma. *Acta Pharmacologica Sinica*, *43*(3), 735–746. https://doi.org/10.1038/S41401-021-00688-3

Mohr, C. J., Steudel, F. A., Gross, D., Ruth, P., Lo, W. Y., Hoppe, R., Schroth, W., Brauch, H., Huber, S. M., & Lukowski, R. (2019). Cancer-Associated Intermediate Conductance Ca2+-Activated K^+ Channel KCa3.1. *Cancers*, *11*(1). https://doi.org/10.3390/CANCERS11010109

Mueller, S., Engleitner, T., Maresch, R., Zukowska, M., Lange, S., Kaltenbacher, T., Konukiewitz, B., Öllinger, R., Zwiebel, M., Strong, A., Yen, H. Y., Banerjee, R., Louzada, S., Fu, B., Seidler, B., Götzfried, J., Schuck, K., Hassan, Z., Arbeiter, A., … Rad, R. (2018). Evolutionary routes and KRAS dosage define pancreatic cancer phenotypes. *Nature*, *554*(7690), 62–68. https://doi.org/10.1038/NATURE25459

Murphy, J. D., Adusumilli, S., Griffith, K. A., Ray, M. E., Zalupski, M. M., Lawrence, T. S., & Ben-Josef, E. (2007). Full-dose gemcitabine and concurrent radiotherapy for unresectable pancreatic cancer. *International Journal of Radiation Oncology, Biology, Physics*, *68*(3), 801–808. https://doi.org/10.1016/J.IJROBP.2006.12.053

Nakahira, S., Nakamori, S., Tsujie, M., Takahashi, Y., Okami, J., Yoshioka, S., Yamasaki, M., Marubashi, S., Takemasa, I., Miyamoto, A., Takeda, Y., Nagano, H., Dono, K., Umeshita, K., Sakon, M., & Monden, M. (2007). Involvement of ribonucleotide reductase M1 subunit overexpression in gemcitabine resistance of human pancreatic cancer. *International Journal of Cancer*, *120*(6), 1355–1363. https://doi.org/10.1002/IJC.22390

Nakano, Y., Tanno, S., Koizumi, K., Nishikawa, T., Nakamura, K., Minoguchi, M., Izawa, T., Mizukami, Y., Okumura, T., & Kohgo, Y. (2007). Gemcitabine chemoresistance and molecular markers associated with gemcitabine transport and metabolism in human pancreatic cancer cells. *British Journal of Cancer*, *96*(3), 457–463. https://doi.org/10.1038/SJ.BJC.6603559

Neoptolemos, J. P., Palmer, D. H., Ghaneh, P., Psarelli, E. E., Valle, J. W., Halloran, C. M., Faluyi, O., O'Reilly, D. A., Cunningham, D., Wadsley, J., Darby, S., Meyer, T., Gillmore, R., Anthoney, A., Lind, P., Glimelius, B., Falk, S., Izbicki, J. R., Middleton, G. W., … Büchler, M. W. (2017). Comparison of adjuvant gemcitabine and capecitabine with gemcitabine monotherapy in patients with resected pancreatic cancer (ESPAC-4): a multicentre, open-label, randomised, phase 3 trial. *Lancet (London, England)*, *389*(10073), 1011–1024. https://doi.org/10.1016/S0140-6736(16)32409-6

Nguyen, T. D., & Moody, M. W. (1998). Calcium-activated potassium conductances on cultured nontransformed dog pancreatic duct epithelial cells. *Pancreas*, *17*(4), 348–358. https://doi.org/10.1097/00006676-199811000-00005

Niemeyer, B. A., Mery, L., Zawar, C., Suckow, A., Monje, F., Pardo, L. A., Stühmer, W., Flockerzi, V., & Hoth, M. (2001). Ion channels in health and disease. 83rd Boehringer Ingelheim Fonds International Titisee Conference. *EMBO Reports*, *2*(7), 568–573. https://doi.org/10.1093/EMBO-REPORTS/KVE145

Norberg, K. J., Liu, X., Fernández Moro, C., Strell, C., Nania, S., Blümel, M., Balboni, A., Bozóky, B., Heuchel, R. L., & Löhr, J. M. (2020). A novel pancreatic tumour and stellate cell 3D co-culture spheroid model. *BMC Cancer*, *20*(1), 1–13. https://doi.org/10.1186/S12885-020-06867-5/FIGURES/7

Novak, I., Haanes, K. A., & Wang, J. (2013). Acid-base transport in pancreas-new challenges. *Frontiers in Physiology*, *4*. https://doi.org/10.3389/FPHYS.2013.00380

Öhlund, D., Handly-Santana, A., Biffi, G., Elyada, E., Almeida, A. S., Ponz-Sarvise, M., Corbo, V., Oni, T. E., Hearn, S. A., Lee, E. J., Chio, I. I. C., Hwang, C. Il, Tiriac, H., Baker, L. A., Engle, D. D., Feig, C., Kultti, A., Egeblad, M., Fearon, D. T., … Tuveson, D. A. (2017). Distinct populations of inflammatory fibroblasts and myofibroblasts in pancreatic cancer. *The Journal of Experimental Medicine*, *214*(3), 579–596. https://doi.org/10.1084/JEM.20162024

Olive, K. P., Tuveson, D. A., Ruhe, Z. C., Yin, B., Willis, N. A., Bronson, R. T., Crowley, D., & Jacks, T. (2004). Mutant p53 gain of function in two mouse models of Li-Fraumeni syndrome. *Cell*, *119*(6), 847–860. https://doi.org/10.1016/j.cell.2004.11.004

Orth, M., Metzger, P., Gerum, S., Mayerle, J., Schneider, G., Belka, C., Schnurr, M., & Lauber, K. (2019). Pancreatic ductal adenocarcinoma: biological hallmarks, current status, and future perspectives of combined modality treatment approaches. *Radiation Oncology (London, England)*, *14*(1), 141. https://doi.org/10.1186/S13014-019-1345-6

Oshi, M., Newman, S., Tokumaru, Y., Yan, L., Matsuyama, R., Endo, I., Katz, M. H. G., & Takabe, K. (2020). High G2M Pathway Score Pancreatic Cancer is Associated with Worse Survival, Particularly after Margin-Positive (R1 or R2) Resection. *Cancers*, *12*(10), 1–18. https://doi.org/10.3390/CANCERS12102871

Palamaris, K., Felekouras, E., & Sakellariou, S. (2021). Epithelial to Mesenchymal Transition: Key Regulator of Pancreatic Ductal Adenocarcinoma Progression and Chemoresistance. *Cancers*, *13*(21). https://doi.org/10.3390/CANCERS13215532

Park, W., Chawla, A., & O'Reilly, E. M. (2021). Pancreatic Cancer. *JAMA*, *326*(9), 851. https://doi.org/10.1001/jama.2021.13027

Parker, S. J., Amendola, C. R., Hollinshead, K. E. R., Yu, Q., Yamamoto, K., Encarnación-Rosado, J., Rose, R. E., LaRue, M. M., Sohn, A. S. W., Biancur, D. E., Paulo, J. A., Gygi, S. P., Jones, D. R., Wang, H., Philips, M. R., Bar-Sagi, D., Mancias, J. D., & Kimmelman, A. C. (2020). Selective Alanine Transporter Utilization Creates a Targetable Metabolic Niche in Pancreatic Cancer. *Cancer Discovery*, *10*(7), 1018–1037. https://doi.org/10.1158/2159-8290.CD-19-0959

Patel, S. H., Bachmann, M., Kadow, S., Wilson, G. C., Abdel-Salam, M. M. L., Xu, K., Keitsch, S., Soddemann, M., Wilker, B., Becker, K. A., Carpinteiro, A., Ahmad, S. A., Szabo, I., & Gulbins, E. (2023). Simultaneous targeting of mitochondrial Kv1.3 and lysosomal acid sphingomyelinase amplifies killing of pancreatic ductal adenocarcinoma cells in vitro and in vivo. *Journal of Molecular Medicine*, *101*(3), 295–310. https://doi.org/10.1007/S00109-023-02290-Y/FIGURES/6

Pedersen, K. A., Koschmieder Jørgensen, N., Skaaning Jensen, B., & Olesen, S.-P. (2000). Inhibition of the human intermediate-conductance, Ca2+-activated K+ channel by

intracellular acidification. *Pflügers Archiv - European Journal of Physiology*, *440*(1), 153–156. https://doi.org/10.1007/s004240000269

Pedersen, S. F., Novak, I., Alves, F., Schwab, A., & Pardo, L. A. (2017). Alternating pH landscapes shape epithelial cancer initiation and progression: Focus on pancreatic cancer. *BioEssays*, *39*(6), 1600253. https://doi.org/10.1002/bies.201600253

Pedersen, S. F., & Stock, C. (2013). Ion channels and transporters in cancer: pathophysiology, regulation, and clinical potential. *Cancer Research*, *73*(6), 1658–1661. https://doi.org/10.1158/0008-5472.CAN-12-4188

Pethő, Z., Najder, K., Beel, S., Fels, B., Neumann, I., Schimmelpfennig, S., Sargin, S., Wolters, M., Grantins, K., Wardelmann, E., Mitkovski, M., Oeckinghaus, A., & Schwab, A. (2023). Acid-base homeostasis orchestrated by NHE1 defines the pancreatic stellate cell phenotype in pancreatic cancer. *JCI Insight*, *8*(19). https://doi.org/10.1172/JCI.INSIGHT.170928

Phillips, P. A., Yang, L., Shulkes, A., Vonlaufen, A., Poljak, A., Bustamante, S., Warren, A., Xu, Z., Guilhaus, M., Pirola, R., Apte, M. V., & Wilson, J. S. (2010). Pancreatic stellate cells produce acetylcholine and may play a role in pancreatic exocrine secretion. *Proceedings of the National Academy of Sciences of the United States of America*, *107*(40), 17397–17402. https://doi.org/10.1073/PNAS.1000359107

Pinilla, E., Sánchez, A., Martínez, M. P., Muñoz, M., García-Sacristán, A., Köhler, R., Prieto, D., & Rivera, L. (2021). Endothelial KCa1.1 and KCa3.1 channels mediate rat intrarenal artery endothelium-derived hyperpolarization response. *Acta Physiologica*, *231*(4), e13598. https://doi.org/10.1111/APHA.13598

Pointer, K. B., Clark, P. A., Eliceiri, K. W., Salamat, M. S., Robertson, G. A., & Kuo, J. S. (2017). Administration of Non-Torsadogenic human Ether-à-go-go-Related Gene Inhibitors Is Associated with Better Survival for High hERG-Expressing Glioblastoma Patients. *Clinical Cancer Research : An Official Journal of the American Association for Cancer Research*, *23*(1), 73–80. https://doi.org/10.1158/1078-0432.CCR-15-3169

Prevarskaya, N., Skryma, R., & Shuba, Y. (2018). Ion Channels in Cancer: Are Cancer Hallmarks Oncochannelopathies? *Physiological Reviews*, *98*(2), 559–621. https://doi.org/10.1152/physrev.00044.2016

Principe, D. R., Narbutis, M., Kumar, S., Park, A., Viswakarma, N., Dorman, M. J., Kamath, S. D., Grippo, P. J., Fishel, M. L., Hwang, R. F., Thummuri, D., Underwood, P. W., Munshi, H. G., Trevino, J. G., & Rana, A. (2020). Long-Term Gemcitabine Treatment Reshapes the Pancreatic Tumor Microenvironment and Sensitizes Murine Carcinoma to Combination Immunotherapy. *Cancer Research*, *80*(15), 3101–3115. https://doi.org/10.1158/0008-5472.CAN-19-2959

Provenzano, P. P., Cuevas, C., Chang, A. E., Goel, V. K., Von Hoff, D. D., & Hingorani, S. R. (2012). Enzymatic Targeting of the Stroma Ablates Physical Barriers to Treatment of Pancreatic Ductal Adenocarcinoma. *Cancer Cell*, *21*(3), 418–429. https://doi.org/10.1016/j.ccr.2012.01.007

Rabjerg, M., Oliván-Viguera, A., Hansen, L. K., Jensen, L., Sevelsted-Møller, L., Walter, S., Jensen, B. L., Marcussen, N., & Köhler, R. (2015). High expression of KCa3.1 in patients

with clear cell renal carcinoma predicts high metastatic risk and poor survival. *PloS One*, *10*(4). https://doi.org/10.1371/JOURNAL.PONE.0122992

Rahib, L., Wehner, M. R., Matrisian, L. M., & Nead, K. T. (2021). Estimated Projection of US Cancer Incidence and Death to 2040. *JAMA Network Open*, *4*(4). https://doi.org/10.1001/JAMANETWORKOPEN.2021.4708

Raphael, B. J., Hruban, R. H., Aguirre, A. J., Moffitt, R. A., Yeh, J. J., Stewart, C., Robertson, A. G., Cherniack, A. D., Gupta, M., Getz, G., Gabriel, S. B., Meyerson, M., Cibulskis, C., Fei, S. S., Hinoue, T., Shen, H., Laird, P. W., Ling, S., Lu, Y., … Zenklusen, J. C. (2017). Integrated Genomic Characterization of Pancreatic Ductal Adenocarcinoma. *Cancer Cell*, *32*(2), 185-203.e13. https://doi.org/10.1016/J.CCELL.2017.07.007

Renkawitz, J., Kopf, A., Stopp, J., de Vries, I., Driscoll, M. K., Merrin, J., Hauschild, R., Welf, E. S., Danuser, G., Fiolka, R., & Sixt, M. (2019). Nuclear positioning facilitates amoeboid migration along the path of least resistance. *Nature*, *568*(7753), 546–550. https://doi.org/10.1038/S41586-019-1087-5

Rhim, A. D., Mirek, E. T., Aiello, N. M., Maitra, A., Bailey, J. M., McAllister, F., Reichert, M., Beatty, G. L., Rustgi, A. K., Vonderheide, R. H., Leach, S. D., & Stanger, B. Z. (2012). EMT and dissemination precede pancreatic tumor formation. *Cell*, *148*(1–2), 349–361. https://doi.org/10.1016/J.CELL.2011.11.025

Rodrigues, D. B., Reis, R. L., & Pirraco, R. P. (2024). Modelling the complex nature of the tumor microenvironment: 3D tumor spheroids as an evolving tool. *Journal of Biomedical Science 2024 31:1*, *31*(1), 1–22. https://doi.org/10.1186/S12929-024-00997-9

Roux, B. (2017). Ion channels and ion selectivity. *Essays in Biochemistry*, *61*(2), 201–209. https://doi.org/10.1042/EBC20160074

Saka, D., Gökalp, M., Piyade, B., Cevik, N. C., Sever, E. A., Unutmaz, D., Ceyhan, G. O., Demir, I. E., & Asimgil, H. (2020). Mechanisms of T-Cell Exhaustion in Pancreatic Cancer. *Cancers*, *12*(8), 1–27. https://doi.org/10.3390/CANCERS12082274

Sarantis, P., Koustas, E., Papadimitropoulou, A., Papavassiliou, A. G., & Karamouzis, M. V. (2020). Pancreatic ductal adenocarcinoma: Treatment hurdles, tumor microenvironment and immunotherapy. *World Journal of Gastrointestinal Oncology*, *12*(2), 173–181. https://doi.org/10.4251/WJGO.V12.I2.173

Sarles, H. (2010). The Exocrine Pancreas. *International Review of Physiology*, *12*, 173–221. https://doi.org/10.4199/C00026ED1V01Y201102ISP014

Sassi, N., De Marchi, U., Fioretti, B., Biasutto, L., Gulbins, E., Franciolini, F., Szabò, I., & Zoratti, M. (2010). An investigation of the occurrence and properties of the mitochondrial intermediate-conductance Ca2+-activated K+ channel mtKCa3.1. *Biochimica et Biophysica Acta*, *1797*(6–7), 1260–1267. https://doi.org/10.1016/J.BBABIO.2009.12.015

Schnipper, J., Dhennin-Duthille, I., Ahidouch, A., & Ouadid-Ahidouch, H. (2020). Ion Channel Signature in Healthy Pancreas and Pancreatic Ductal Adenocarcinoma. *Frontiers in Pharmacology*, *11*, 568993. https://doi.org/10.3389/FPHAR.2020.568993

Schwab, A., Fabian, A., Hanley, P. J., & Stock, C. (2012). Role of ion channels and transporters in cell migration. *Physiological Reviews*, *92*(4), 1865–1913. https://doi.org/10.1152/PHYSREV.00018.2011

Sevelsted Møller, L., Fialla, A. D., Schierwagen, R., Biagini, M., Liedtke, C., Laleman, W., Klein, S., Reul, W., Koch Hansen, L., Rabjerg, M., Singh, V., Surra, J., Osada, J., Reinehr, R., De Muckadell, O. B. S., Köhler, R., & Trebicka, J. (2016). The calcium-activated potassium channel KCa3.1 is an important modulator of hepatic injury. *Scientific Reports*, *6*. https://doi.org/10.1038/SREP28770

Sforna, L., Megaro, A., Pessia, M., Franciolini, F., & Catacuzzeno, L. (2018). Structure, Gating and Basic Functions of the Ca2+-activated K Channel of Intermediate Conductance. *Current Neuropharmacology*, *16*(5), 608–617. https://doi.org/10.2174/1570159X15666170830122402

Sharma, P., Guo, A., Poudel, S., Boada-Romero, E., Verbist, K. C., Palacios, G., Immadisetty, K., Chen, M. J., Haydar, D., Mishra, A., Peng, J., Madan Babu, M., Krenciute, G., Glazer, E. S., & Green, D. R. (2024). Rapid metabolic regulation of a novel arginine methylation of KCa3.1 attenuates T cell exhaustion. *BioRxiv : The Preprint Server for Biology*. https://doi.org/10.1101/2024.05.09.593421

Sheikh, A. A., & Utzschneider, D. T. (2022). IRF2 integrates inflammatory signals to balance T cell exhaustion. *Immunity*, *55*(12), 2225–2227. https://doi.org/10.1016/J.IMMUNI.2022.11.010

Siegel, R. L., Miller, K. D., Fuchs, H. E., & Jemal, A. (2022). Cancer statistics, 2022. *CA: A Cancer Journal for Clinicians*, *72*(1), 7–33. https://doi.org/10.3322/CAAC.21708

Song, K., Yu, Z., Zu, X., Li, G., Hu, Z., & Xue, Y. (2022). Collagen Remodeling along Cancer Progression Providing a Novel Opportunity for Cancer Diagnosis and Treatment. *International Journal of Molecular Sciences 2022, Vol. 23, Page 10509*, *23*(18), 10509. https://doi.org/10.3390/IJMS231810509

Soret, B., Hense, J., Lüdtke, S., Thale, I., Schwab, A., & Düfer, M. (2023). Pancreatic KCa3.1 channels in health and disease. In *Biological Chemistry* (Vol. 404, Issue 4, pp. 339–353). De Gruyter Open Ltd. https://doi.org/10.1515/hsz-2022-0232

Sperb, N., Tsesmelis, M., & Wirth, T. (2020). Crosstalk between Tumor and Stromal Cells in Pancreatic Ductal Adenocarcinoma. *International Journal of Molecular Sciences*, *21*(15), 5486. https://doi.org/10.3390/ijms21155486

Srivastava, S., Panda, S., Li, Z., Fuhs, S. R., Hunter, T., Thiele, D. J., Hubbard, S. R., & Skolnik, E. Y. (2016). Histidine phosphorylation relieves copper inhibition in the mammalian potassium channel KCa3.1. *ELife*, *5*. https://doi.org/10.7554/eLife.16093

Staal, R. G. W., Weinstein, J. R., Nattini, M., Cajina, M., Chandresana, G., & Möller, T. (2017). Senicapoc: Repurposing a Drug to Target Microglia KCa3.1 in Stroke. *Neurochemical Research*, *42*(9), 2639–2645. https://doi.org/10.1007/S11064-017-2223-Y

Steudel, F. A., Mohr, C. J., Stegen, B., Nguyen, H. Y., Barnert, A., Steinle, M., Beer-Hammer, S., Koch, P., Lo, W. Y., Schroth, W., Hoppe, R., Brauch, H., Ruth, P., Huber, S. M., & Lukowski, R. (2017). SK4 channels modulate Ca2+ signalling and cell cycle

progression in murine breast cancer. *Molecular Oncology*, *11*(9), 1172–1188. https://doi.org/10.1002/1878-0261.12087

Stewart, C. M., Siegler, E. L., Sakemura, R. L., Cox, M. J., Huynh, T., Kimball, B., Mai, L., Can, I., Roman, C. M., Yun, K., Sirpilla, O., Girsch, J. H., Ogbodo, E., Ismail, W., Maia, A. G., Budka, J., Kim, J., Scholler, N., Mattie, M., … Kenderian, S. S. (2023). Title: The Identification of IL-4 as a Regulator of Chimeric Antigen Receptor T Cell Exhaustion. *BioRxiv*. https://doi.org/10.1101/2023.09.28.560046

Stocker, J. W., De Franceschi, L., McNaughton-Smith, G. A., Corrocher, R., Beuzard, Y., & Brugnara, C. (2003). ICA-17043, a novel Gardos channel blocker, prevents sickled red blood cell dehydration in vitro and in vivo in SAD mice. *Blood*, *101*(6), 2412–2418. https://doi.org/10.1182/BLOOD-2002-05-1433

Storck, H., Hild, B., Schimmelpfennig, S., Sargin, S., Nielsen, N., Zaccagnino, A., Budde, T., Novak, I., Kalthoff, H., & Schwab, A. (2017). Ion channels in control of pancreatic stellate cell migration. *Oncotarget*, *8*(1), 769–784. https://doi.org/10.18632/oncotarget.13647

Strupp, M., Staub, F., & Grafe, P. (1993). A Ca(2+)- and pH-dependent K+ channel of rat C6 glioma cells and its possible role in acidosis-induced cell swelling. *Glia*, *9*(2), 136–145. https://doi.org/10.1002/GLIA.440090207

Sugunan, S., Nampoothiri, S. S., Garg, T., & Krishnamurthy, R. G. (2016). Role of KCa3.1 Channels in CNS Diseases: A Concise Review. *CNS & Neurological Disorders - Drug Targets*, *15*(10), 1299–1305. https://doi.org/10.2174/1871527315666160822111913

Sun, Q., Zhao, X., Li, R., Liu, D., Pan, B., Xie, B., Chi, X., Cai, D., Wei, P., Xu, W., Wei, K., Zhao, Z., Fu, Y., Ni, L., & Dong, C. (2023). STAT3 regulates CD8+ T cell differentiation and functions in cancer and acute infection. *The Journal of Experimental Medicine*, *220*(4). https://doi.org/10.1084/JEM.20220686

Szabo, I., & Zoratti, M. (2014). Mitochondrial Channels: Ion Fluxes and More. *Physiol Rev*, *94*, 519–608. https://doi.org/10.1152/physrev.00021.2013.-The

Tao, J., Yang, G., Zhou, W., Qiu, J., Chen, G., Luo, W., Zhao, F., You, L., Zheng, L., Zhang, T., & Zhao, Y. (2021). Targeting hypoxic tumor microenvironment in pancreatic cancer. *Journal of Hematology & Oncology*, *14*(1), 14. https://doi.org/10.1186/s13045-020-01030-w

Tempero, M. A., Pelzer, U., O'Reilly, E. M., Winter, J., Oh, D. Y., Li, C. P., Tortora, G., Chang, H. M., Lopez, C. D., Bekaii-Saab, T., Ko, A. H., Santoro, A., Park, J. O., Noel, M. S., Frassineti, G. L., Shan, Y. S., Dean, A., Riess, H., Van Cutsem, E., … Fuloria, J. (2023). Adjuvant nab-Paclitaxel + Gemcitabine in Resected Pancreatic Ductal Adenocarcinoma: Results From a Randomized, Open-Label, Phase III Trial. *Journal of Clinical Oncology : Official Journal of the American Society of Clinical Oncology*, *41*(11), 2007–2019. https://doi.org/10.1200/JCO.22.01134

Thompson-Vest, N., Shimizu, Y., Hunne, B., & Furness, J. B. (2006). The distribution of intermediate-conductance, calcium-activated, potassium (IK) channels in epithelial cells. *Journal of Anatomy*, *208*(2), 219–229. https://doi.org/10.1111/J.1469-7580.2006.00515.X

Tirpe, A., Streianu, C., Isachesku, E., Simon, I., & Berindan-Neagoe, I. (2024). The road to overcome pancreatic cancer: Where are we? *Heliyon*, *10*(19), e38196. https://doi.org/10.1016/J.HELIYON.2024.E38196

Todesca, L. M., Gerke, M., Bulk, E. E., Bachmann, M., Rudersdorf, A., Antonuzzo, L., Pillozzi, S., Düfer, M., Szabo, I., & Schwab, A. (2024). Targeting KCa3.1 channels to overcome erlotinib resistance in non-small cell lung cancer cells. *Cell Death Discovery*, *10*(1). https://doi.org/10.1038/S41420-023-01776-5

Todesca, L. M., Maskri, S., Brömmel, K., Thale, I., Wünsch, B., Koch, O., & Schwab, A. (2021). Targeting Kca3.1 Channels in Cancer. *Cellular Physiology and Biochemistry*, *55*(S3), 131–144. https://doi.org/10.33594/000000374

Valsecchi, M. E., Holdbrook, T., Leiby, B. E., Pequignot, E., Littman, S. J., Yeo, C. J., Brody, J. R., & Witkiewicz, A. K. (2012). Is there a role for the quantification of RRM1 and ERCC1 expression in pancreatic ductal adenocarcinoma? *BMC Cancer*, *12*. https://doi.org/10.1186/1471-2407-12-104

van Erning, F. N., Mackay, T. M., van der Geest, L. G. M., Groot Koerkamp, B., van Laarhoven, H. W. M., Bonsing, B. A., Wilmink, J. W., van Santvoort, H. C., de Vos-Geelen, J., van Eijck, C. H. J., Busch, O. R., Lemmens, V. E., & Besselink, M. G. (2018). Association of the location of pancreatic ductal adenocarcinoma (head, body, tail) with tumor stage, treatment, and survival: a population-based analysis. *Acta Oncologica (Stockholm, Sweden)*, *57*(12), 1655–1662. https://doi.org/10.1080/0284186X.2018.1518593

Veite-Schmahl, M. J., Rivers, A. C., Regan, D. P., & Kennedy, M. A. (2017). The Mouse Model of Pancreatic Cancer Atlas (MMPCA) for classification of pancreatic cancer lesions: A large histological investigation of the Ptf1aCre/+;LSL-KrasG12D/+ transgenic mouse model of pancreatic cancer. *PloS One*, *12*(11). https://doi.org/10.1371/JOURNAL.PONE.0187552

Vergara, C., Latorre, R., Marrion, N. V., & Adelman, J. P. (1998). Calcium-activated potassium channels. *Current Opinion in Neurobiology*, *8*(3), 321–329. https://doi.org/10.1016/S0959-4388(98)80056-1

Versteijne, E., Van Dam, J. L., Suker, M., Janssen, Q. P., Groothuis, K., Akkermans-Vogelaar, J. M., Besselink, M. G., Bonsing, B. A., Buijsen, J., Busch, O. R., Creemers, G. J. M., Van Dam, R. M., Eskens, F. A. L. M., Festen, S., De Groot, J. W. B., Groot Koerkamp, B., De Hingh, I. H., Homs, M. Y. V., Van Hooft, J. E., … Van Eijck, C. H. J. (2022). Neoadjuvant Chemoradiotherapy Versus Upfront Surgery for Resectable and Borderline Resectable Pancreatic Cancer: Long-Term Results of the Dutch Randomized PREOPANC Trial. *Journal of Clinical Oncology : Official Journal of the American Society of Clinical Oncology*, *40*(11), 1220–1230. https://doi.org/10.1200/JCO.21.02233

Von Hoff, D. D., Ervin, T., Arena, F. P., Chiorean, E. G., Infante, J., Moore, M., Seay, T., Tjulandin, S. A., Ma, W. W., Saleh, M. N., Harris, M., Reni, M., Dowden, S., Laheru, D., Bahary, N., Ramanathan, R. K., Tabernero, J., Hidalgo, M., Goldstein, D., … Renschler, M. F. (2013). Increased survival in pancreatic cancer with nab-paclitaxel plus gemcitabine. *The New England Journal of Medicine*, *369*(18), 1691–1703. https://doi.org/10.1056/NEJMOA1304369

Waddell, N., Pajic, M., Patch, A. M., Chang, D. K., Kassahn, K. S., Bailey, P., Johns, A. L., Miller, D., Nones, K., Quek, K., Quinn, M. C. J., Robertson, A. J., Fadlullah, M. Z. H., Bruxner, T. J. C., Christ, A. N., Harliwong, I., Idrisoglu, S., Manning, S., Nourse, C., … Grimmond, S. M. (2015). Whole genomes redefine the mutational landscape of pancreatic cancer. *Nature*, *518*(7540), 495–501. https://doi.org/10.1038/NATURE14169

Wang, J., Haanes, K. A., & Novak, I. (2013). Purinergic regulation of CFTR and Ca 2-activated Cl channels and K channels in human pancreatic duct epithelium Wang J, Haanes KA, Novak I. Purinergic regulation of CFTR and Ca 2-activated Cl channels and K channels in human pancreatic duct epithelium. *Am J Physiol Cell Physiol*, *304*, 673–684. https://doi.org/10.1152/ajpcell.00196.2012

Wang, S., Huang, S., & Sun, Y. L. (2017). Epithelial-Mesenchymal Transition in Pancreatic Cancer: A Review. *BioMed Research International*, *2017*, 2646148. https://doi.org/10.1155/2017/2646148

Wang, S., Li, Y., Xing, C., Ding, C., Zhang, H., Chen, L., You, L., Dai, M., & Zhao, Y. (2020). Tumor microenvironment in chemoresistance, metastasis and immunotherapy of pancreatic cancer. *American Journal of Cancer Research*, *10*(7), 1937. https://pmc.ncbi.nlm.nih.gov/articles/PMC7407356/

Wang, Y., Ji, P., Liu, J., Broaddus, R. R., Xue, F., & Zhang, W. (2009). Centrosome-associated regulators of the G2/M checkpoint as targets for cancer therapy. *Molecular Cancer*, *8*, 8. https://doi.org/10.1186/1476-4598-8-8

Werner, J., Combs, S. E., Springfeld, C., Hartwig, W., Hackert, T., & Büchler, M. W. (2013). Advanced-stage pancreatic cancer: therapy options. *Nature Reviews. Clinical Oncology*, *10*(6), 323–333. https://doi.org/10.1038/NRCLINONC.2013.66

Wong, R., & Schlichter, L. C. (2014). PKA reduces the rat and human KCa3.1 current, CaM binding, and Ca2+ signaling, which requires Ser332/334 in the CaM-binding C terminus. *The Journal of Neuroscience : The Official Journal of the Society for Neuroscience*, *34*(40), 13371–13383. https://doi.org/10.1523/JNEUROSCI.1008-14.2014

Wu, B. M., Liu, J. Da, Li, Y. H., & Li, J. (2020). Margatoxin mitigates CCl4-induced hepatic fibrosis in mice via macrophage polarization, cytokine secretion and STAT signaling. *International Journal of Molecular Medicine*, *45*(1), 103–114. https://doi.org/10.3892/IJMM.2019.4395

Wulf, A., & Schwab, A. (2002). Regulation of a Calcium-sensitive K+ Channel (cIK1) by Protein Kinase C. *The Journal of Membrane Biology*, *187*(1), 71–79. https://doi.org/10.1007/s00232-001-0149-3

Wulff, H., & Castle, N. A. (2010). Therapeutic potential of KCa3.1 blockers: recent advances and promising trends. *Expert Review of Clinical Pharmacology*, *3*(3), 385–396. https://doi.org/10.1586/ECP.10.11

Wulff, H., Knaus, H.-G. N., Pennington, M., & Chandy, K. G. (2004). K Channel Expression during B Cell Differentiation: Implications for Immunomodulation and Autoimmunity

1. *The Journal of Immunology*, *173*, 776–786. http://journals.aai.org/jimmunol/article-pdf/173/2/776/1187805/776.pdf

Wulff, H., Miller, M. J., Hänsel, W., Grissmer, S., Cahalan, M. D., & Chandy, K. G. (2000). Design of a potent and selective inhibitor of the intermediate-conductance Ca2+-activated K+ channel, IKCa1: A potential immunosuppressant. *Proceedings of the National Academy of Sciences of the United States of America*, *97*(14), 8151. https://doi.org/10.1073/PNAS.97.14.8151

Xu, R., Li, C., Wu, Y., Shen, L., Ma, J., Qian, J., & Ge, J. (2017). Role of KCa3.1 channels in macrophage polarization and its relevance in atherosclerotic plaque instability. *Arteriosclerosis, Thrombosis, and Vascular Biology*, *37*(2), 226–236. https://doi.org/10.1161/ATVBAHA.116.308461/SUPPL_FILE/XU_226.PDF

Yi, M., Yu, P., Lu, Q., Geller, H. M., Yu, Z., & Chen, H. (2016). KCa3.1 constitutes a pharmacological target for astrogliosis associated with Alzheimer's disease. *Molecular and Cellular Neurosciences*, *76*, 21. https://doi.org/10.1016/J.MCN.2016.08.008

Zaccagnino, A., Pilarsky, C., Tawfik, D., Sebens, S., Trauzold, A., Novak, I., Schwab, A., & Kalthoff, H. (2016). In silico analysis of the transportome in human pancreatic ductal adenocarcinoma. *European Biophysics Journal*, *45*(7), 749–763. https://doi.org/10.1007/s00249-016-1171-9

Zhang, T., Ameen, S., Ghosh, S., Kim, K., Thanh, M., Patteson, A. E., Wu, M., & Schwarz, J. M. (2024). Enhanced extracellular matrix remodeling due to embedded spheroid fluidization. *ArXiv*. /pmc/articles/PMC10996774/

Zhang, Z., Zhang, H., Liao, X., & Tsai, H. I. I. (2023). KRAS mutation: The booster of pancreatic ductal adenocarcinoma transformation and progression. *Frontiers in Cell and Developmental Biology*, *11*, 1147676. https://doi.org/10.3389/FCELL.2023.1147676/BIBTEX

Zhen, D. B., Rabe, K. G., Gallinger, S., Syngal, S., Schwartz, A. G., Goggins, M. G., Hruban, R. H., Cote, M. L., McWilliams, R. R., Roberts, N. J., Cannon-Albright, L. A., Li, D., Moyes, K., Wenstrup, R. J., Hartman, A. R., Seminara, D., Klein, A. P., & Petersen, G. M. (2015). BRCA1, BRCA2, PALB2, and CDKN2A mutations in familial pancreatic cancer: a PACGENE study. *Genetics in Medicine : Official Journal of the American College of Medical Genetics*, *17*(7), 569–577. https://doi.org/10.1038/GIM.2014.153

Zheng, W., Thorne, N., & McKew, J. C. (2013). Phenotypic screens as a renewed approach for drug discovery. *Drug Discovery Today*, *18*(21–22), 1067–1073. https://doi.org/10.1016/J.DRUDIS.2013.07.001